EFFECT OF COLUMN RETROFITTING ON THE SEISMIC RESPONSE OF CONCRETE FRAMES

by

Emmet D. Poon

April 1999

Department of Civil Engineering and Applied Mechanics

McGill University

Montréal, Canada

A thesis submitted to the Faculty of Graduate Studies
and Research in partial fulfilment of the requirements
for the degree of Master of Engineering

0-612-55024-9

EFFECT OF COLUMN RETROFITTING ON THE SEISMIC RESPONSE OF CONCRETE FRAMES

ABSTRACT

A full-scale exterior beam-column-slab subassemblage was tested under reversed cyclic loading to investigate the influence of retrofitting with steel corner angles and batten plates to increase the column strength. The response of this specimen was compared to two specimens previously constructed and tested at McGill University (Castele, 1988). Each specimen was designed and detailed according to the 1984 CSA A23.3-M84 Standard with a force modification factor, R, of 2.0 (NBCC 1995). The first specimen represented a deficient subassemblage before retrofit. The response of the retrofitted specimen using steel corner angles and batten plates was compared to the response of a specimen retrofitted using reinforced concrete sleeving (tested by Castele, 1988). The test specimens were instrumented to enable detailed strain, load and deflection measurements at critical locations during the testing procedure. The results of the two retrofit specimens provides some insight into the rehabilitation of older structures containing "weak column" or deficiently designed and detailed columns.

In addition, three full-scale column specimens were constructed and tested under monotonic axial compression to determine the effectiveness of the two column retrofitting techniques used in the subassemblage specimens. These tests provided a means of assessing the assumptions used in predicting the responses of retrofitted columns.

EFFET DU RENFORCEMENT DE COLONNES SUR LE COMPORTEMENT SISMIQUE DE CADRES EN BÉTON ARMÉ

RÉSUMÉ

Cette étude porte sur des essais en vraie grandeur réalisés sur un spécimen de sous-assemblages poutres-dalles-colonnes en béton armé afin d'évaluer l'efficacité d'une technique de réhabilitation sismique de colonnes à l'aide de cornières et lattes en acier. Le comportement de ce spécimen a été comparé à celui de deux autres spécimens préalablement construits et testés à l' l'Université McGill (Castele, 1988): le premier représentait un sous-assemblage déficient, i.e. avant réhabilitation, alors que le deuxième avait été renforcé par un manchon en béton armé. Chacun des spécimens a été conçu et construit selon la norme CSA A23.3-M84 pour des conditions de ductilité nominale correspondant à un facteur de réduction de charge, R, égal à 2.0 selon le Code National du Bâtiment du Canada 1995. Les essais ont été réalisés sous charges cycliques réversibles, avec mesures détaillées des déformations aux endroits critiques, des déplacements et de la charge appliquée.

Trois essais supplémentaires ont été réalisés sur des spécimens en vraie grandeur de colonnes seules soumises à des charges monotones de compression axiale, afin d'évaluer l'efficacité des deux techniques de réhabilitation sismique utilisées dans les sous-assemblages. Ces essais ont permis de vérifier les hypothèses utilisées pour la prédiction du comportement des colonnes renforcées.

ACKNOWLEDGEMENTS

The author wishes to sincerely thank Professor Denis Mitchell for his guidance and encouragement throughout the course of this research program. The patience and invaluable assistance of both Dr. William D. Cook and Stuart Bristowe was also tremendously appreciated. In addition, the author expresses his gratitude to Daniel Castele for the construction and testing of Specimens S1 and RS1.

The research presented in this thesis was carried out in the Jamieson Structures Laboratory at McGill University. The author would like extend special thanks to Ron Sheppard, Marek Przykorski, John Bartczak, and Damon Kiperchuk for their assistance in the laboratory. Special thanks are also extended to: Pierre Koch, Bryce Tupper, Kevin Li, Carla Ghannoum, Wassim Ghannoum and Pedro Da Silva for their assistance during this study.

The completion of this project would not have been possible without the patience and valuable help of the office staff of the Civil Engineering Department.

Finally, the author would like to thank his family and friends, and especially Kira Rich, for their incredible support and understanding throughout his stay at McGill University.

Emmet D. Poon
April, 1999

TABLE OF CONTENTS

LIST OF FIGURES

Chapter 4

Chapter 5

Chapter 6

Appendix A

Appendix B

LIST OF TABLES

LIST OF SYMBOLS

a	depth of equivalent rectangular stress block
A_c	area of spandrel beam cross-section
A_{ch}	area of confined core
A_g	gross area of concrete column
A_{jh}	total effective transverse reinforcement in the joint
A_o	area enclosed by torsional shear flow path
A_{oh}	area enclosed by centreline of closed transverse torsion reinforcement
A_s	area of longitudinal reinforcement
$A_s{}^*$	area of slab bars within the distance s_s
A_{sh}	total cross sectional area of transverse reinforcement within spacing, s, and perpendicular to dimension, h_c
A_{sl}	area of slab reinforcement contributing to the negative flexural capacity of the beam
$A_{s,max}$	maximum permitted longitudinal reinforcement
$A_{s,min}$	minimum permitted longitudinal reinforcement
A_{st}	area of column vertical reinforcement
A_t	area of one leg of the closed hoop reinforcement
A_v	effective area of transverse reinforcement
b_e	effective width of T-beam in negative bending
b_o	width between corner longitudinal bars of the spandrel beam
b_w	minimum effective width in shear
c	size of rectangular or equivalent rectangular column
d	distance from extreme compression fibre to centroid of tension reinf.
d''	diameter of concrete core
d_{bh}	nominal diameter of hoop reinforcement
d_{bl}	nominal diameter of longitudinal reinforcement
d_v	distance between the resultants of the tensile and compressive forces due to flexure
e	eccentricity of slab reinforcement about the centre of twist of the spandrel beam
f'_c	specified compressive strength of concrete
f_m	magnification factor
f_{sp}	splitting strength of concrete
f_r	modulus of rupture
f_y	specified yield strength of reinforcement
f_{yh}	yield strength of transverse reinforcement
f_{yt}	yield strength of spiral
f_{ult}	ultimate strength of reinforcement
F	foundation factor of a structure
F_{cr}	force in slab bars at cracking
g	acceleration due to gravity
h_c	cross-sectional dimension of column core
h_f	thickness of the slab
h_n	total height of a structure
h_o	height between corner longitudinal bars of the spandrel beam
I	importance factor of a structure
jd	moment lever arm
k_u	stiffness at a deflection of Δ_u
k_y	stiffness at a deflection of Δ_y
l	distance from loading point to the column face
l_n	length of clear span
m	$f_y/0.85f'_c$
M_{cr}	cracking moment
M_f	factored moment
M_{max}	maximum moment obtained in the beam
M_{nb}	nominal flexural resistance of a beam
M_{pr}^-	negative probable moment in the beam

M_r	factored moment resistance
M_r^+	positive moment resistance
M_r^-	negative moment resistance
M_R	flexural strength ratio
M_{rc}	factored flexural resistance of a column
n	number of effective slab bars
N	number of storeys in a structure
N*	design axial load at ultimate limit state
p_c	outside perimeter of concrete cross-section
p_h	perimeter of the centreline of the closed transverse hoop reinforcement
P	axial load on column
P_r	factored axial load resistance of a member
P_{peak}	applied load corresponding to the peak of the cycle
$P_{r(max)}$	maximum factored axial load resistance of a column
P_u	applied load corresponding to Δ_u
P_y	applied load corresponding to Δ_y
R	force modification factor
s	spacing of transverse reinforcement
s_{max}	maximum stirrup spacing for shear
s_s	spacing between slab bars
S	seismic response factor of a structure
T	fundamental period of vibration of a structure
T_y	yield torque of a beam
T_{cr}	cracking torque of a beam
U	calibration factor of a structure
v	zonal velocity ratio
V	seismic base shear of a structure
V_c	factored shear resistance provided by the concrete
V_f	factored shear resistance
V_j	net horizontal joint shear
V_s	factored shear resistance provided by the steel
V_r	factored shear resistance of a member
V_y	yield force
W	dead load of a structure plus 25% of design snow load
x	effective width of the slab
Z_a	acceleration-related seismic zone
Z_v	velocity-related seismic zone
Δ_f	component of beam tip deflection due to flexure
Δ_j	component of beam tip deflection due to bond slip and joint shear deformation
Δ_{peak}	cycle peak tip deflection
Δ_s	component of beam tip deflection due to shear
Δ_{tip}	beam tip deflection
Δ_u	maximum recorded tip deflection
Δ_y	deflection at general yielding
Δ_y^+	deflection at general yielding in the positive direction
Δ_y^-	deflection at general yielding in the negative direction
ε_c'	concrete strain corresponding to f_c'
ε_s	strain in reinforcement
ε_y	yield strain of reinforcement
ϕ_c	resistance factor for concrete
ϕ_s	resistance factor for reinforcement
γ	shear strain in the beam
γ_j	joint shear factor
φ	beam curvature
φ_u	ultimate curvature of beam
φ_y	yield curvature of beam
λ	factor to account for density of concrete
ν	shear stress
ν_{cr}	cracking shear stress of beam
ν_t	shear stress due to torsion in the beam
ν_v	shear stress due to shearing in the beam
ν_j	joint shear stress
θ	angle of principal compression
θ_{jb}	rotation of joint due to bond slip
θ_{jv}	rotation of joint due to shear
ρ_s	ratio of spiral reinforcement
ρ_{sh}	shear reinforcement ratio
ρ_t	ratio of non prestressed longitudinal column reinforcemnet
ρ_{tm}	modified transverse reinforcement ratio
ρ_{tmi}	modified and increased reinforcement ratio

CHAPTER 1

INTRODUCTION

The objective of earthquake resistant design according to the National Building Code of Canada (1995) is such that structures "should be able to resist moderate earthquakes without significant damage and major earthquakes without collapse." Experimental research, as well as lessons learned from previous earthquakes have shown the need for proper design and detailing of structural members to provide the necessary strength and ductility. The 1995 National Building Code of Canada (NBCC) contains detailed provisions for the earthquake resistant design of structures. The NBCC incorporates the use of a force modification factor, R, that reflects the "capability of a structure to dissipate energy through inelastic behaviour" and ranges from 1.0 for unreinforced masonry construction, to 4.0 for ductile moment-resisting space frames. The necessary design and detailing requirements are described in the 1994 Canadian Standard Association A23.3-94, Design of Concrete Structures (CSA).

Reinforced concrete frames are designed and detailed as either ductile moment-resisting frames (R = 4.0) in accordance with Clause 21.4, nominally ductile frames (R = 2.0) in accordance with Clause 21.9, or as "ordinary" frames (R = 1.5) satisfying the non-seismic provisions of the CSA Standard. Figure 1.1 summarises the detailing requirements for beams and columns in frames designed with an R factor of 1.5, 2.0 and 4.0. Because this research project will be examining the retrofit of a beam-column-slab subassemblage designed and detailed for a force modification factor, R of 2.0, the code requirements for nominally ductile frames are discussed below.

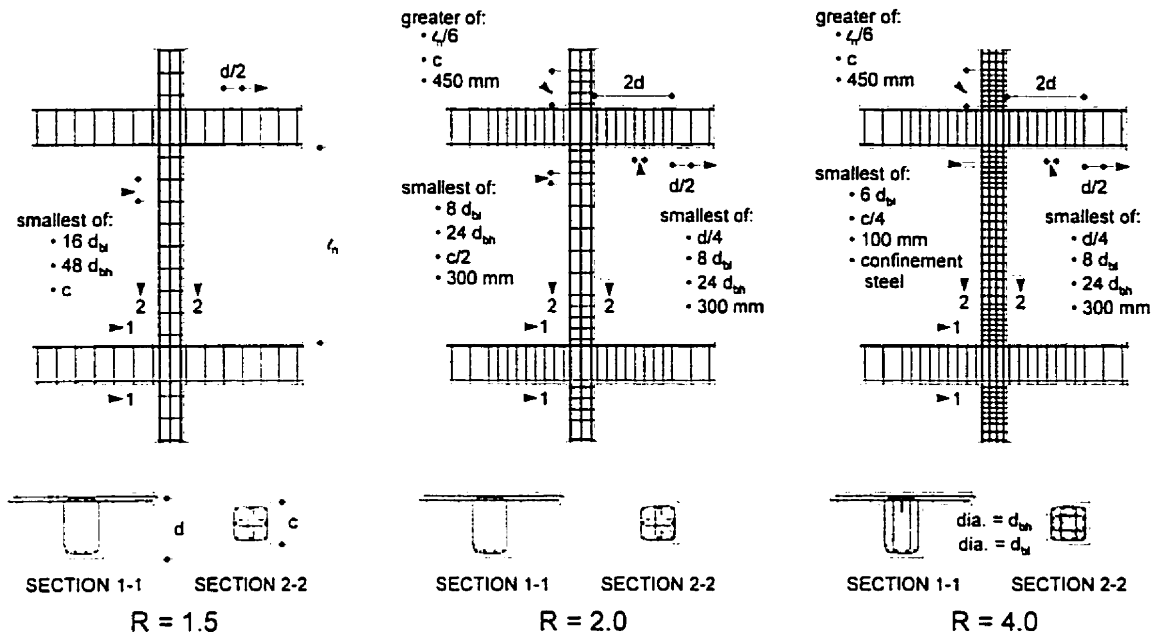

Figure 1.1: Summary of detailing requirements for beams and columns (from CSA, 1994)

1.1 Design Criteria for Nominally Ductile Moment-resisting Frames

The structural members of a nominally ductile moment-resisting frame are designed and detailed to provide adequate amounts of seismic energy dissipation through inelastic deformation. The CSA Standard (1994) contains provisions for nominally ductile moment-resisting frames which are described in detail in Clause 21.9. Detailing of the beams of a nominally ductile moment-resisting frame are described in Clause 21.9.2.1. All of the stirrups must be detailed as hoops and must be provided over a distance of twice the member depth measured from the face of the supporting member towards midspan. The first hoop shall be located not more than 50 mm from the face of the supporting member, with subsequent hoops having spacing not exceeding the smallest of:

(i) d/4;

(ii) 8 times the diameter of the smallest longitudinal bar;

(iii) 24 tie diameters; or

(iv) 300 mm.

Outside of this region, stirrups must be provided with a maximum spacing of d/2.

The detailing requirements of the column in a nominally ductile moment-resisting frame are described in Clause 21.9.2.2. All transverse reinforcement in the columns must be detailed as hoops and cross-ties. Where plastic hinging is expected to develop in the columns, the spacing of the hoops and cross-ties over a distance of not less than:

(i) one-sixth of the clear height of the column;

(ii) the maximum cross sectional dimension; or

(iii) 450 mm.

and having a spacing of the lesser of one-half the value specified in Clause 7.6.5 or 300 mm.

Therefore, in regions where plastic hinges are expected to develop these provisions result in hoop spacings not exceeding the least of:

(i) 8 times the diameter of the smallest longitudinal bar;

(ii) 24 tie diameters;

(iii) one-half of the least dimension of the compression member; or

(iv) 300 mm.

The design and detailing of the joint region is defined in Clause 21.9.2.4. Minimum joint reinforcement is required over the depth of the joint and must be spaced at no more than 150 mm. This clause requires the limiting of the centre-to-centre spacing of the longitudinal column bars to not exceed 300 mm. In addition, the maximum joint shear cannot exceed the limits specified in Clause 21.6.4.1.

It is noted that in the 1984 CSA Standard, regular column ties with 90° bend anchorages were permitted, while the 1994 CSA Standard requires that hoops or cross ties having seismic hooks be provided throughout the height of the column. The 1984 CSA Standard also permitted stirrups to be used throughout the length of the beam, whereas the 1994 CSA Standard requires hoops with seismic hooks to be used as transverse reinforcement in the plastic hinge region of the beams.

1.2 The Need for Research on Retrofitting of Reinforced Concrete Structures

Recent earthquakes have emphasised the need to retrofit existing poorly designed and detailed reinforced concrete structures. The lessons learned from past earthquakes have influenced design codes resulting in significant changes to codes of practice over the last 25 years. Most older structures possess a number of deficiencies and are in need of strengthening in order to provide adequate levels of strength and ductility.

The majority of retrofitting techniques used are very expensive, time consuming and require the interruption of the use of the structure during the construction process. The Federal Emergency Management Agency (FEMA) has numerous publications to deal with the seismic risk associated with existing buildings. The first step is to determine if a building is in need of an in-depth review of the seismic capacity of the structure. A rapid screening procedure, developed by FEMA, permits a visual inspection of a building (ATC-21, 1988). If the structure is determined to need further evaluation by an engineer, a technical manual that offers guidelines for engineers is used to evaluate the seismic capabilities of the existing structure (ATC-21-1, 1989). Seismic rehabilitation of a building can be accomplished with a variety of different techniques. The benefits and limitations of these approaches are discussed in the technical handbook, ATC-22 (1989). It should be pointed out that the main deterrent to retrofit is the "reluctance to invest money in an activity that probably does not increase the market value or income" of the structure as well as "the incomplete understanding of the true benefits of pursuing this course of action" (FEMA-157, 1988). Therefore, it is imperative to develop new, improved, low cost and less disruptive retrofitting techniques in order to make retrofitting an economically viable option.

1.3 Retrofit Techniques for Reinforced Concrete Moment-resisting Frames

Field reports following various damaging earthquakes have shown that reinforced concrete frame structures are particularly susceptible to earthquake damage. The column and joint regions are at great risk when the structures possess "strong beam-weak column" conditions. Following the 1985 Mexico City earthquake, Mitchell *et al* (1988), reported that many of the structures which experienced severe damage or total collapse contained columns and beam-column joints with inadequate details to reach the required levels of ductility. Recent Canadian design codes possess much more stringent design and detailing requirements for ductile and nominally-ductile moment-resisting frames, and hence older Canadian structures may reflect similar design and detailing deficiencies as those in Mexico City. It is imperative to strengthen and/or improve the ductility of these older structures, in order to prevent a catastrophe in the event of a major earthquake.

The strengthening of an existing structure requires close examination of details and usually a more extensive structural analysis than the design of a new structure. The analysis would consist of determining the strengths and weaknesses of the existing lateral force resisting system. The strengthening technique chosen would have to be consistent with the strength, stiffness and ductility of the original structure, as well as considerations for aesthetics and functionality of the structure.

The most important objective of strengthening a structure with inadequate lateral load resisting elements is to increase the strength and ductility, as well as provide uniform stiffness throughout the structure. In structures containing "weak column-strong beam" designs, the most common solution is to strengthen the columns.

A number of different retrofitting techniques are used in practice to strengthen deficient reinforced concrete members. The most common forms of retrofitting reinforced concrete columns involves some form of steel or fibre reinforced plastic (FRP) jacketing or sleeving with reinforced concrete.

1.3.1 Reinforced Concrete Sleeving

The technique of reinforced concrete sleeving is one of the most popular methods of retrofitting building columns. The procedure involves the addition of a reinforced concrete layer around the existing concrete column. The new concrete may be cast in-situ, however, shotcrete reduces the cost of form-work and speeds up the retrofit process. The added confinement reinforcement typically consists of closely spaced perimeter hoops with added vertical bars. If it is desired not to increase the flexural capacity of the column, a gap of 50 mm is left at the top and bottom of the new concrete sleeve to avoid contact with the other frame members.

The main disadvantage of this type of retrofit is the time-consuming process, causing extended interruptions of the use of the structure while work is being carried out, and the fact that it involves enlargement of the columns, interfering with the architectural finishes of the structure.

1.3.2 Steel Jacketing

This form of retrofitting can be further subdivided into two categories: steel encasement and steel caging. Steel encasement is when the column is completely encased within steel plates or a steel shell, placed a small distance away from the surface of the column. The gap is then filled with non-shrink grout to ensure composite action between the steel jacket and the existing column. This method is most commonly used on circular columns. The process involves two-half circular steel shells placed around the column and then welded along the seams. Similarly, for rectangular columns, two half elliptical shaped shells are used, using a normal strength concrete to fill the gap between the shell and the existing column. However, using elliptical shaped columns is not always possible due to structural and architectural restraints. Another option is to use rectangular steel jackets to retrofit rectangular columns. However, this method while being fully effective in increasing the shear resistance of the column, provides additional confinement only at the corners of the retrofit column.

Steel caging is normally best suited for rectangular columns. This method usually consists of using vertical angle sections at the corners of the column with transverse batten plates welded to the angles. Alternatively, the steel corner angles may be omitted, using only thin steel strips wrapped around the column attached by an epoxy resin. This method is of particular interest when the increase in column dimensions are to be minimised, but its influence on confinement is questionable. There have been cases where a thin cover concrete or shotcrete has been provided over the steel retrofit to increase the fire protection.

It is worth noting that this method has been extensively used in emergency situations, to provide post-earthquake temporary support of the structure after failure of columns. This can be attributed to the speed of construction and simplicity of this type of retrofit technique. However, more commonly, this method is used on a permanent basis to enhance the confinement of the column and the strength and ductility of the column in shear and flexure.

The main advantages of a steel corner angle and batten plate retrofit method consist of the minimal increase in column dimensions, minimal skilled-labour required for construction and speed of construction. In addition, the cost of interruption of the normal use of the structure is minimised.

1.3.3. Composite Wraps

Recently, various strengthening techniques have been developed using various fibre reinforced plastics (FRP), made of high-strength fibres impregnated with an epoxy resin. These FRPs, which were originally used in the aerospace industry, have found use in strengthening concrete structures, due to their high corrosion resistance and large strength-to-weight ratio. Two approaches are used to strengthen damaged or deficient concrete columns. The first method uses full composite jackets placed around the column and secured to the column using an epoxy resin. In the second method, thin composite strips are wrapped in continuous spirals or in discontinuous straps around the column.

1.4 Previous Research on Column Retrofitting

This section briefly reviews some of the research which has been previously conducted on the performance of retrofitting techniques used to strengthen deficient moment-resisting frames. It focuses primarily on research that was conducted on the retrofit of columns using reinforced concrete sleeving, steel jacketing or FRP wraps.

1.4.1 Reinforced Concrete Sleeving

Jirsa (1981), conducted a series of experiments at the University of Texas at Austin, focusing on the various strengthening techniques for reinforced concrete members. The nearly full-scale specimens represented frames with "weak columns" and "strong beams" The columns were strengthened by adding new reinforced concrete. The author reported that the enlarged column caused the frame to fail in a ductile manner by forcing plastic hinging to occur in the beam. Jirsa also conducted another series of tests to investigate the effects of different repair techniques on the shear strength characteristics of the bond between new and existing concrete. The author concluded that roughening the surface of the concrete prior to adding the new concrete improved the shear strength at the interface, however the actual method in which the concrete surface was roughened seem to have little importance. The author also noted that the relative compressive strengths of the new and the existing concrete appeared to influence the characteristics of bond failure.

In 1986, a research program began at McGill University involving the testing of full-scale, exterior beam-column-slab subassemblages. Castele (1988) was involved in the investigation of strengthening a deficient moment-resisting frame having a "strong beam-weak column" condition, using a reinforced concrete sleeve to strengthen the column. The author concluded that this particular retrofit technique was effective in improving the strength and ductility of the specimen. The strengthened column and joint permitted the full flexural capacity of the beam to be achieved, resulting in the flexural hinging of the beam. The author also concluded that to properly strengthen a beam column joint, the added longitudinal column bars need to pass continuously through the joint and any lap splices should be made at mid-height of the column.

1.4.2 Steel Jacketing

Frangrou *et al* (1995) investigated at the University of Sheffield, the effectiveness and efficiency of strengthening reinforced concrete columns using post-tensioned metal strips. It was determined that the strapping technique was effective in strengthening the columns by increasing the confinement and shear resistance. The authors concluded that this method of retrofitting was very competitive due to the low material costs as well as the ease and speed of construction.

Masri and Goel (1996) constructed a one-third scale, two-bay, two-storey reinforced concrete slab-column frame to represent a seismically inadequate structure. The frame was strengthened to improve its behaviour under seismic loading. The columns in the frame were strengthened using vertical steel corner angles and batten plates. The authors determined that the performance of the vertical steel corner angles are greatly dependant on the strength and spacing of the batten plates which tie these important elements together.

Abdoutaha *et al* (1996) constructed and tested three large-scale columns with inadequate lap splices as well as four large-scale columns with inadequate shear strength. The authors determined that the use rectangular steel jackets connected to the original column with adhesive anchor bolts significantly improved the reversed cyclic loading responses of the columns by increasing their strength, ductility and energy dissipation.

Dritsos (1997) examined the effectiveness of using steel corner angles and pretensioned transverse steel ties on one-third scale columns. Experimental evidence shows that this method was successful in increasing the strength and the peak strain of the column concrete. The author concluded that if the longitudinal steel corner angles were adequately stiff, the spacing of the horizontal steel ties was less important. It was also concluded that this retrofit technique became less effective if low or no pretensioning were applied to the steel ties.

1.4.3 Composite Wraps

Some of the previous research conducted to determine the performance of wrapping a damaged or deficient column with FRP wrapping include: Hanna and Jones (1997), Hoppel *et al* (1997), Howie *et al* (1997), Mirmiran *et al* (1998), Tontanji and Balaguru (1998) and Ye *et al* (1998). It is noted that although this method of retrofitting damaged or deficient columns is very effective, FRP wraps have not been extensively used in practice due to their high cost.

1.5 Objectives of this Research Project

One of the main objectives of this study is to investigate the effectiveness of a column retrofit technique using vertical steel corner angles and transverse batten plates welded to the angles. This retrofit will be carried out on a nominally ductile moment-resisting frame which will be subjected to reversed cyclic loading. The results of this test specimen will be compared to the two specimens previously tested at McGill University by Castele (1988). Castele's first specimen contains a deficient column in the subassemblage, in order to determine the response of the subassemblage before retrofit. His second specimen was retrofit with a reinforced concrete sleeve around the column. All specimens were instrumented to determine behavioural aspects, such as:

(i) Load versus deflection responses,

(ii) moment versus curvature responses,

(iii) strain distribution in the slab reinforcement,

(iv) effective slab widths,

(v) curvatures and shear strains in the beams

(vi) tip deflection components, and

(vii) energy dissipation characteristics.

The behaviour of the full-scale subassemblage tested in this project will provide useful data on the performance of a steel corner angle and batten plate retrofit and will permit a comparison with the response of the subassemblage before retrofit and the response using a reinforced concrete sleeving retrofit.

In addition to testing a full-scale subassemblage retrofit with vertical steel corner angles and batten plates, a series of three full-scale columns will be constructed and tested under monotonically increasing axial compressive loading. The first column represents the deficient column before retrofit. The second column utilises a reinforced concrete sleeving technique to increase the strength of the column. The third specimen consists of retrofitting the deficient column using steel corner angles and batten plates to increase both the strength and ductility of the column. The three columns of this series will provide an indication of the effectiveness of these two different retrofit techniques.

CHAPTER 2

DESCRIPTION OF TEST SPECIMENS

2.1 Column Retrofit Specimens

Three full-scale column specimens were constructed and tested to investigate different methods of retrofitting existing columns with deficient details. The first column Specimen, C1 was constructed with a large tie spacing resulting in inadequate confinement and poor control of buckling of the vertical bars. The other two specimens in this series, RC1 and RC2 represent the deficient column C1, which has been retrofit using either reinforced concrete sleeving or steel batten plates welded to the corner angles. All columns had an overall height of 1500 mm and the cross section of column Specimen C1 was 325 by 325 mm.

2.1.1 Reinforcement Details for Specimen C1

Column Specimen C1 contained 8 - No. 15 longitudinal reinforcing bars welded to 12 mm thick end plates. The transverse reinforcement was provided by 6 - No. 10 ties with 90° bend anchorages, having straight bar end extensions of $6d_b$. The resulting centre-to-centre spacing of 240 mm satisfied the requirements of Clause 7.6.5.2 of the CSA A23.3 Standard for the Design of Concrete Structures (CSA 1994). The reinforcement details are given in Fig. 2.1. These "non-seismic" details do not meet the "Special Provisions for Seismic Design" given in Clause 21 of the CSA Standard for either ductile columns or columns with nominal ductility. For example, in regions where plastic hinges are expected to develop, columns with nominal ductility must be confined with hoops anchored with seismic hooks, with a maximum spacing not exceeding the least of:

(i) 8 longitudinal bar diameters;

(ii) 24 tie diameters;

(iii) one half the least dimension of the column; and

(iv) 300 mm.

Therefore in order to satisfy the requirements for a nominally ductile column (Clause 21.9) the ties would have to be hoops and would have a maximum spacing of 120 mm.

Three column specimens with the same reinforcement and details were cast at the same time with the same batch of concrete in order to provide column Specimen C1 and two essentially identical specimens for retrofit (RC1 and RC2).

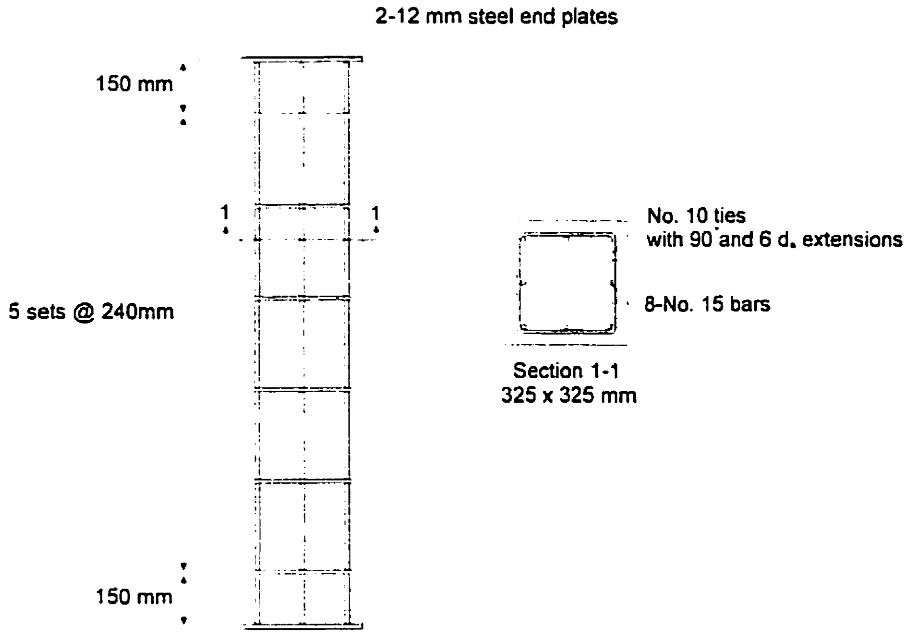

Figure 2.1: Reinforcement Details for Specimen C1

2.1.2 Reinforcement Details for Specimen RC1

Column Specimen RC1 represents the retrofit of column C1 using a reinforced concrete sleeve to strengthen the column and to improve the confinement. As shown in Fig. 2.2, a reinforced concrete layer of 87.5 mm was added to the original C1 column, giving overall cross-sectional dimensions of 500 by 500 mm. The first step in the retrofit technique was to roughen the surface of the original column to improve the bond between the existing and the retrofit concrete. In the retrofit, 4 - No. 25 longitudinal bars were added at the corners. Added transverse reinforcement was provided by 9 - No.10 hoops with 135° bend anchorages, having straight bar extensions of $6d_b$. These hoops had a spacing of 200 mm, which satisfy the requirements of Clause 21.9. All of the longitudinal bars were welded to 12 mm thick end plates. The reinforcement details are shown in Fig. 2.2.

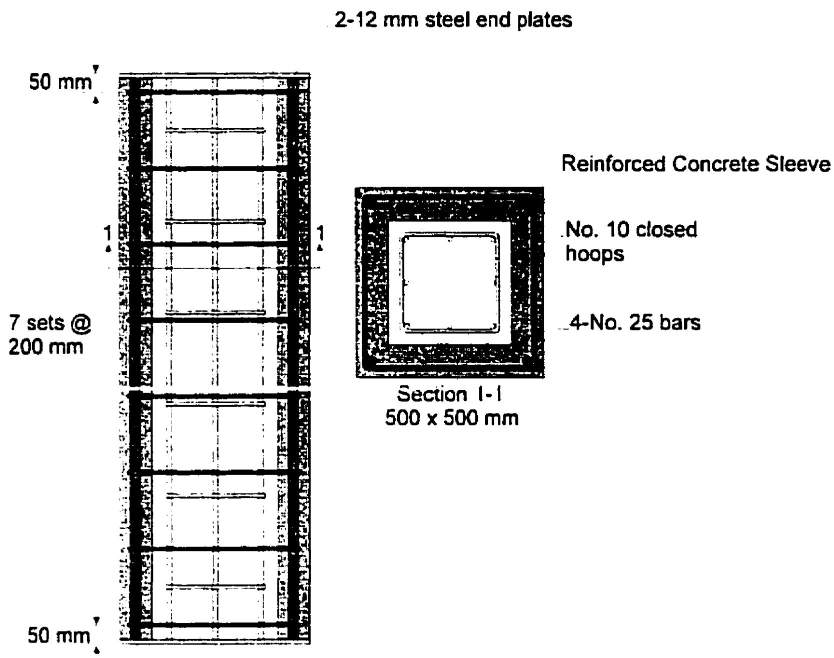

Figure 2.2: Reinforcement Details for Specimen RC1

2.1.3 Reinforcement Details for Specimen RC2

Column Specimen RC2 represents the retrofit of column C1 using external reinforcement consisting of vertical steel corner angles with batten plates welded to the steel angles (see Fig. 2.3). The first step was to grind down the corners of the original column to enable proper contact of the steel angles against the concrete. Four 51 mm x 51 mm x 6 mm thick steel angles were added to the corners of the column and were welded to the 12 mm thick end plates. Steel batten plates (100 mm wide by 6 mm thick), providing a centre-to-centre spacing of 300 mm, were welded to the outside face of the corner angles. The spacing of these batten plates was chosen to provide a clear spacing between the plates of 200 mm All fillet welds were designed to resist the shears corresponding to the development of yield in the batten plates. The externally applied steel retrofit was not attached to the concrete except for the welding of the corner angles to the end plates. The reinforcement details can be seen in Fig. 2.3.

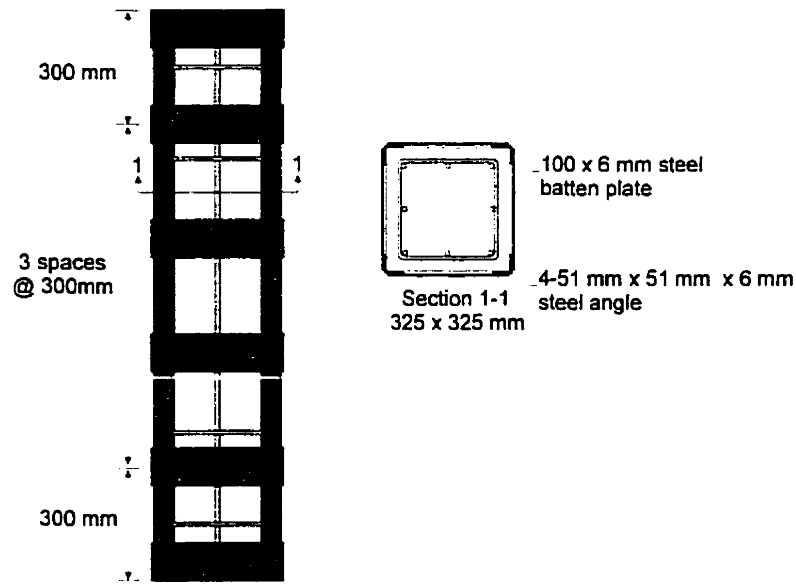

Figure 2.3: Reinforcement Details for Specimen RC2

2.2 Description of Prototype Structure for Beam-Column-Slab Subassemblage Specimens

The prototype structure for the study of the retrofit of beam-column-slab subassemblages is a six-storey reinforced concrete office building situated in Montreal, designed in accordance to the National Building Code of Canada (NBCC). The original structure was designed by Paultre (1987) to evaluate the seismic response and performance of reinforced concrete beam-column-slab subassemblages. Additional experimental investigations on similar beam-column-slab subassemblages were carried out by Rattray (1987) and Castele (1988). This research project will compare the results of two of the specimens tested by Castele (1988) with the full scale subassemblage tested in this research project.

2.2.1 Building Description

The six-storey rectangular office building has overall dimensions of 42 m by 24 m, containing seven equal six metre bays in the N-S direction and two nine metre bays separated by a six metre corridor in the E-W direction. The ground floor height is 4.85 m with each additional storey having a height of 3.65 m, resulting in a total height of 23.1 m, as shown in Fig. 2.4. The original structure designed by Paultre (1987) used 500 x 500 mm interior columns and

450 x 450 mm exterior columns. The main beams between the columns were 400 mm wide and 600 mm deep for the first three storeys. In all remaining storeys the main beams were reduced in depth to 550 mm. The 110 mm thick slab was supported by secondary beams, 300 mm wide by 350 mm deep, spanning between the main beams in the N-S direction.

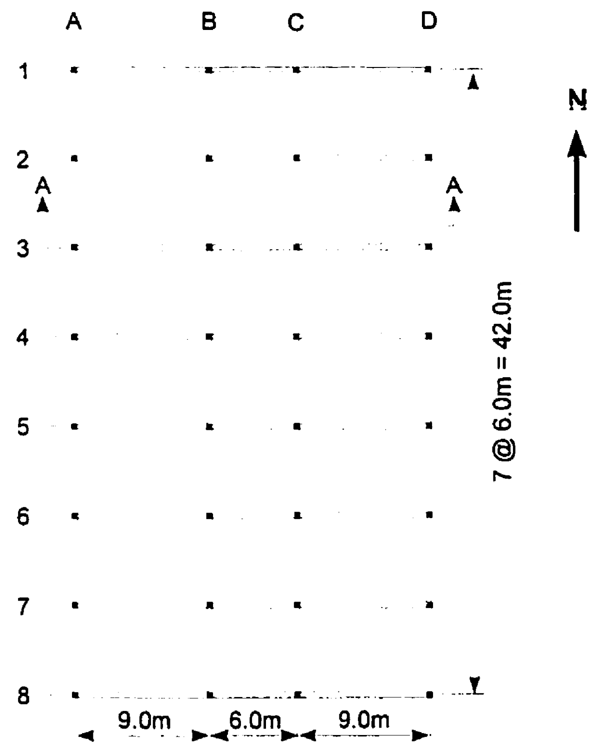

(a) Plan View

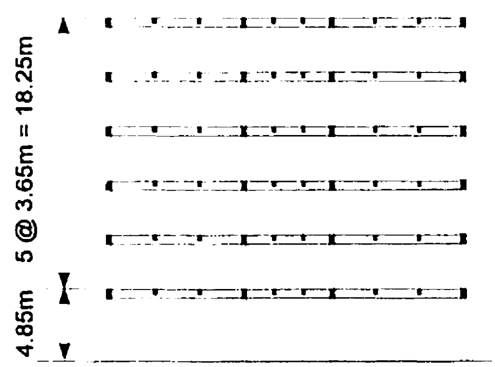

(b) Section A-A

Figure 2.4: Plan and elevation view of prototype structure

2.2.2 Loading and Analysis Assumptions

The original loadings, determined by Paultre (1987), were in accordance with the 1985 NBCC. The original design used a K-factor to account for ductility. For nominally ductile moment resisting frames, the 1985 NBCC used a K-factor equal to 1.3 for determining the base shear, while the 1995 NBCC uses a force modification factor, R, of 2.0. However, the resulting design forces from the base shear equation remain practically the same using these two different codes. The load parameters used to design this structure, using the provisions of the 1995 NBCC are as follows:

Floor live load:	2.4	kN/m^2 on typical office floors
	4.8	kN/m^2 on 6 m wide corridor bay
Roof load:	2.2	kN/m^2 full snow load
	1.6	kN/m^2 mechanical services loading in 6 m wide strip over corridor bay
Dead loads:	24	kN/m^3 self weight of concrete members
	1.0	kN/m^2 partition loading on all floors
	0.5	kN/m^2 mechanical service loading on all floors
	0.5	kN/m^2 roof insulation
Wind loading	1.24	kN/m^2 net lateral pressure for top four floors
	1.18	kN/m^2 net lateral pressure for bottom two floors

Seismic loading:

Z_a = acceleration-related seismic zone = 4
Z_v = velocity-related seismic zone = 2
v = zonal velocity ratio = 0.1
T = fundamental period = 0.1N = 0.6 s.
S = seismic response factor = $1.5/\sqrt{T}$ = 1.94
I = importance factor, taken as 1.0 for an office building
F = foundation factor, taken as 1.0
U = calibration factor specified as 0.6
W = dead load plus 25% of design snow load

Hence for this structure, the minimum lateral seismic force, V, at the base of the structure is:

$$V = \frac{vSIFW}{R}U = \frac{0.1 \times 1.94 \times 1.0 \times 1.0W}{2.0}0.6 = 0.0582W \qquad (2-1)$$

Details for the design of this six storey frame structure are given by Mitchell *et al.* (1995), for the case of a ductile moment resisting frame (R = 4). In order to simplify the analysis, the floor slab was assumed to act as a rigid diaphragm. This then allowed the system to be reduced to a series of two-dimensional frames. It was determined that frame 2 was the most critical frame for design since it has a significant torsional eccentricity effect, together with significant gravity loads effects. To account for the reduction in stiffness after cracking it was assumed that the columns and beams have stiffness values equal to 50% and 20% of their gross stiffness values, respectively.

2.3 Beam-Column-Slab Subassemblage Specimens

The analysis of the prototype structure determined that the critical beam-column-slab subassemblage was the exterior joint connection located on the second storey as seen in Fig. 2.5. All specimens described in this study are comprised of four main components: exterior column, main beam, spandrel beam and floor slab.

The test specimens were full-scale beam-column-slab subassemblages The column height of 3000 mm was chosen such that the ends represented the points of contraflexure in the prototype columns. All beams had a 600 mm overall depth, including a 110 mm thick slab. Since the beams were placed at the centre of the 3000 mm column, the columns projected 1200 mm above and below the 600 mm deep joint region. The width of the slab was chosen to be 1900 mm due to the limitations of specimen width in the universal testing machine. A beam length of 2200 mm, measured from the centre of the column was chosen, giving a lever arm of 2000 mm from the centre of the column. The overall dimensions are shown in Fig. 2.6.

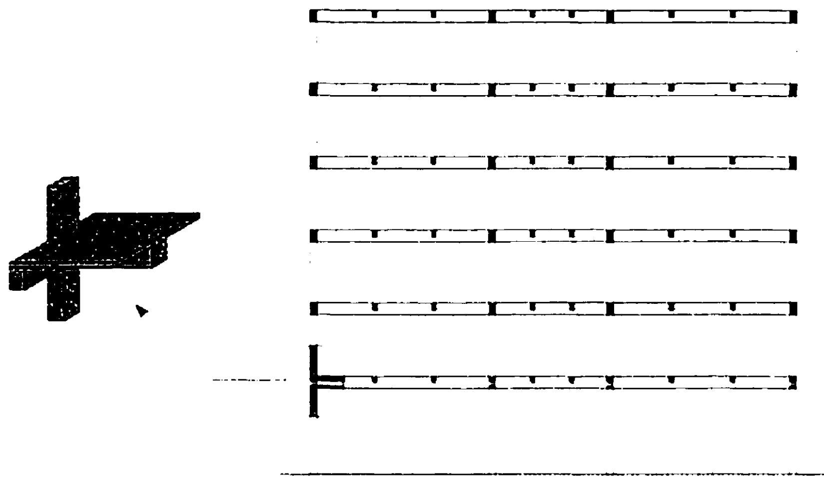

Figure 2.5: Location of full scale specimen

The first specimen of the series, S1 constructed and tested by Castele (1988), was designed for normal strength concrete and detailed according to the NBCC with a force modification factor ,R = 2.0. The purpose of this specimen was to investigate the behaviour of a "weak column" and "strong beam" situation under reversed cyclic loading. This was achieved by reducing the column size of Specimen R2, tested by Rattray (1987), from 450 by 450 mm to 400 by 400 mm. Specimens RS1 (Castele, 1988) and RS2 (reported in this thesis), represent different retrofit techniques applied to the same deficient subassemblage Specimen S1. Specimen RS1 was strengthened using a normal-strength reinforced concrete sleeve retrofit increasing the overall dimensions of the column to 600 by 700 mm. Whereas Specimen RS2, used a steel corner angle and batten plate column retrofit rendering the overall dimensions of the column relatively unchanged.

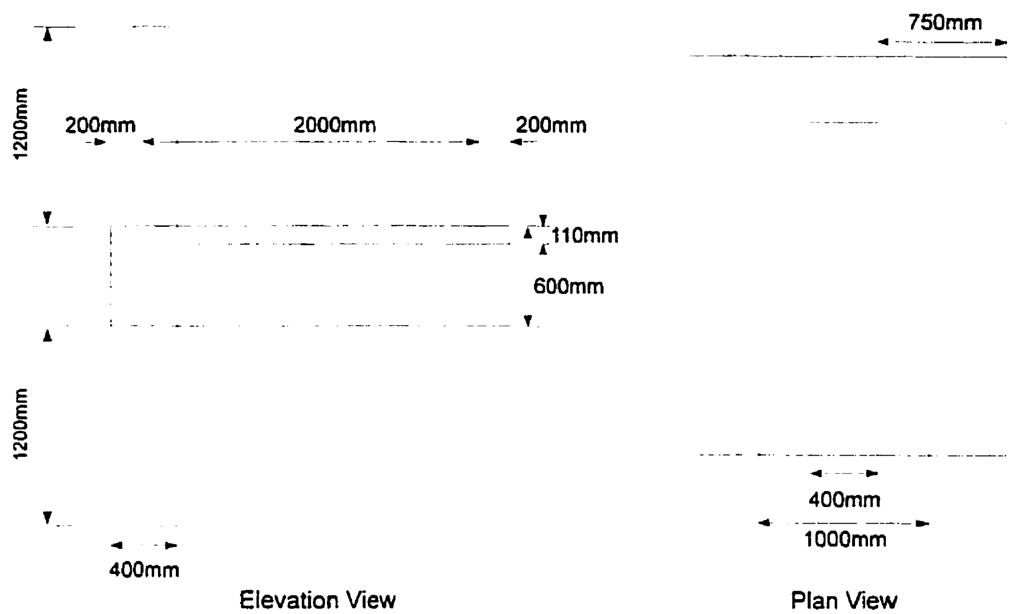

Figure 2.6: Dimensions of Specimens S1 and Specimens RS1 and RS2 Before Retrofit

2.3.1 Reinforcement Details for Specimen S1

Specimen S1 represents a "weak column-strong beam" subassemblage designed and detailed as a nominally ductile frame subassemblage, for a force modification factor, R of 2.0. The reinforcement details for Specimen S1 are given in Fig. 2.7. The 400 by 400 mm column contains 8 - No. 15 vertical bars and No. 10 column ties with 90° bend anchorages having straight bar extensions of $6d_b$. Since the column above and below the joint will yield before the beam will yield in flexure, the CSA requirements indicate that a maximum tie spacing of 125 mm is required over a distance of 500 mm above and below the joint. Outside of these regions, tie spacing can be increased to 170 mm (d/2). It must be noted that the 1994 CSA Standard requires that all column ties in nominally ductile frames be detailed as hoops. Since 90° bend anchorages were used for the ties, this transverse reinforcement does not meet the requirement for hoops, anchored with 135° bends.

A minimum concrete cover of 20 mm was provided for the slab bars while 40 mm was provided for beam and column reinforcement. The reinforcement details are shown in Fig. 2.7 and Fig. 2.8.

Negative moment resistance in the main beam consisted of 8 - No. 15 bars placed in two rows of four bars. To satisfy Clause 21.9.2.1.1 requires the positive moment resistance of the beam at the joint face be at least 1/3 of the negative moment resistance. Therefore 4 No. 15 bars were placed at the bottom of the section, resulting in an effective depth, d of 542.5 mm. The shear reinforcement was provided by No. 10 U-stirrups with 180° bend anchorages spaced at 260 mm (d/2). However, in order to satisfy the requirements for "nominal ductility" (Clause 21.9.2.1.2), the stirrup spacing was reduced to 130 mm (d/4) over a distance of 2d from the joint face.

The slab reinforcement was provided by two mats of No. 10 bars spaced at 300 mm in both directions. The longitudinal slab bars where anchored into the core of the spandrel beam with 90° bend anchorages and straight bar end extensions of $12d_b$. Additional slab reinforcement was provided around the loading points to ensure no local failures would occur.

The spandrel beam longitudinal reinforcement consisted of 8 - No. 15 bars , with 4 top bars and 4 bottom bars. The shear and torsion reinforcement in this spandrel beam was provided by No. 10 closed hoops with 135° bend anchorages with $6d_b$ end extensions spaced at 125 mm (d/4).

For this exterior joint, a minimum amount of joint reinforcement was provided to satisfy Clause 7.7.3, resulting in 2 - No. 10 ties with 90° bend anchorages and $6d_b$ straight bar end extensions.

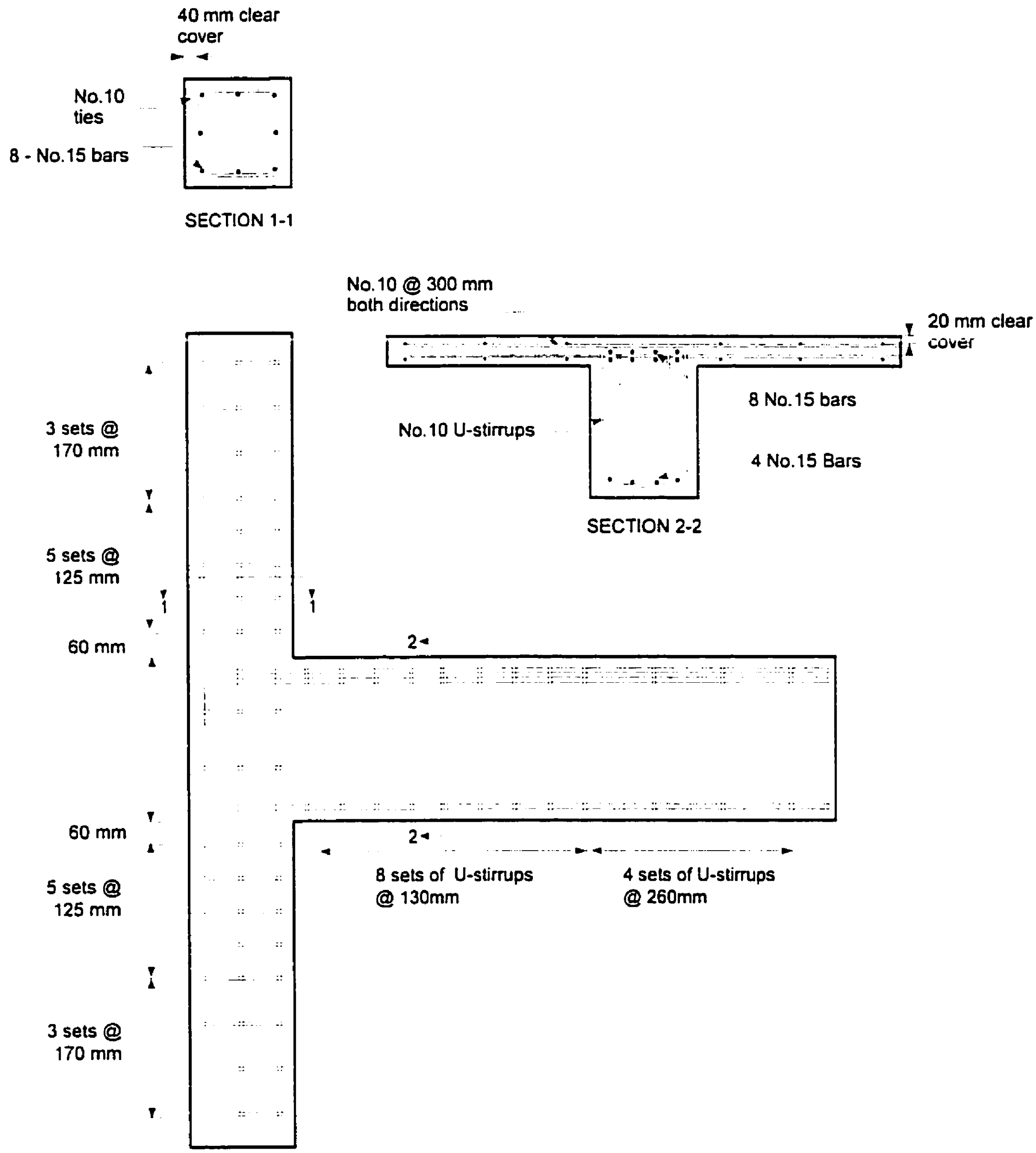

Figure 2.7: Reinforcement details for Specimen S1

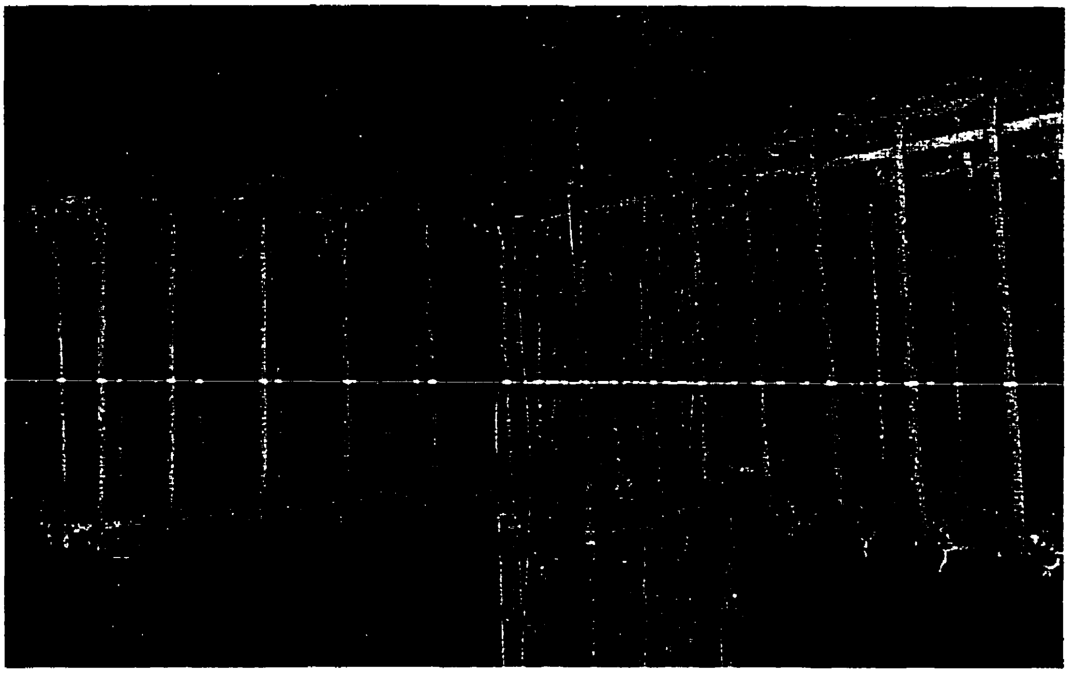

Fig. 2.8: Reinforcing cage for Specimen SI

2.3.2 Reinforcement Details for Specimen RS1

The goal of constructing and testing retrofit Specimen RS1 (Castele, 1988) was to strengthen the column of Specimen S1 to improve its behaviour under reversed cyclic loading. The column strengthening changed hierarchy of yielding among the frame members, resulting in a desirable "weak beam-strong column" response.

The strengthening of the column was achieved by adding reinforcement and increasing its size to 600 by 700 mm. As is often the case, due to the presence of exterior finishes, exterior column dimensions cannot be drastically altered and therefore changes to the column dimensions may be somewhat limited. In order to limit the interference near the exterior face, the resulting retrofit column was rectangular in shape as shown in Fig. 2.9. The increase in column dimension must also accommodate room to place the reinforcement and provide sufficient space for the 135° bend anchorages of the added hoops (Fig. 2.9, 2.10).

The strengthening of this specimen consisted of first roughening the concrete surface over the full height of the column. This technique was used to ensure proper bond between the new and existing concrete. Four No. 30 vertical bars were added around the existing column along with the new transverse reinforcement. Holes were drilled through the floor slab to allow continuity of the longitudinal reinforcement through the joint region. In an actual structure these bars would be lap spliced at the mid-height of the column. The transverse reinforcement consisted of No. 10 ties with 135° bend anchorages and $10d_b$ straight bar end extensions. This end extension was chosen to ensure good anchorage of the of the added hoops in the concrete. These hoops were spaced at 200 mm over the 700 mm height above and below the joint region, with the first tie being placed 100 mm from the face of the joint. Outside of this region, the hoop spacing was increased to 270 mm. No additional ties could be placed directly through the joint due to the presence of the spandrel beams and the main beam framing into the joint. In order to keep this retrofit as simple as possible, the option of drilling dowels into the joint core was dismissed. With the aid of a two dimensional non linear finite element program, FIELDS (Cook and Mitchell, 1988) the flow of compressive stresses through the joint region was determined. The results of the analysis demonstrated that hoops placed immediately above and below the joint would help resist shear in the joint. Therefore double hoops were provided immediately above and below the joint (see Fig. 2.9).

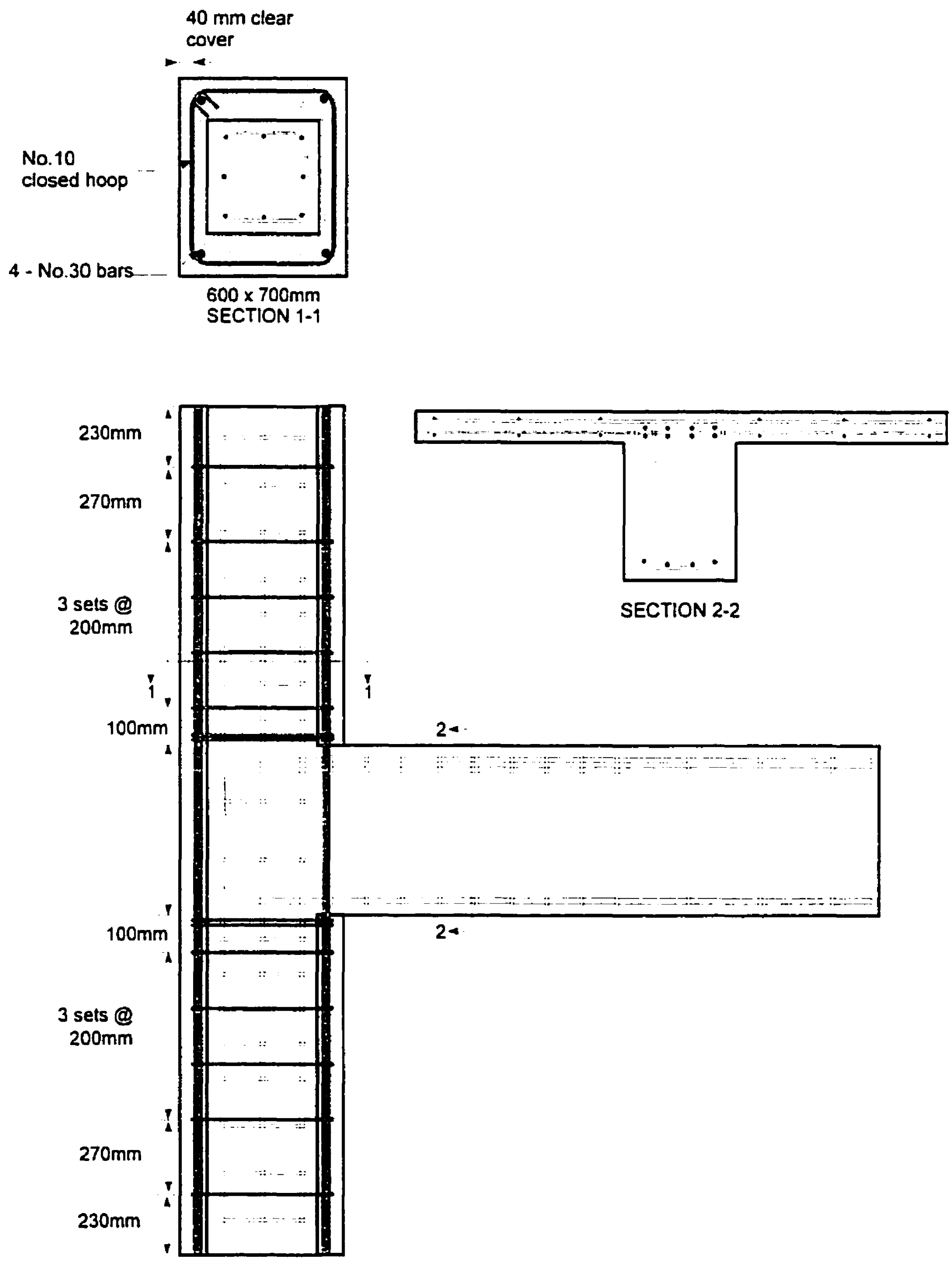

Figure 2.9: Reinforcement details for Specimen RS1

a) Details of added hoops

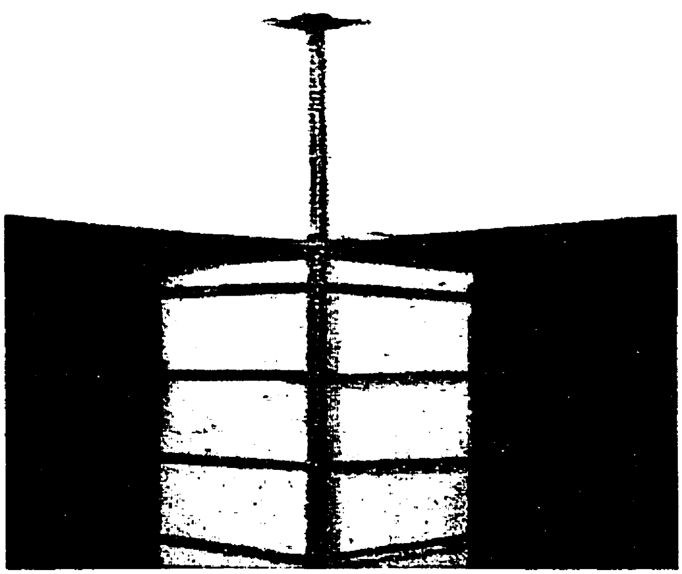

b) Close-up of joint region

Figure 2.10: Construction of Specimen RS1

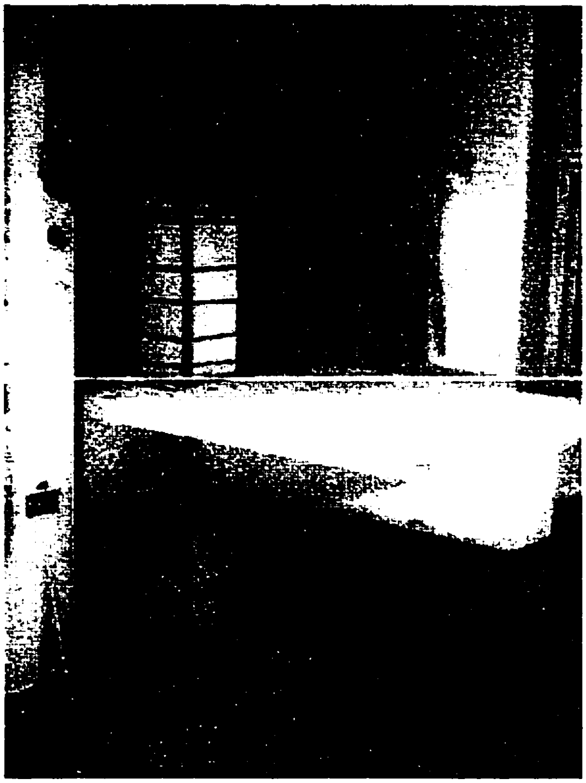

c) Overall view of added reinforcement

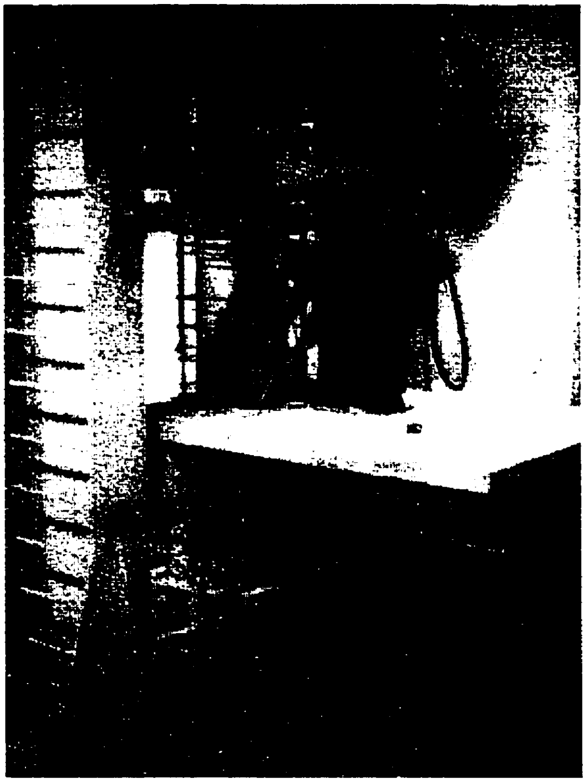

d) Vibrating concrete in lower column

Figure 2.10 ***(con't)*****: Construction of Specimen RS1**

2.3.4 Reinforcement Details for Specimen RS2

The goal of constructing and testing retrofit Specimen RS2 was to strengthen the column of Specimen S1 to improve its behaviour under reversed cyclic loading and to provide an alternative to retrofitting with reinforced concrete sleeving. The column strengthening changed the hierarchy of yielding among the frame members, resulting in a desirable "weak beam-strong column" response.

Specimen RS2 enhanced the strength and ductility of the original column by adding external steel corner angles and batten plates (see Fig. 2.11). This technique forces hinging to occur in the beam, allowing for greater rotations and thereby more energy dissipation while maintaining overall stability of the structure. The steel corner angle and welded batten plate retrofit can be applied without significant disruption to the building and its occupants and avoids major changes to the column dimensions. This retrofit technique would avoid or limit problems associated with increased column size, such as: disturbance to exterior finishes and loss of useable occupancy space.

The first step in the retrofit procedure was to grind down the corners of the column to permit seating of the steel corner angles. Four vertical 51 mm x 51 mm x 6 mm thick structural steel angles were placed at the corners of the original column. The corner angles greatly enhanced the flexural resistance of the column so that hinging would form in the beam.

Additional shear reinforcement and confinement was provided by welding 100 x 6 mm thick steel plates to the four corner angles, as shown in Fig. 2.11. The batten plates were bolted with Hilti HSL M12/25 anchor bolts to the exterior and interior column faces (see Fig. 2.11 and 2.13) to ensure adequate anchorage and connection of the steel retrofit to the concrete column. Holes were drilled into the concrete column core to a depth of 80 mm just inside the location of the existing vertical column bars. The location of the anchor bolts are shown in Fig. 2.11 and 2.13. The spacing of the batten plates was chosen such that a sufficient number of anchor bolts would be provided to produce the shear necessary to develop the nominal yield capacity of the corner angles. This resulted in a clear spacing of 200 mm between batten plates. The first batten plates were placed immediately above and below the joint. The fillet welds connecting the batten plates to the corner columns were designed to resist the shear forces required to develop the nominal resistance of the batten plates.

In order to avoid drilling large holes in the critical shear periphery to allow for the angles to be continuous through the joint, two different load transfer methods were used. On the interior face, 2 - 30 mm holes were drilled through the slab. Four 102 mm x 102 mm x 16 mm thick collar angles were welded to the corner angles immediately above and below the joint region on two sides of the column. Two 28 mm solid round bars were passed through the slab and welded to the collar angles. The construction of this load transfer mechanism is shown in Fig. 2.11 and 2.14. To ensure the adequacy of the stiffness of each collar angle 2 - 6 mm plate stiffeners were used as shown in Fig. 2.11. On the exterior face, 2 - 100 by 6 mm thick plates were butt welded to the vertical angles, to provide continuity to these angles through the joint region.

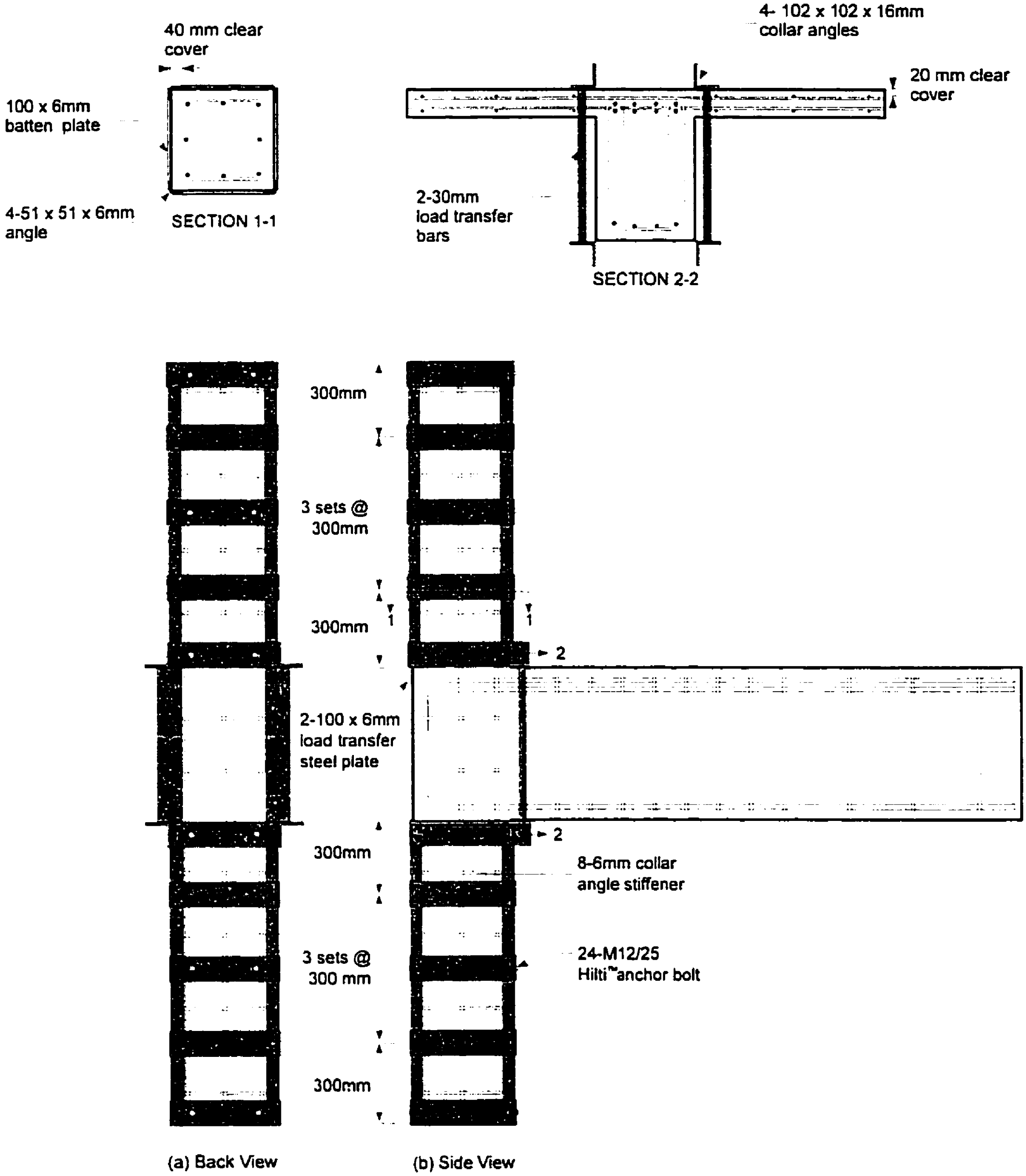

Figure 2.11: Reinforcement details for Specimen RS2

Figure 2.12: Batten Plate Retrofit Construction

Figure 2.13: Placement of Anchor Bolts for Specimen RS2

Figure 2.14: Construction of load transfer mechanism through joint region

CHAPTER 3

TEST SET-UP, INSTRUMENTATION AND MATERIAL PROPERTIES OF TEST SPECIMENS

3.1 Test Set-up

All specimens were tested in the Jamieson Structures Laboratory in the Department of Civil Engineering and Applied Mechanics at McGill University.

3.1.1 Column Retrofit Specimens

The three column retrofit specimens were tested using the 11400 kN capacity MTS universal testing machine. Each column was carefully aligned under the spherically seated compression head of the loading machine to ensure concentric loading.

3.1.2 Beam-Column-Slab Subassemblage Specimens

The test set-up for all three of the beam-column-slab subassemblage specimens was identical and is shown in Fig. 3.1 and Fig. 3.2.

The subassemblage specimens were constructed and tested under the Baldwin universal testing machine, having an axial compressive capacity of 1800 kN and braced to the strong floor in order to accommodate horizontal forces on the testing machine. The column of each specimen was pinned at its top and bottom to simulate points of contraflexure, as shown in Fig. 3.2. The 6 mm thick plate used to prevent horizontal movement at the top and bottom of the column, was thin enough to reduce moment restraint to a negligible level. A constant axial load of 1076 kN was applied by the universal testing machine through 75 mm diameter rollers at the top and bottom of the column. This load simulates 90% of the gravity load of the prototype structure at the second storey level.

The reversed cyclic loading was simulated using four hydraulic loading jacks. The jacks were located at a distance of 2000 mm from the centre of the column. Two jacks were used simultaneously in each direction. The two jacks located under the reaction floor used two 32 mm diameter high-strength threaded rods to apply the load in the positive direction. The negative loading was applied using a 50 mm diameter roller reacting against a steel plate under the main beam.

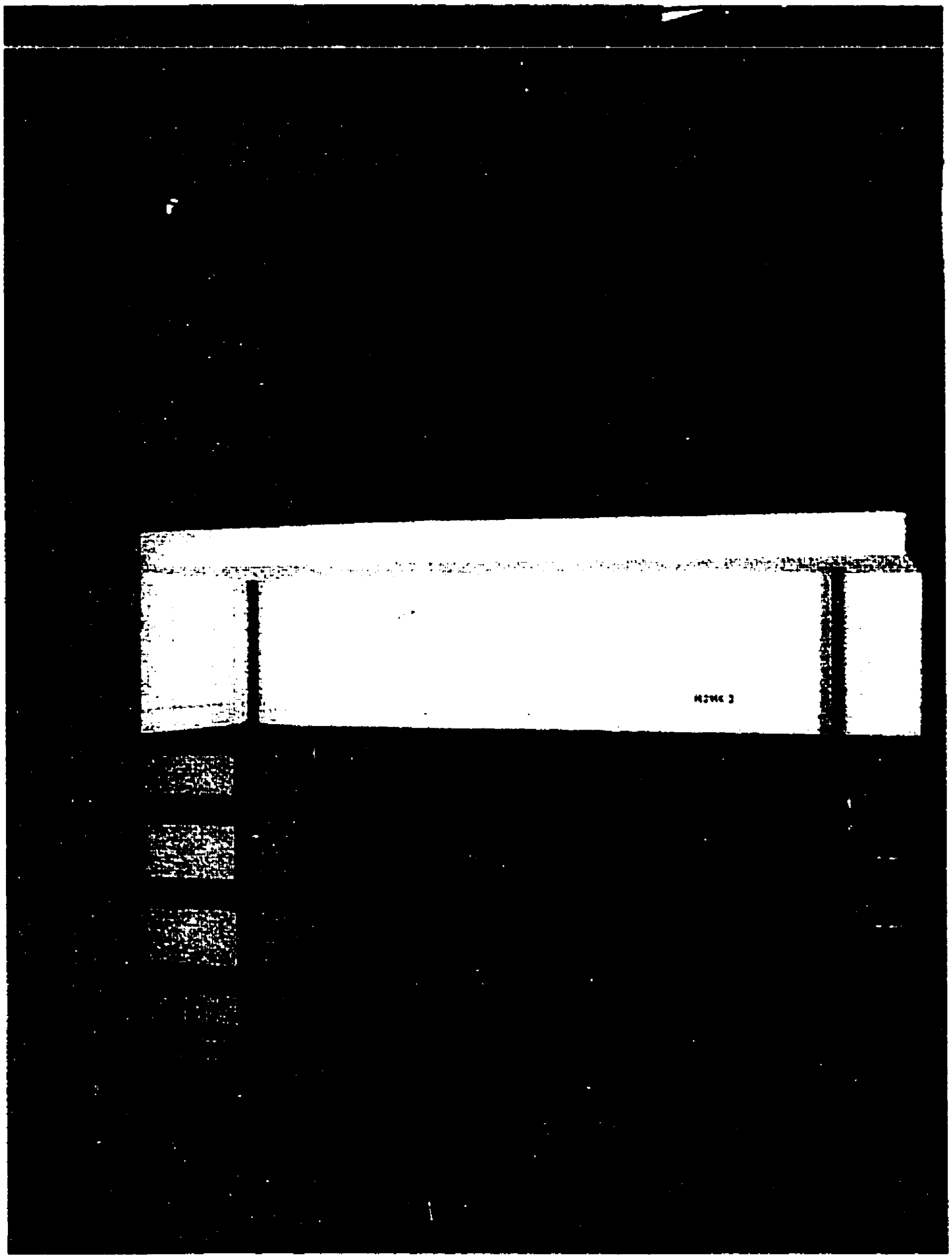

Fig. 3.1: Test set-up

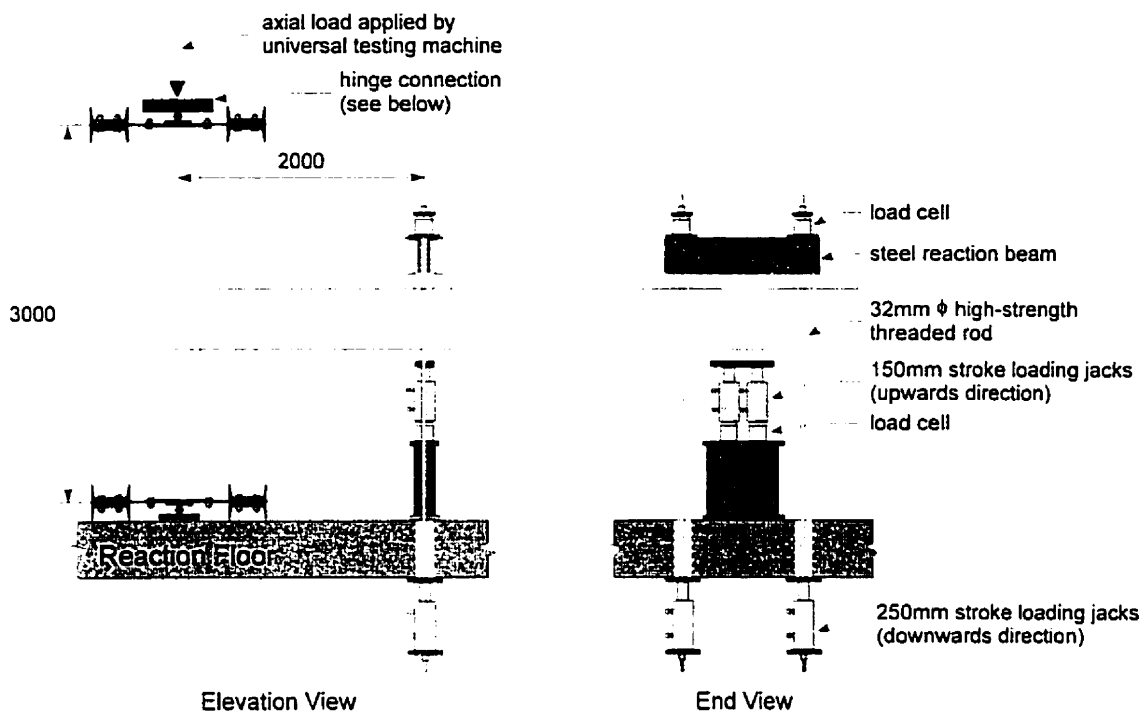

(a) Details of Loading Mechanism.

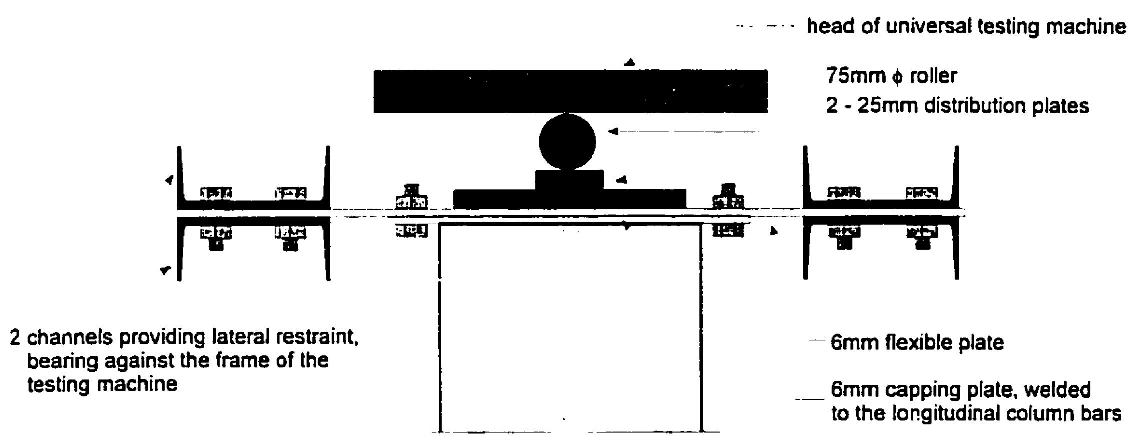

(b) Details of Hinge Connection.

Figure 3.2: Details of subassemblage test set-up

3.2 Instrumentation for Column Retrofit Specimens

The behaviour of each specimen was monitored continually during each test by electronic instrumentation. All electronic readings were taken at small intervals throughout the test by means of a computerised data acquisition system. The linear voltage differential transducers (LVDTs) were used to measure external deflections, while electrical strain gauges were glued to the reinforcing bars to measure strains in the steel. Load cells were used to measure the applied loads.

3.2.1 Load Measurements

The axial load applied to the column retrofit specimens was measured by the internal load cell connected to the universal testing machine.

3.2.2 Deflection Measurements

A total of eleven LVDTs were used on each specimen. Four LVDTs were placed vertically at the corners of the column by means of an aluminium frame connected to the top end of each specimen with the bottom of these full-height LVDTs being attached to the bearing plate at the bottom of each specimen. These LVDTs were used to measure the full-height shortening of each specimen at the four corners. Five other LVDTs were placed vertically on the back face of the column to measure deflections over shorter segments of the height of the column. Furthermore, two more LVDTs were placed horizontally at the mid-height of the column on adjacent faces to measure horizontal expansion during the loading of the specimen. The placement of these LVDTs can be seen in Fig. 3.3.

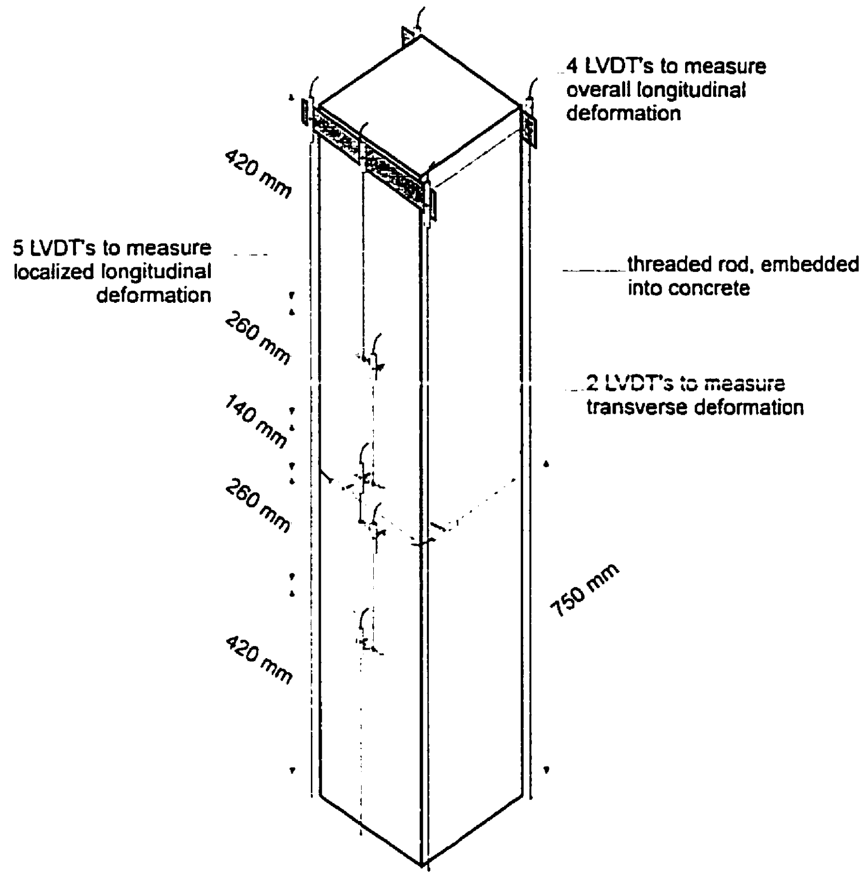

Figure 3.3: Location of LVDT's

3.3.3 Strain Measurements

Strains were measured by the use of electrical resistance strain gauges. The electrical resistance strain gauges were glued to reinforcing steel and monitored local strains in the steel. The placement of the gauges correspond to critical locations throughout the specimen. The location of electrical resistance strain gauges on Specimens C1, RC1 and RC2 are shown in Fig. 3.4. All electrical resistance strain gauges had a gauge length of 5.0 mm except strain gauges used on the No. 10 hoops where the gauge length was 2.0 mm.

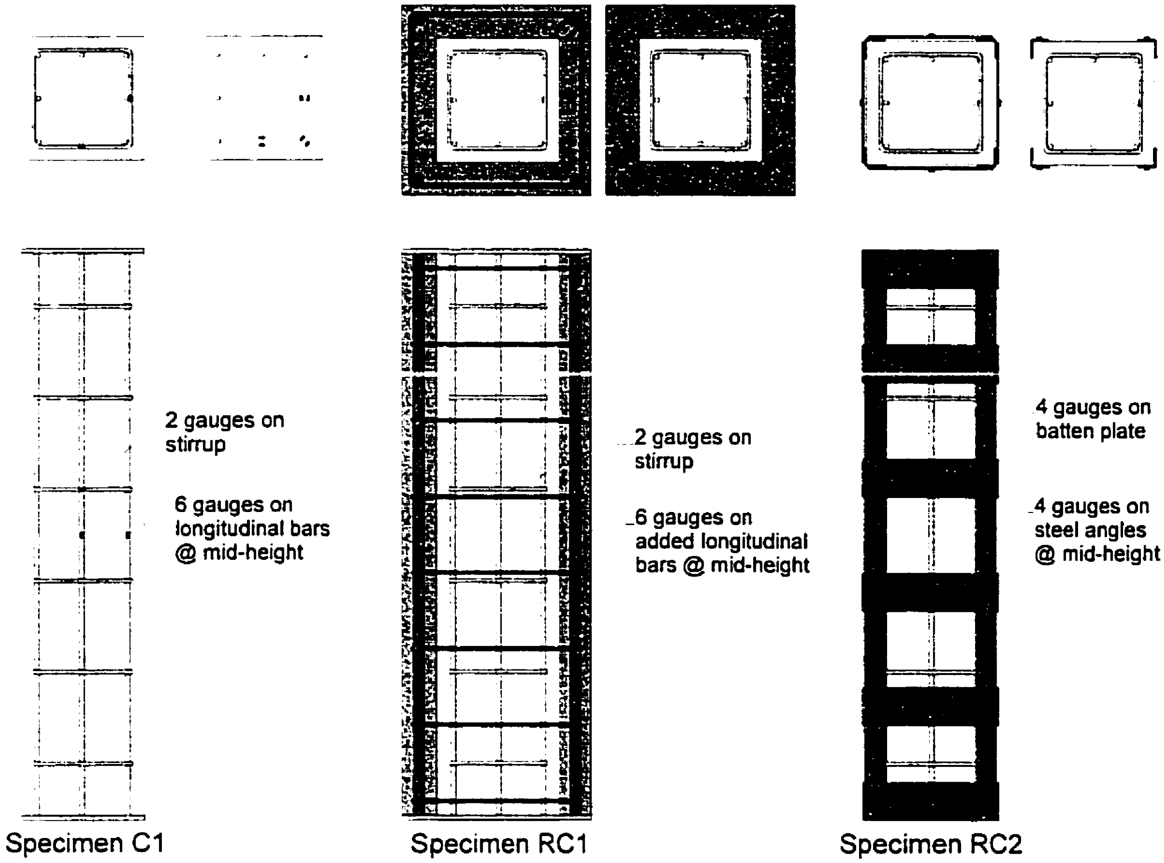

Figure 3.4: Location of electrical resistance strain gauges

3.3 Instrumentation for Beam-Column-Slab Subassemblage Specimens

The behaviour of each specimen was monitored continually during the test by both electronic and mechanical instrumentation. All electronic readings were taken at small intervals throughout the test by means of a computerised data acquisition system. The mechanical readings were manually taken at the peak of each loading cycle. The linear voltage differential transducers (LVDTs) were used to measure external deflections, while electrical strain gauges were placed on the reinforcing steel to measure strains in the steel. Load cells were used in conjunction with the hydraulic jacks to measure the applied loads. The mechanical instrumentation consisted of small targets glued to the concrete surface to measure concrete strains.

3.3.1 Load Measurements

Four load cells, each having a capacity of 350 kN, were used to record the applied loads during the reversed cyclic loading. Two load cells were used in each loading direction of the main beam, as shown in Fig. 3.2. The axial load applied to the specimens was measured by the load cell of the Baldwin universal testing machine.

3.3.2 Deflection Measurements

Each subassemblage specimen was instrumented with sixteen LVDTs in order to determine important deflections and to enable strains to be determined over the gauge length of the LVDTs. The locations of the LVDTs are shown in Fig. 3.5. Two LVDTs, one for upwards deflections and one for downwards deflections, were mounted onto an aluminium frame to measure the vertical tip deflection of the main beam relative to the column at the point of load application.

The twist of the spandrel beam was determined by the measured horizontal deflections provided by two pairs of LVDTs attached to the back of the spandrel beam. In order to ensure readings after spalling of the concrete, threaded rods were glued into holes which were drilled into the concrete to provide attachment points for each end of each LVDT. Four additional LVDTs were located vertically on the back of the spandrel beam at hoop locations to enable average strains of the outside legs of these hoops to be determined. Two more LVDTs were attached to the concrete to the outside face of the column and were placed across the joint between the column and spandrel beam to measure the relative movement.

Two LVDTs, one vertical and one horizontal, were connected to the aluminium frame at the interface of the upper column and the slab to measure both horizontal and vertical movement at the joint interface. A similar set-up was used to determine the relative movement of the lower column with respect to the main beam.

3.3.3 Strain Measurements

Strains were measured by the use of both mechanical and electrical strain gauges. Mechanical targets were glued to the surface of the concrete at locations shown in Fig. 3.6. All targets were identical and placed to provide a gauge length of 200 mm. The readings were taken manually with the aid of an extensometer with a precision of measuring strain to the nearest 1×10^{-5}. Six sets of targets were placed on the top surface of the slab immediately above the longitudinal slab bars to determine strains in the bars and the effective slab width. A row of five sets of targets were placed on the slab surface immediately above the longitudinal reinforcement of the main beam to determine the extent of yielding along the beam. A matching row of targets was placed on the side of the beam at the level of the bottom longitudinal reinforcing bars in the beam. These two rows of targets will be used to determine the curvature of the main beam and furthermore provide an estimation of the contribution of the flexural deformation to the tip deflection of the main beam. Five sets of mechanical target rosettes were glued at mid-height along the length of the beam. These targets enabled the calculation of shear strain, principal strain and direction of principal strains. The shear strains are used to estimate the contribution of shear deformations to the total tip deflection of the main beam, while the transverse strains indicate the strains in the hoops.

The electrical resistance strain gauges were glued to reinforcing bars at critical locations throughout the specimen. The location of the electrical resistance strain gauges on Specimen RS2 are shown in Fig. 3.7. All electrical resistance strain gauges had a gauge length of 5.0 mm except the strain gauges used on the No. 10 hoops which had a gauge length of 2.0 mm. The maxumum specified strain associated with these electrical resistance gauges was 2%, (0.02 mm/mm).

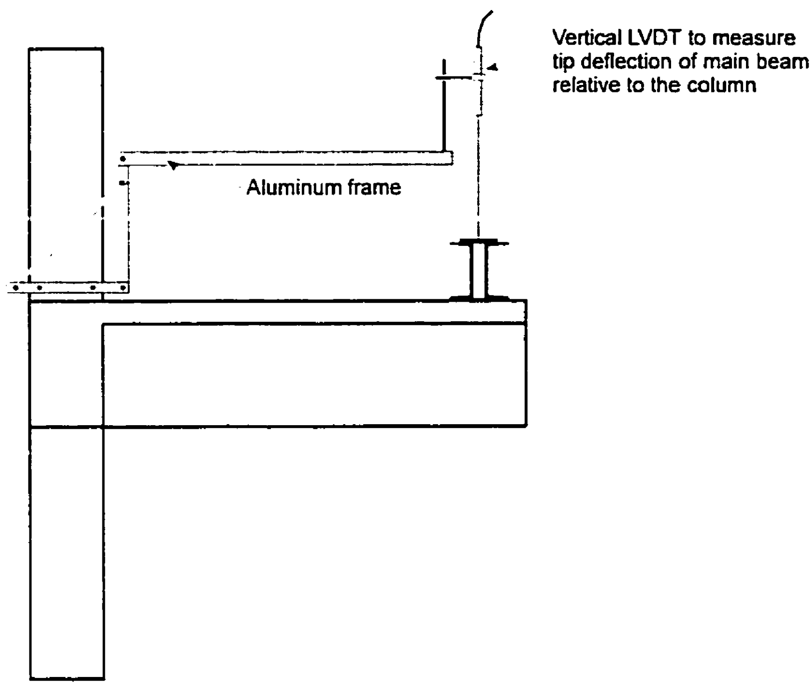

(a) Elevation View

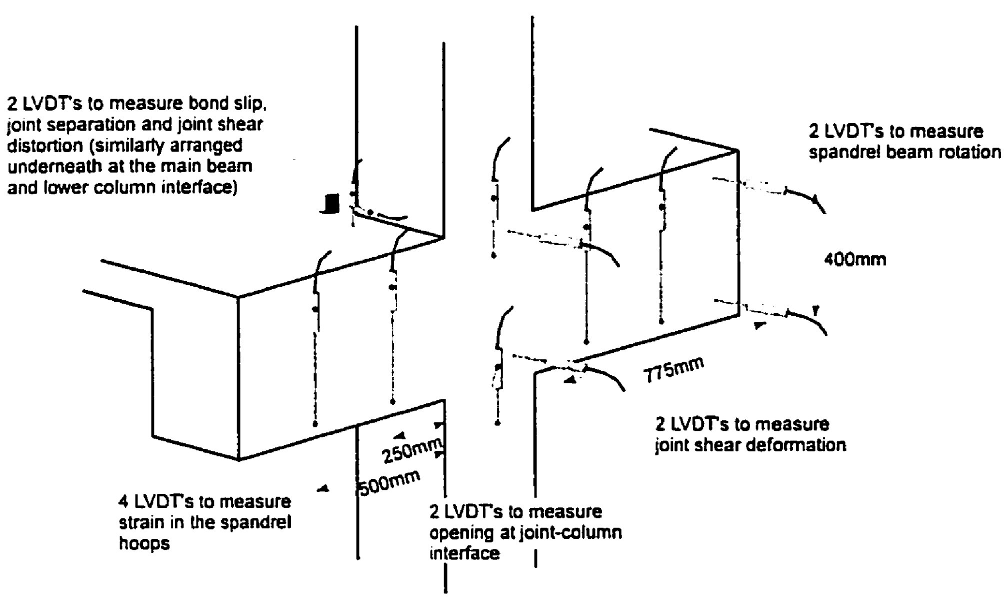

(b) View of Exterior of Spandrel Beam

Figure 3.5: Location of LVDT's

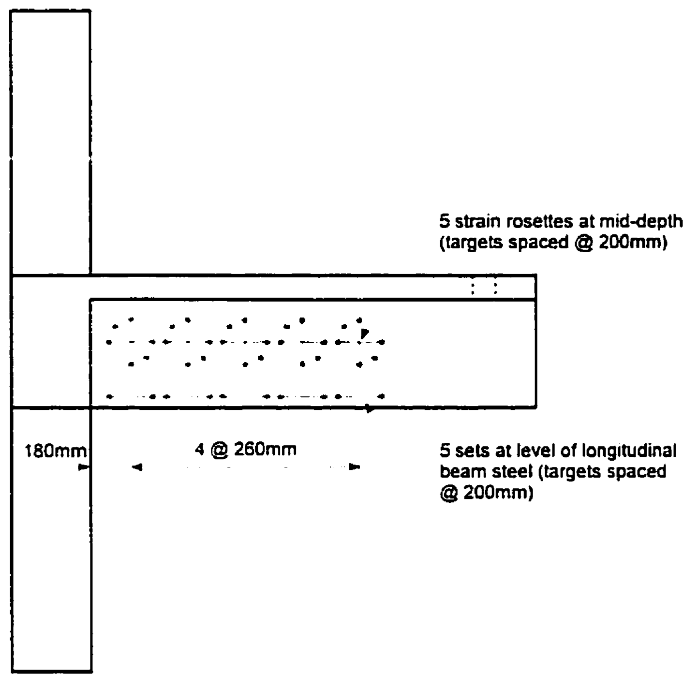

(a) Elevation View

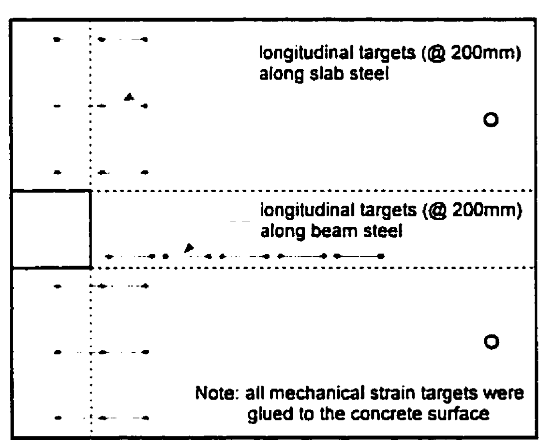

(b) Plan View

Figure 3.6: Location of mechanical strain targets

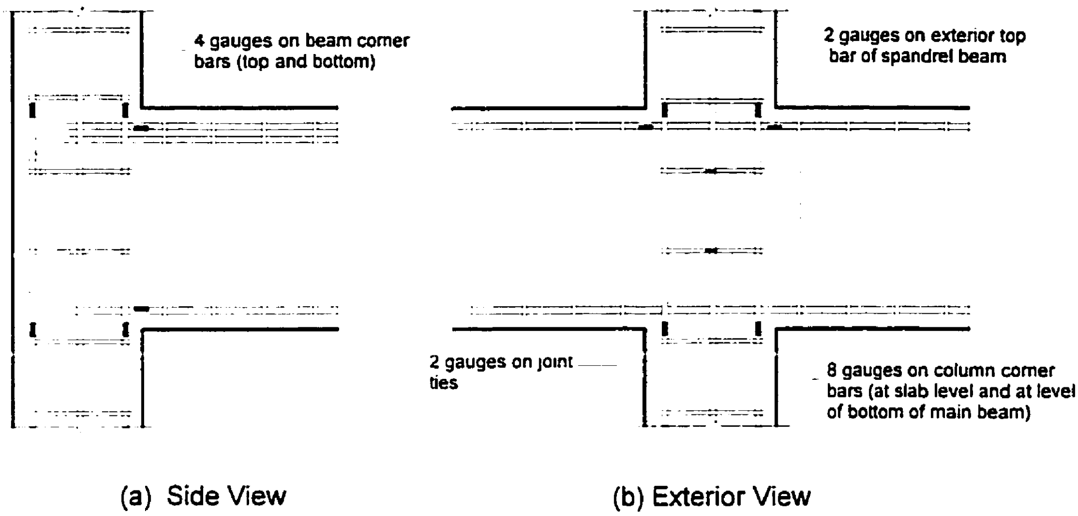

Figure 3.7: Locations of electrical resistance strain gauges

3.4 Testing Procedure

A general testing procedure was followed for all specimens, although slightly altered to specific characteristics inherent to each specimen.

3.4.1 Testing Procedure for Column Retrofit Specimens

The column retrofit specimens were tested under concentric axial load controlled by the 11400 kN MTS universal testing machine. A loading rate of 4 kN per second was used, up to 80% of the expected yield strength. When this point was reached, the loading rate was "displacement controlled" at a rate of 0.003 mm per second. This rate was used until failure was reached in the specimen.

Other information such as crack patterns and failure mechanisms were also observed throughout the duration of the test. Photographs were also taken of the specimens at regular intervals.

3.4.2 Testing Procedure for Beam-Column-Slab Subassemblages

The first stage of the testing began by the application of the axial compressive load of 1076 kN. Once applied, reversed cyclic loading was simulated by applying downwards and upwards loads to the end of the main beam. Each cycle consisted of one downwards or "positive" half cycle (peak labelled "A") and one upwards or "negative" half cycle (peak labelled "B").

The peak of the first cycle was the load necessary to reach a moment in the main beam corresponding to 1.2 times the calculated first cracking moment. The peak of the second cycle was determined by the first yielding of the longitudinal beam bars. The peak of the third cycle corresponded to general yielding of the beam. General yielding was considered to occur when a significant reduction in the loading stiffness was observed. The subsequent cycles were taken as multiples of the vertical tip deflection at general yielding. The complete idealised loading sequence is shown in Fig. 3.8.

Other information such as crack patterns, crack widths, as well as photographs were taken at the peaks of each cycle.

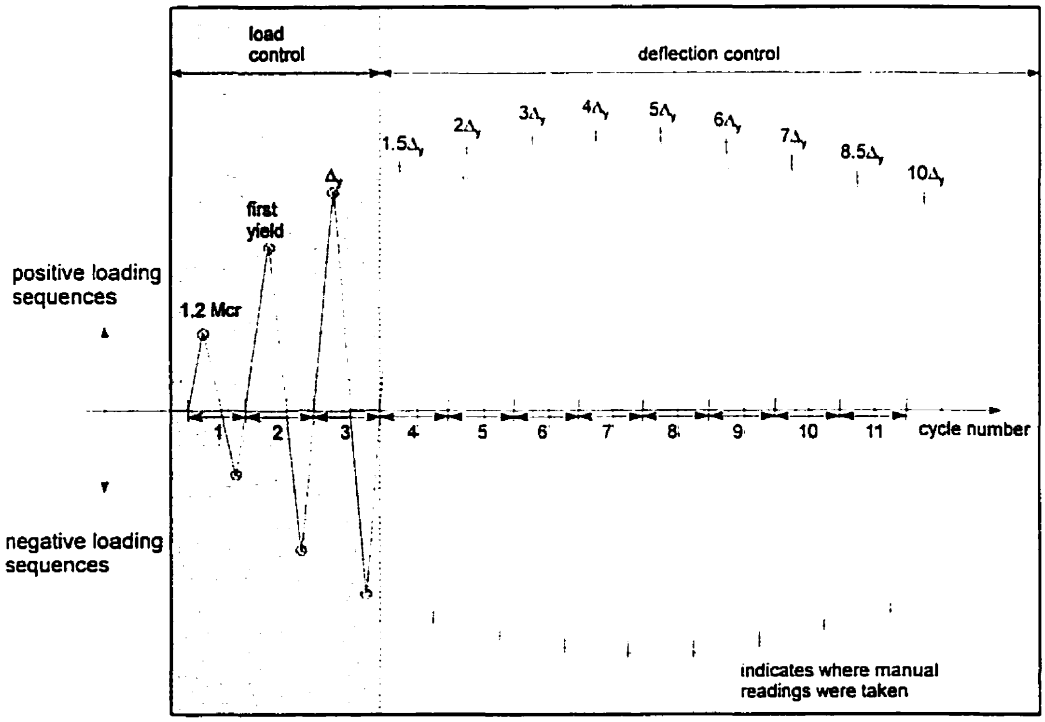

Figure 3.8: Loading sequence for specimens

3.5 Material Properties

3.5.1 Reinforcing Steel

The reinforcing steel used in all specimens was hot-rolled, non-weldable 400 Grade satisfying CSA standard G30.18-M (CSA 1992). However, Specimen RC1 used hot-rolled, weldable Grade 400 bars for the reinforcement in the concrete retrofit. The mechanical properties of the reinforcing steel are summarised in Table 3.1. The stress-strain curves for Specimens C1, RC1, RC2 and RS2 are shown in Fig. 3.9, while stress-strain curves for the RC1 strengthening are shown in Fig. 3.10. Three samples were tested for each bar size.

3.5.2 Structural Steel

The structural steel used in Specimens RC2 and RS2 was Grade 300 steel as specified by CSA-S16.1-94. The mechanical properties are summarised in Table 3.2. The stress-strain curves are shown in Fig. 3.11. Three coupons where tested for each steel shape used.

Table 3.1: Properties of Reinforcing Steel

Specimen	Bar Description	f_y (MPa)	ε_y (mm/mm)	f_{ult} (MPa)
C1 RC1, RC2 and RS2	No.10	434	0.0020	653
	std. deviation	9.5	0.0004	13.9
	No. 15	445	0.0023	588
	std. deviation	3.5	-	5.0
RC1 retrofit	No. 10	488	0.0028	597
	std. deviation	6.6	0.0003	2.7
	No. 25	433	0.0023	592
	std. deviation	1.9	0.00013	0.3
S1 and RS1	No. 10	441	-	667
	No. 15	494	-	794
RS1 retrofit	No. 10	458	-	695
	No. 30	433	-	671

Table 3.2: Properties of Structural Steel

Specimen	Steel Description	Area (mm^2)	f_y (MPa)	ε_y (mm/mm)	f_{ult} (MPa)
RC2 and RS2	51 x 51 x 6 mm angle std. deviation	605	342 4.51	0.00101 0.00025	499 2.08
	100 x 6 mm plate std. deviation	600	359 11.1	0.00111 0.00018	510 13.75
	28 mm solid round bar std.deviation	616	387 2.08	0.00191 0.00002	519 1.0

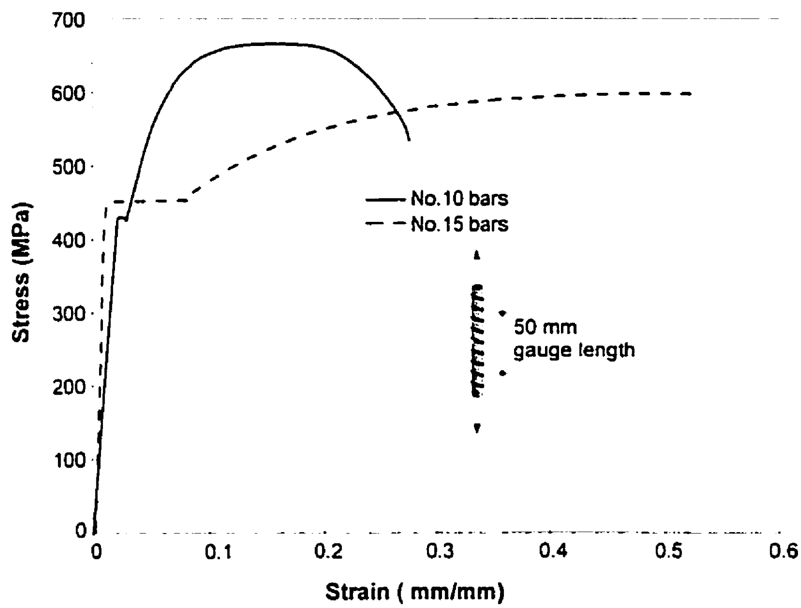

Figure 3.9: Stress - strain responses for reinforcing bars for Specimens C1, RC1, RC2 and RS2

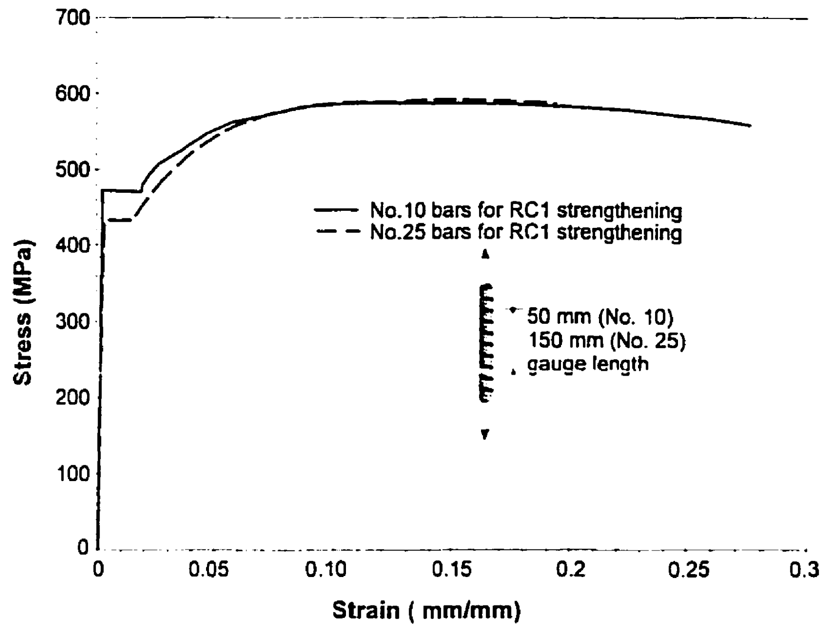

Figure 3.10: Stress - strain responses for reinforcing bars for RC1 retrofit

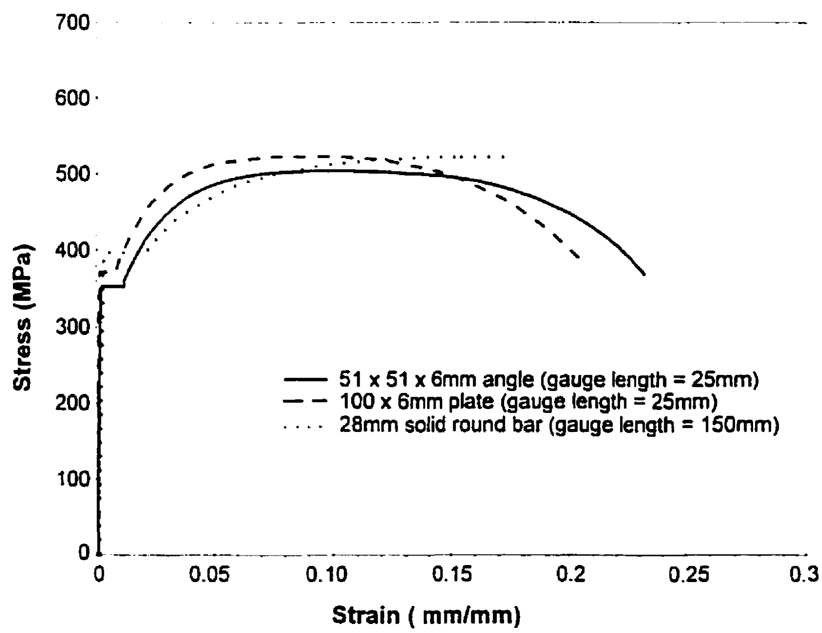

Figure 3.11: Stress - strain responses for structural steel for Specimens RC2 and RS2

3.5.3 Concrete

All six specimens used a high-early strength ready-mix concrete with a specified 28-day concrete strength of 30 MPa. Table 3.3 summarises the mix proportions used for the normal-strength concrete.

The three column retrofit specimens were cast in one stage, with the exception of RC1, which required two stages. The results from the concrete material tests are shown in Table 3.4 and typical stress-strain curves are given in Fig. 3.12.

The three beam-column-slab subassemblage specimens where each cast in two stages. The first cast included the lower column, both beams and the slab. The upper column was cast after the slab had hardened. The compressive stress-strain curve for Specimen RS2 is given in Fig. 3.13.

Specimen RS1, constructed and tested by Castele (1988), required special attention to ensure that proper vibration was performed even though the working space was very limited. The reinforced concrete sleeve for the lower column up to the middle of the joint region was cast in one lift. This was achieved by placing the concrete at the back of the joint. Small inspection holes were drilled into the formwork to verify that the concrete was filling the formwork. A 25 mm diameter vibrator used to consolidate the concrete retrofit. The upper column retrofit was completed in two separate casts, requiring no patching after the removal of the formwork.

For each concrete batch a minimum of six concrete cylinders, three beam specimens and two shrinkage specimens were cast. These specimens were used to determine the following properties: compressive strength, f'_c, split-cylinder strength, f_{sp}, modulus of rupture and the variation of shrinkage with time. The cylinders used to determine f'_c (three specimens) and f_{sp} (three specimens) were 150 mm in diameter and 300 mm in height. The modulus of rupture beams had a cross section of 100 by 100 mm and an overall length of 400 mm and was subjected to third-point loading over a span of 300 mm. A summary of these properties are given in Table 3.4. Shrinkage measurements were also taken for RS2 as well as for the three column retrofit specimens. This was done by the use of 2 -50 mm x 50 mm x 275 mm long rectangular concrete prisms which were cast and cured in the same environment as the full-scale specimens. The shrinkage measurements are shown in Fig. 3.14 and 3.15 for the column retrofit specimens and Specimen RS2, respectively.

Table 3.3: Mix proportions for concrete of Specimen RS2

Component	30 MPa
Cement (kg/m^3)*	*340
Fine Aggregate (kg/m^3)	795
Coarse Aggregate (kg/m^3)	**1055
Water (kg/m^3)	160
Water-Cement ratio	0.47
Superplasticizer (L/m^3)	2.9
Retarding Agent (L/m^3)	0.2
Slump (mm)	170
Air Content	5%
Density (kg/m^3)	2350

* Type 30 high early strength

** 20 mm maximum aggregate

Table 3.4: Concrete properties

Specimen	Cast No.	f'_c (MPa)	ε'_c (mm/mm)	f_{sp} (MPa)	f_r (MPa)
C1, RC1 RC2	1 std. deviation	39.6 1.73	0.0022 0.00007	3.2 (0.3)	3.7 (0.5)
RC1 retrofit	1 std. deviation	43.7 0.25	0.00246 0.00029	3.0 (0.2)	3.9 (0.3)
S1	1 2	29.6 34.5	- -	1.94 2.77	- -
RS1	1 2	30.0 38.7	- -	1.78 1.98	- -
RS1 retrofit	1 2	32.1 34	- -	2.02 2.10	- -
RS2	1 std. deviation	43.7 0.25	0.00246 0.00029	3.0 (0.2)	3.9 (0.3)

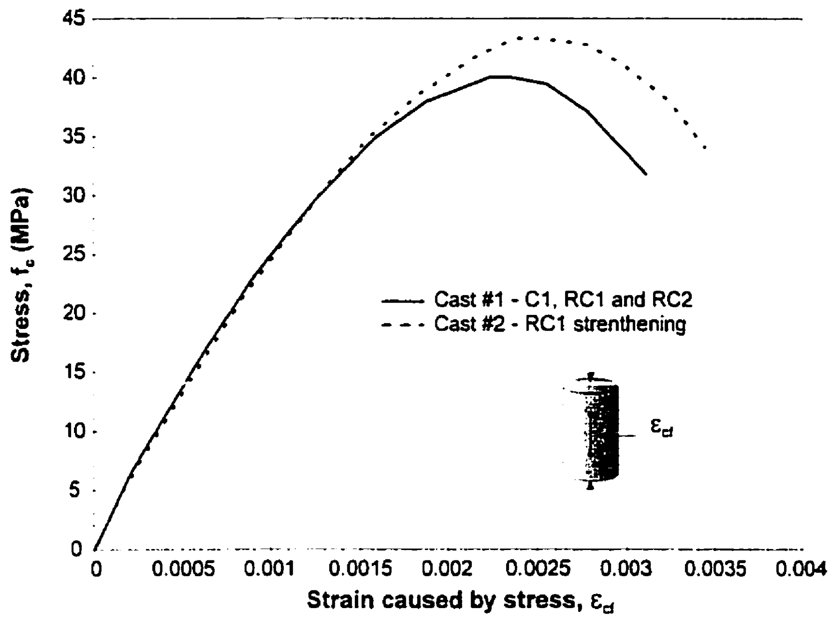

Figure 3.12: Compressive stress-strain response for Concrete of Column Retrofit Specimens

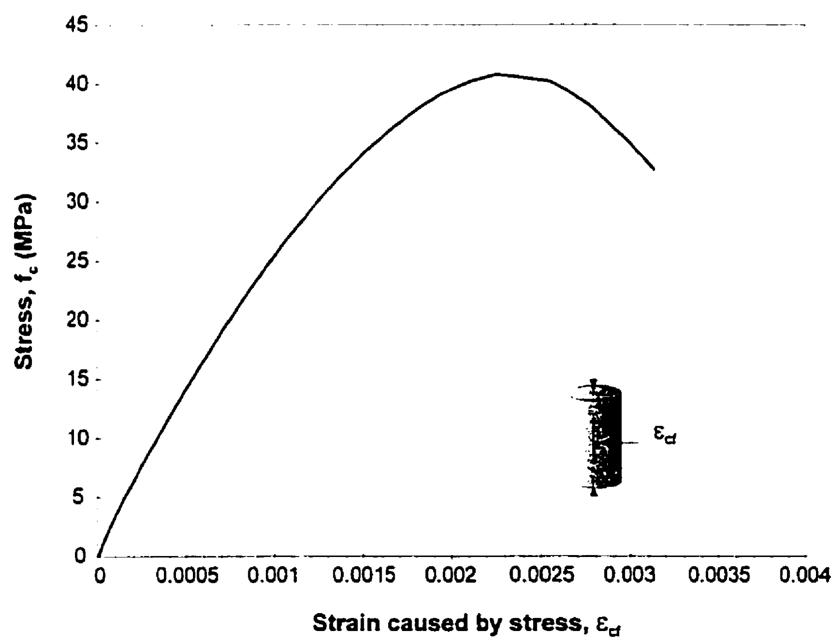

Figure 3.13: Compressive stress-strain response for Concrete of Specimen RS2

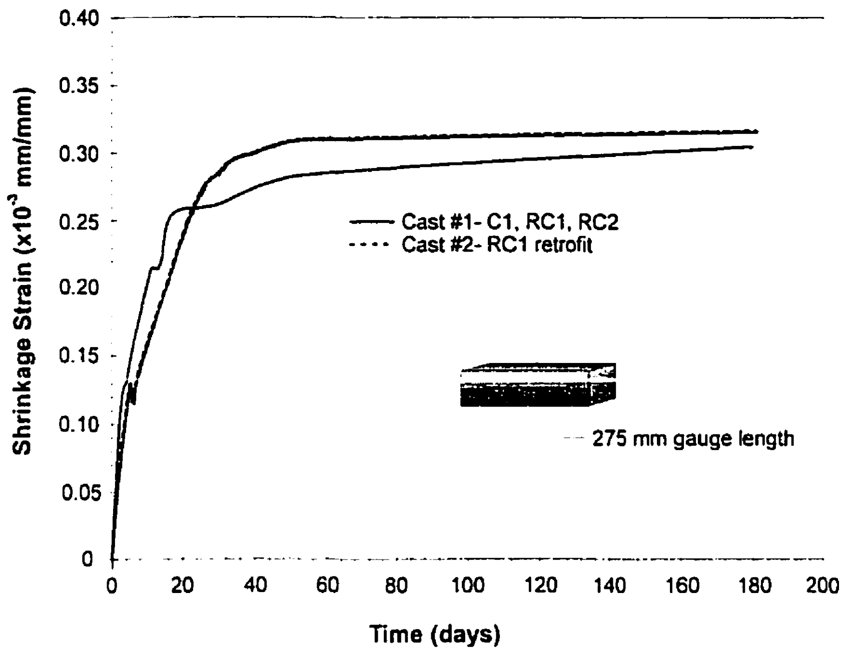

Figure 3.14: Shrinkage strains measured in concrete prisms for concrete of column retrofit specimens

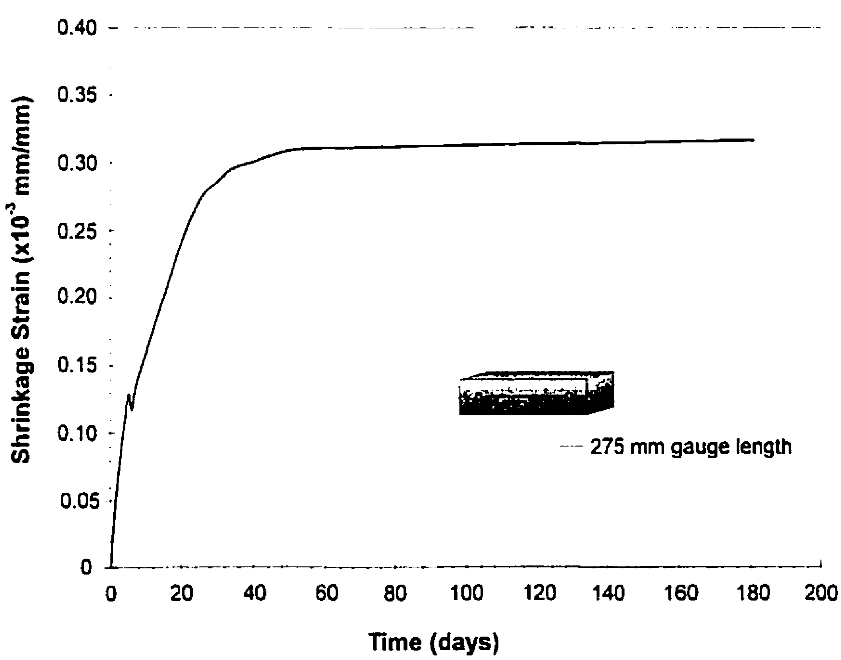

Figure 3.15: Shrinkage strains measured in concrete prisms for concrete of Specimen RS2

CHAPTER 4

EXPERIMENTAL RESULTS AND ASSESSMENT OF COLUMN RETROFIT TECHNIQUES

This chapter presents the behaviour and predictions of the responses of the three column Specimens, C1, RC1 and RC2. In addition, the performance of the retrofitted Specimens RC1 and RC2 are compared with the unretrofitted Specimen C1.

4.1 Observed Behaviour of Column Specimens

All three specimens were tested under concentric axial load under the 11400 kN capacity MTS universal testing machine, as described in Section 3.1.1. The instrumentation of each of the specimens is described in Section 3.2. The results of the three tests are described below.

4.1.1 Response of Column Before Retrofit (Column C1)

Specimen C1 is a column before retrofit, with deficient amounts and details of the confinement reinforcement. The load deflection response for this column is shown in Fig. 4.1. First signs of splitting cracks were observed at a load of 3900 kN on the north face of the column. The splitting cracks had a maximum width of approximately 0.1 mm. The loading was increased to a peak load of 4369 kN. At the peak load, significant splitting and significant spalling of the concrete cover were observed at the midheight of the column. Immediately after the peak load, a sudden drop in the load carrying capacity, down to 50% of the peak load occurred. The failure zone which occurred at midheight was caused primarily by the loss of concrete cover and loss of the concrete section in between the column ties, with some signs of concrete crushing. Specimen C1 at the end of the test is shown in Fig. 4.2. It should also be noted that the initial portion of the load deflection response shown in Fig. 4.1, demonstrates a softer initial response up to a deflection of about 1.5 mm, with a steeper load-deflection response beyond this deflection. After studying the data, it seems clear that this phenomenon is probably due to a column "seating" problem at the base of the column. This becomes clear when the overall deformations measured by the full height LVDTs are compared with the local strains observed over the five different segments as shown in Fig. 4.3. The applied load versus strain response for the lower most segment indicates this strain stiffening response, whereas the other segments show very normal responses up to the peak load level, with some relieving of the load once failure occurs at midheight of the column. The test was terminated due to the buckling of the longitudinal bars as well as the inability of the column to sustain compressive load.

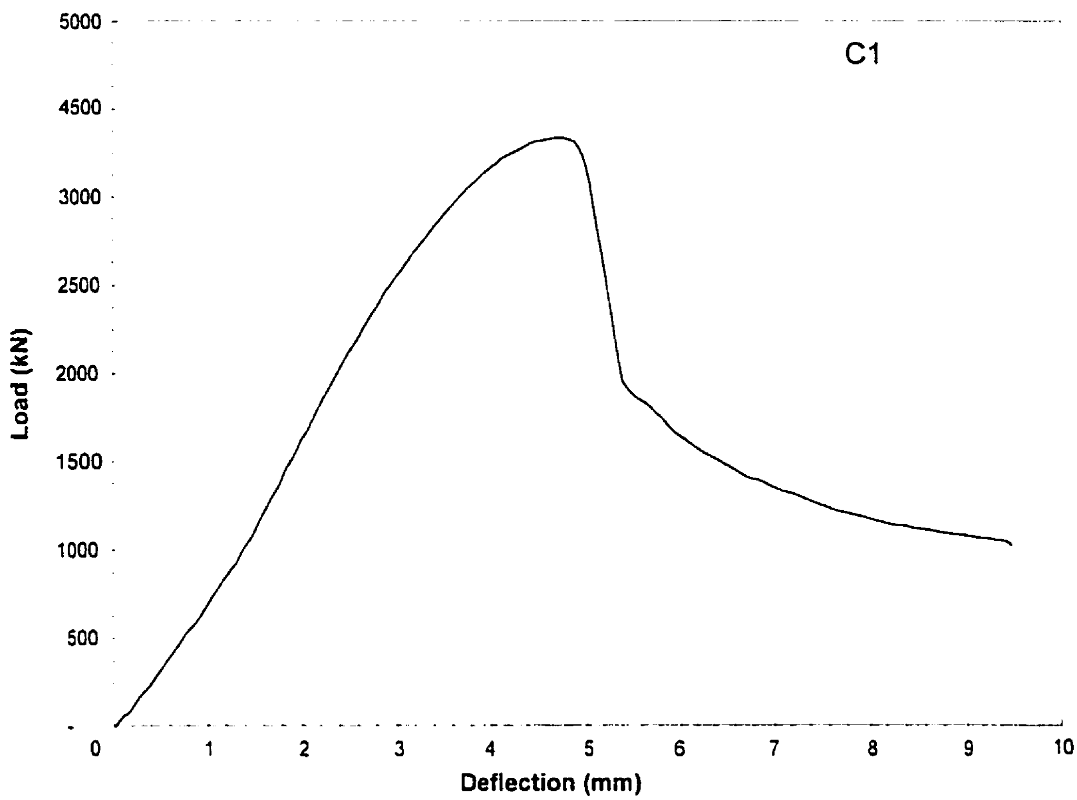

Figure 4.1: Load versus deflection response for Specimen C1

Figure 4.3 shows the longitudinal strain distribution along the height of the column. The grey segments in Fig. 4.3 indicate the load versus versus local strain response in that segment. these load versus strains responses are compared for the different segments and are compared with the load versus strain response obtained over the full height of the column (all segments shaded in Fig. 4.3). The most brittle segment response occurs in the middle region of the column where significant spalling occurred. Strains measured on the vertical reinforcing bars by electrical resistance strain gauges are shown in Fig. 4.4. Regions outside the shaded zones in Fig. 4.4 indicate yielding of the vertical bars. It is noted that the inner and outer gauges, L5 and L6, which are placed at the same level on the same bar, indicate that at a load of 4100 kN, the outer face experiences a large increase in compression while the inner face jumps into tension. This indicates that severe buckling of this mid-side bar has occurred.

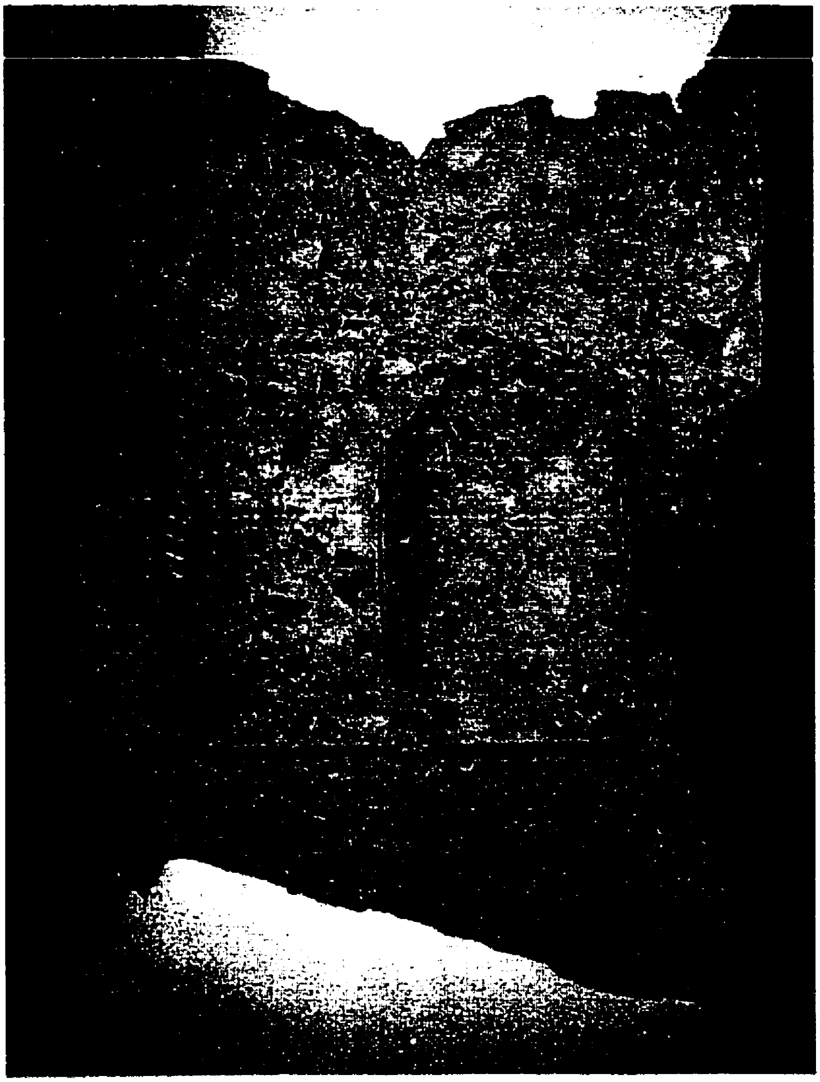

Figure 4.2: Specimen C1 at end of test

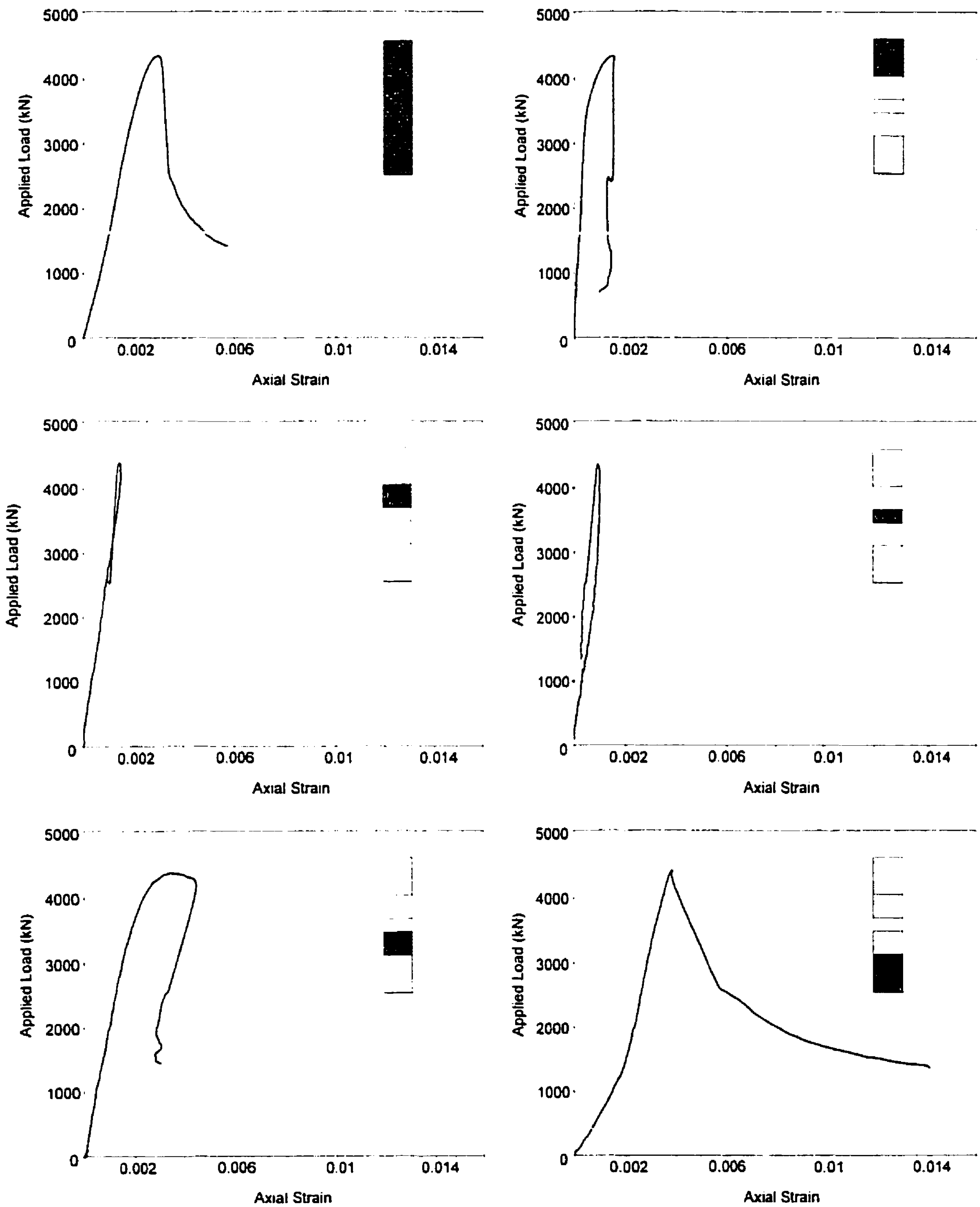

Figure 4.3: Axial Strain in Specimen C1

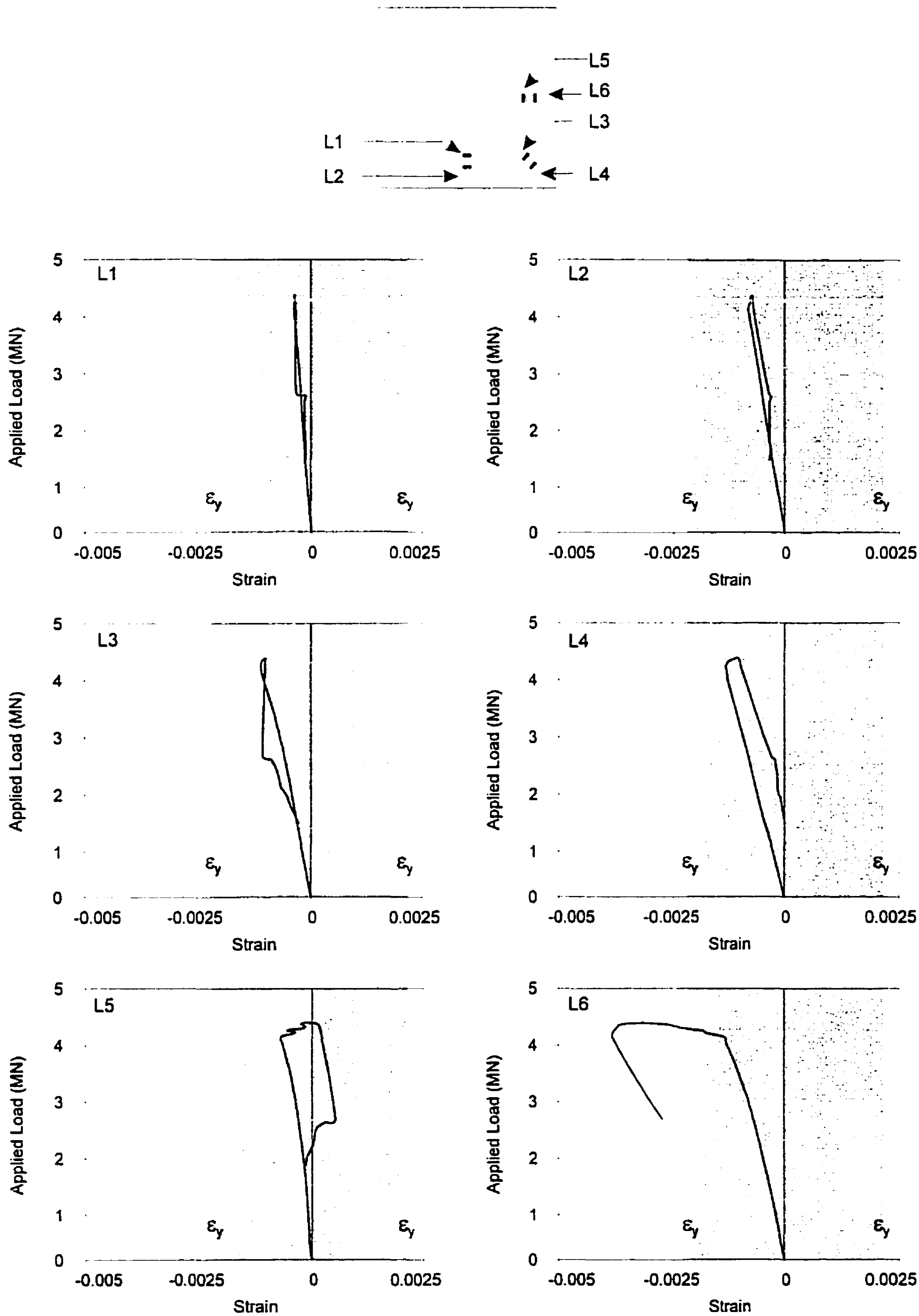

Figure 4.4 Measured strains in longitudinal reinforcement of Specimen C1

Strains in two legs of the column tie at midheight were also monitored using electrical resistance strain gauges, as shown in Fig. 4.5. It is noted that one of these gauges indicates yielding of the transverse tie close to the peak load obtained in the column.

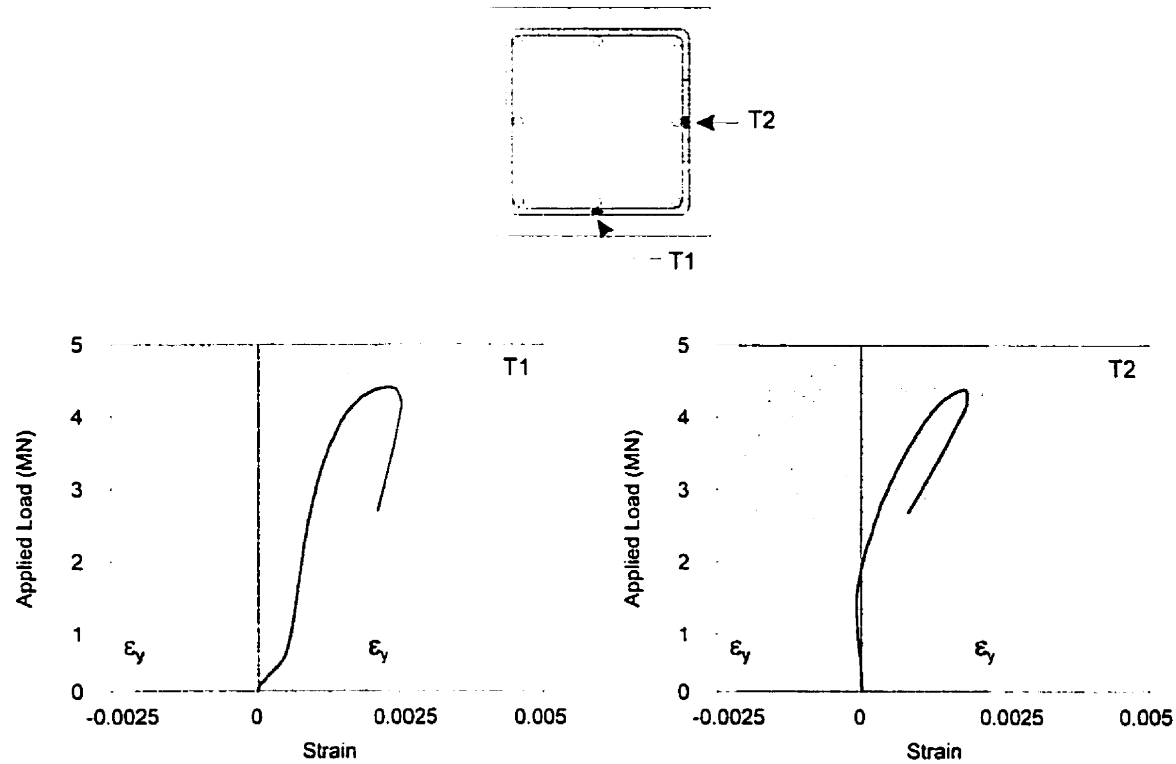

Figure 4.5: Measured strains in transverse reinforcement of Specimen C1

4.1.2 Response of Column with Reinforced Concrete Sleeving Retrofit (Column RC1)

Specimen RC1 is a retrofit of a column with the same deficient confinement details and design as Specimen C1, with an added layer of reinforced concrete to increase its strength. The reinforced concrete sleeve of Specimen RC1 increased in cross sectional area to 500 x 500 mm from 325 x 325 mm. Differential shrinkage caused the new reinforced concrete to crack at 200 mm intervals along the height of the column, coinciding with the placement of the added hoops. Vertical cracks due to restraint of shrinkage strains were also observed on all four faces at the centre of each face.

The load deflection response is given in Fig. 4.6. At a load of approximately 4000 kN it was observed that the shrinkage cracks had completely closed. No other indications of distress were observed until an axial load of 7600 kN, where small splitting cracks were observed near the bottom of the column on the west face immediately over the added vertical bars. When the peak axial load was reached, extensive splitting cracks as well as spalling of the added concrete cover occurred very suddenly, resulting in a sudden drop in load of about 50%. The post peak response of the retrofitted specimen behaved in a brittle manner, very similar to the response of Specimen C1. After the peak was reached, buckling of the added vertical bars as well as bond failure between the old and new concrete occurred. Upon closer inspection, it was clear that spalling of the concrete cover of the original column had occurred, indicated by a "hollow" sound when hit with a hammer.

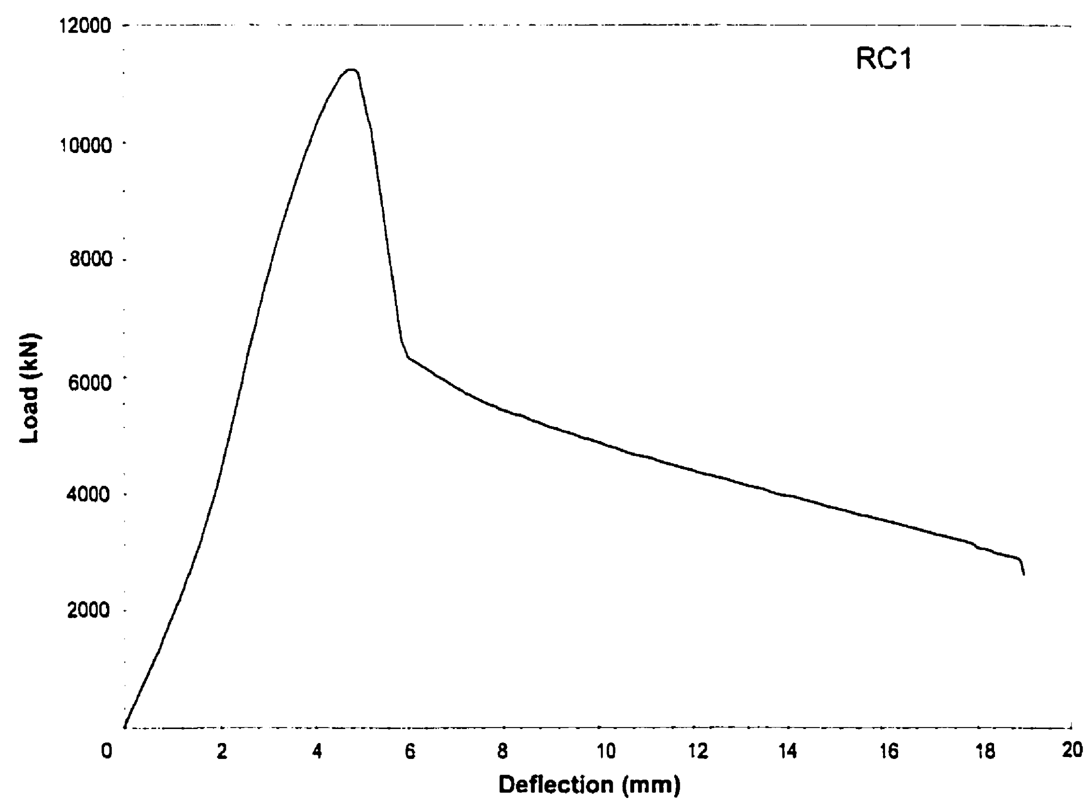

Figure 4.6: Load versus deflection response for Specimen RC1

The appearance of Specimen RC1 at the end of the testing procedure is shown in Fig. 4.7. The soft initial response of this specimen, shown in Fig. 4.6, can be explained by the specimen having a "seating" problem at the base of the column. This is evident from Fig. 4.8 by comparing the overall vertical strains to the local strains measured over the five different segments over the height of the column. The bottom-most segment shown in Fig. 4.8, shows a large strain concentration in this segment, with an initial strain stiffening response, similar to the response measured from the four full length LVDTs.

Vertical and transverse strain measurements using electrical resistance gauges were recorded in the same manner as for column Specimen C1. However, 6 strain gauges were placed on the added vertical bars and 2 strain gauges were placed on the added transverse hoop at mid height of the column. The plots of the recorded strains versus the applied loading are shown in Fig. 4.9. Buckling of one of the added No. 25 bars occurred at a load of 6400 kN after the peak load had been reached. At this load level, the inner and outer gauges, L3 and L4, showed some signs of buckling. With gauge L3 having a large jump in compressive strain while gauge L4 experienced a reduction in compressive strain. It is clear from Fig. 4.9 that yielding of the vertical bars in both the original column and in the retrofit sleeving occurred.

The strains in the transverse reinforcement of the column, are shown in Fig. 4.10 for both the original tie and the added hoop at midheight. The strains in the existing tie were found to be slightly larger than the strains in the added tie. One of the gauges on the existing tie measured strains greater than yield when the maximum compressive load was reached.

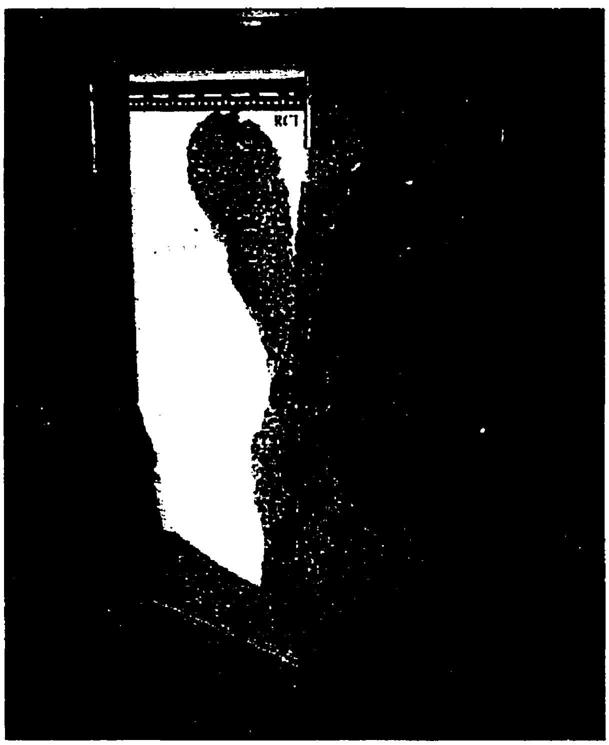

Figure 4.7: Specimen RC1 at end of test

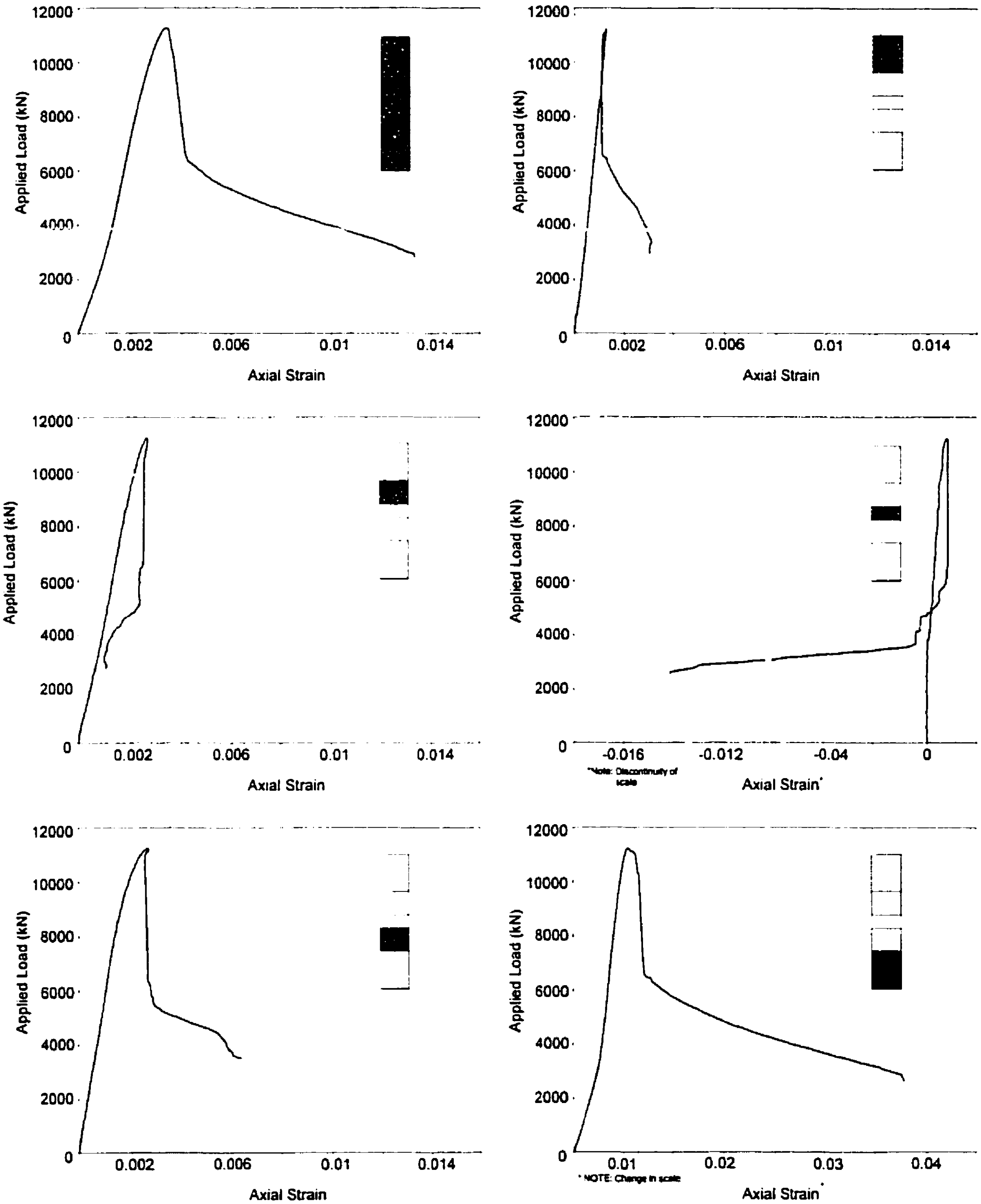

Figure 4.8: Axial Strain in Specimen RC1

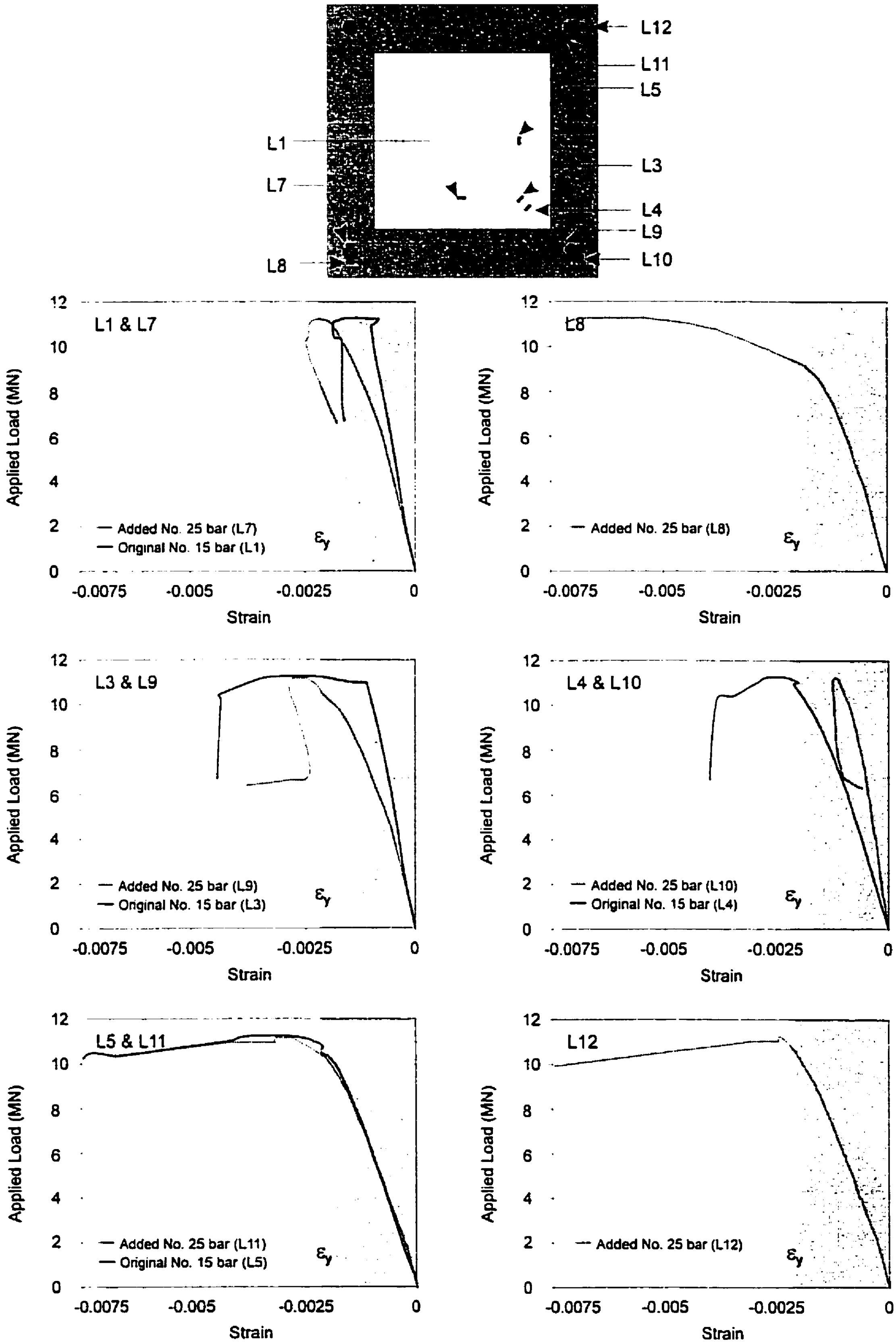

Figure 4.8 Measured strains in longitudinal reinforcement of Specimen RC1

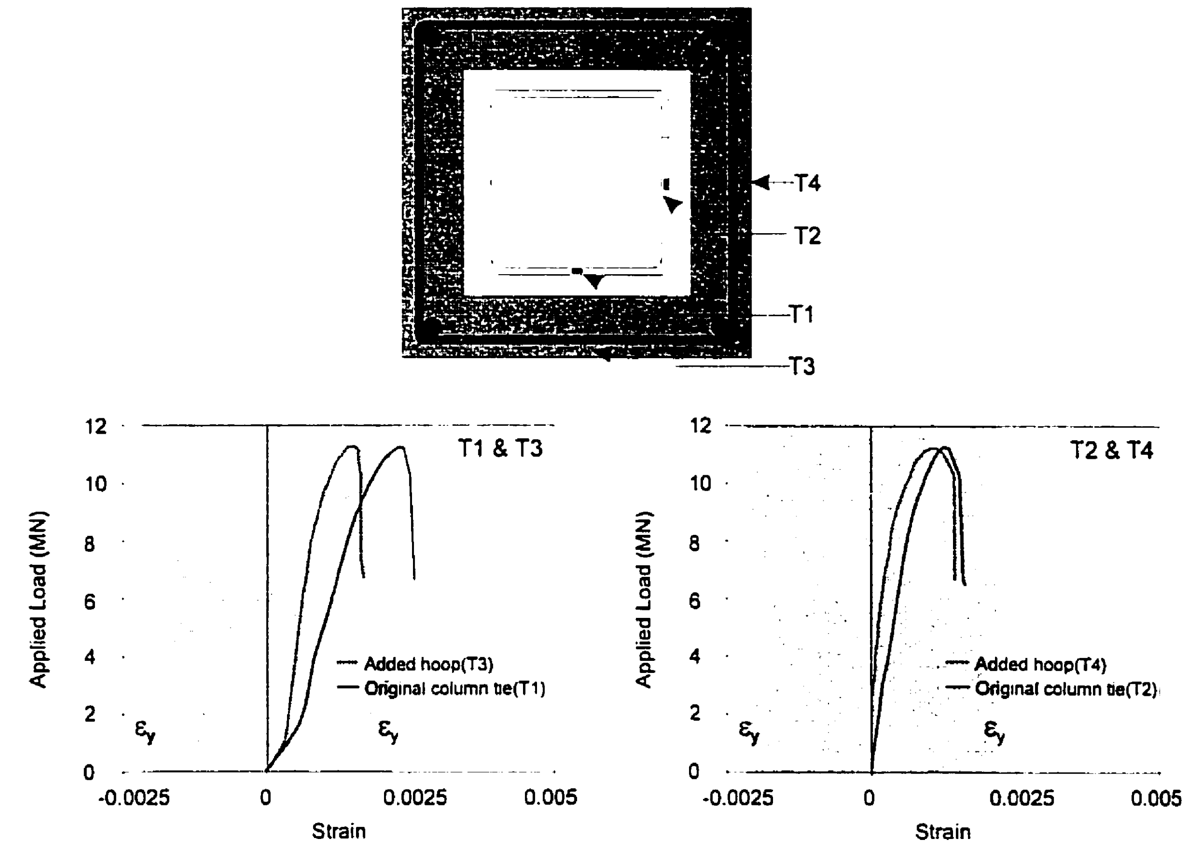

Figure 4.10: Measured strains in transverse reinforcement of Specimen RC1

4.1.3 Response of Column with Steel Angles and Batten Plate Retrofit (Column RC2)

Specimen RC2 incorporated the use of steel corner angles and batten plates to retrofit a companion specimen to column C1. The construction of this specimen is detailed in Section 2.1.3. The load deflection response for this specimen is shown in Fig. 4.11. The first observed signs of distress were observed at a load of 5100 kN where small splitting cracks appeared on one of the faces. However, there may have been earlier signs of distress prior to this point but observation was obscured by the presence of the angles and batten plates. At a load of 5200 kN concrete crushing was observed on one of the faces. A peak axial compressive load of 5240 kN was obtained. In comparison to the two other specimens (C1 and RC1), RC2 displayed great post peak response, dropping initially only 21% from the peak load. The load versus deflection response following this initial drop in load carrying capacity, showed the ability of this specimen to sustain significant axial compressive loads while undergoing increasingly larger deformations.

Concrete spalling was observed throughout the height of the specimen after the peak load was reached. The improved post peak behaviour arises from the fact that the spalled concrete cover was restrained by the batten plates and steel angles, which improved the confinement of the concrete core and allowed spreading of concrete crushing over the height. The angles showed signs of overall bending between batten plates, as well as bending of the legs of the angles. The batten plates also showed outward bending between the angles due to lateral expansion of the concrete. The test was stopped when a weld between a batten plate and a corner angle failed, even though the specimen showed signs of greater deflection capacity. The appearance of Specimen RC2 at the end of the test is shown in Fig. 4.12. This specimen also showed signs of "seating" problems, this can be seen when comparing the bottom vertical LVDT to the other four measured strain regions shown in Fig. 4.13. The bottom region demonstrated a much softer initial response with strain stiffening being apparent at a load of 1500 kN.

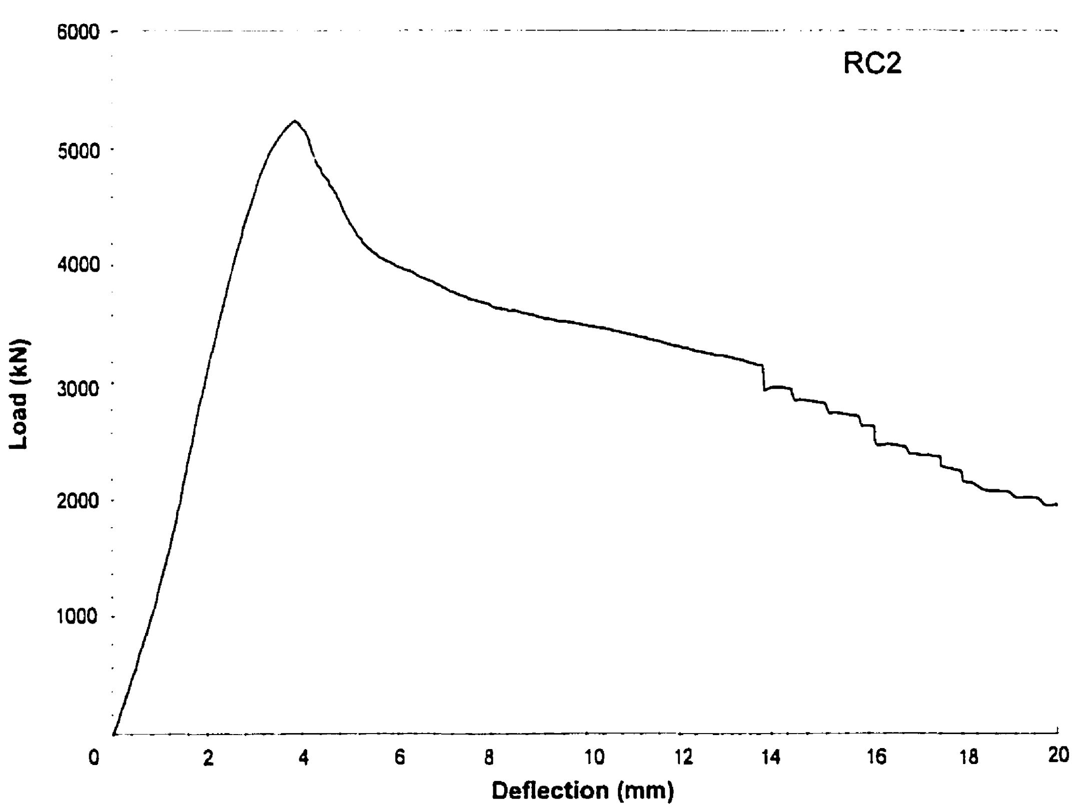

Figure 4.11: Load versus deflection response for Specimen RC2

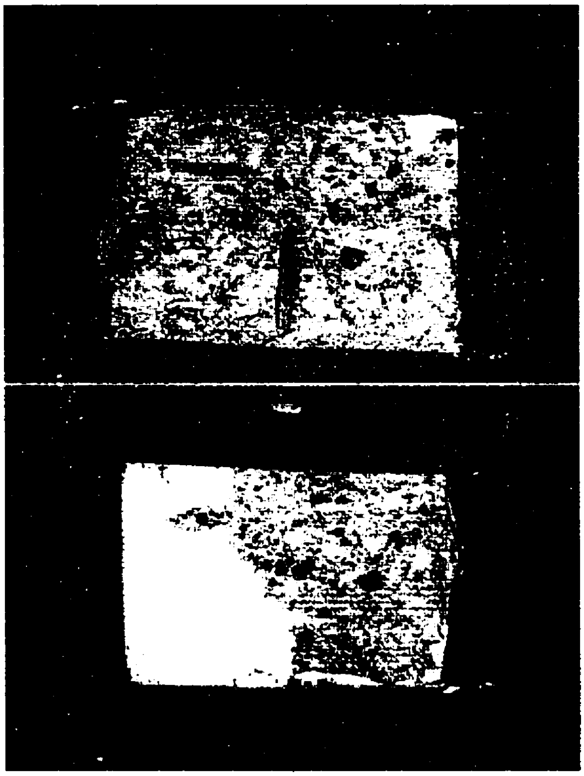

a) buckling of vertical steel corner angles

b) bending of batten plates and concrete crushing

Figure 4.12: Specimen RS2 at the end of the test

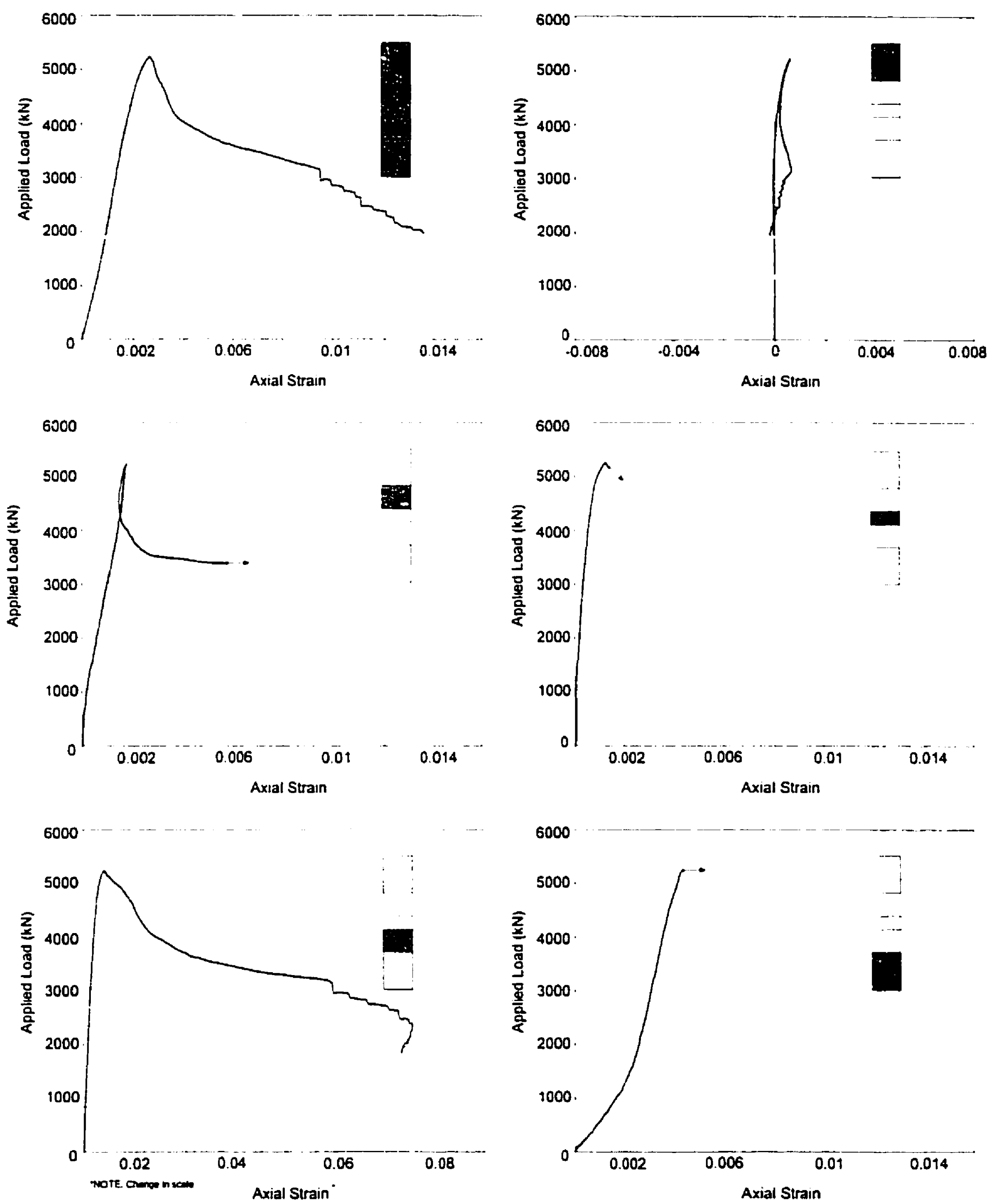

Figure 4.13: Axial Strain in Specimen RC2

In addition to the electrical resistance strain gauges placed in the original section, four additional gages were placed on the longitudinal angles as well as four gauges on the batten plates at mid-height of the column. The results of the electrical resistance strain gauges for the original longitudinal steel are shown in Fig. 4.14, whereas the results for the added vertical angles are shown in Fig. 4.15. It is apparent from Fig. 4.14, that all vertical reinforcing bars reached strains well beyond yield levels. Similarly, the added steel corner angles also reached strains greater than yield. It is noted that the recorded axial strains in the corner angles shown in Fig. 4.15, were probably influenced by the outwards buckling of the angles after the peak load was reached. It is apparent from observations during the test, that these angles experienced strains well above the yield strain.

Figure 4.16 shows the measured strains in two legs of the original tie and in the four batten plates located at the mid-height of the column. It is apparent that the batten plates, as well as the column tie, reached strain levels greater than yield. It is noted that the strain in the batten plates lagged behind the strain in the original column tie. This is to be expected because it takes some lateral expansion of the concrete before the added external reinforcement becomes fully effective. It is important to realise that the yield strain of the batten plates is significantly lower than the yield strain of the column tie. The batten plates however, are extremely effective in confinement since the area of one batten plate is six times greater than the area of one tie leg.

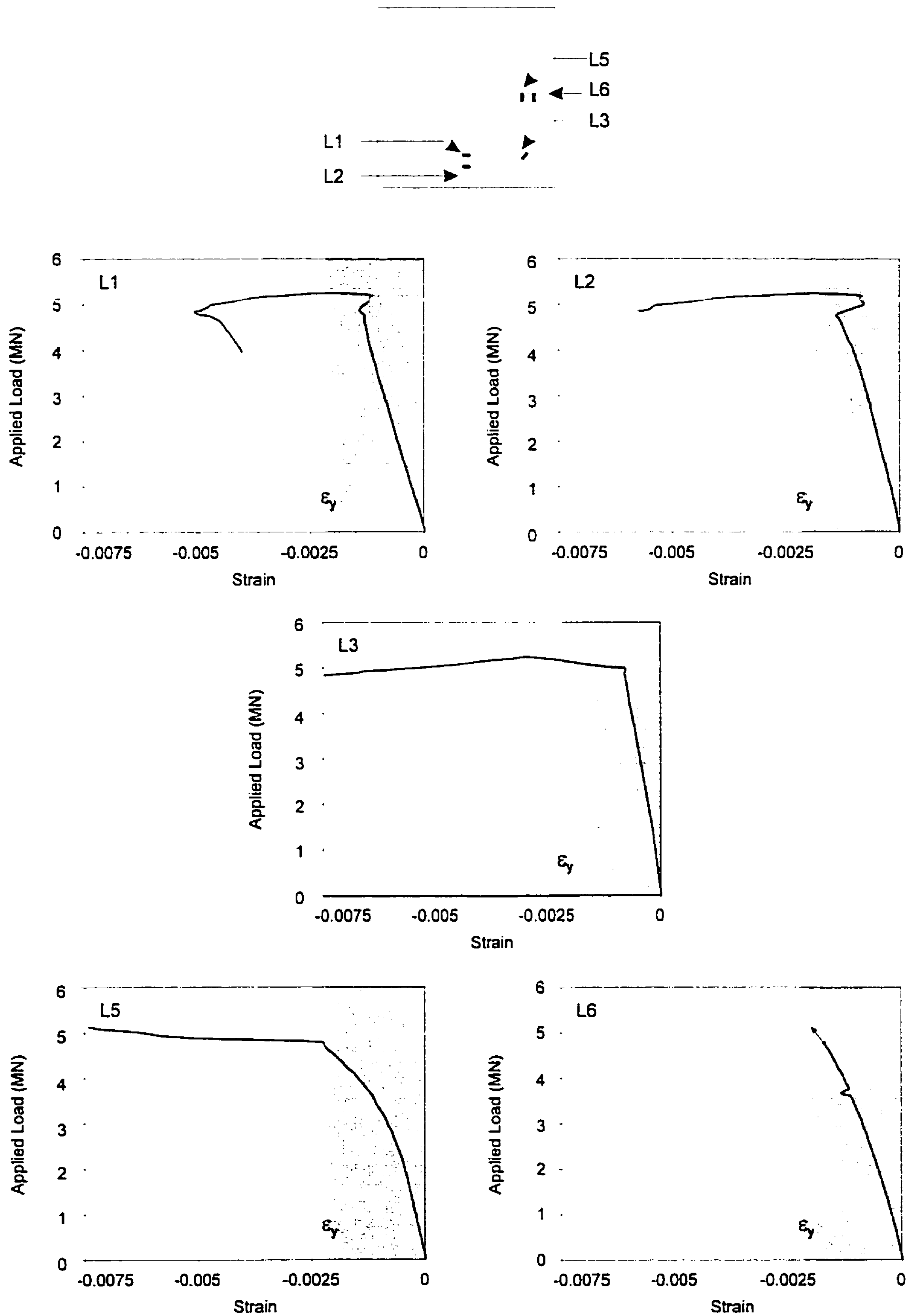

Figure 4.14: Measured strains in longitudinal reinforcement of Specimen RC2

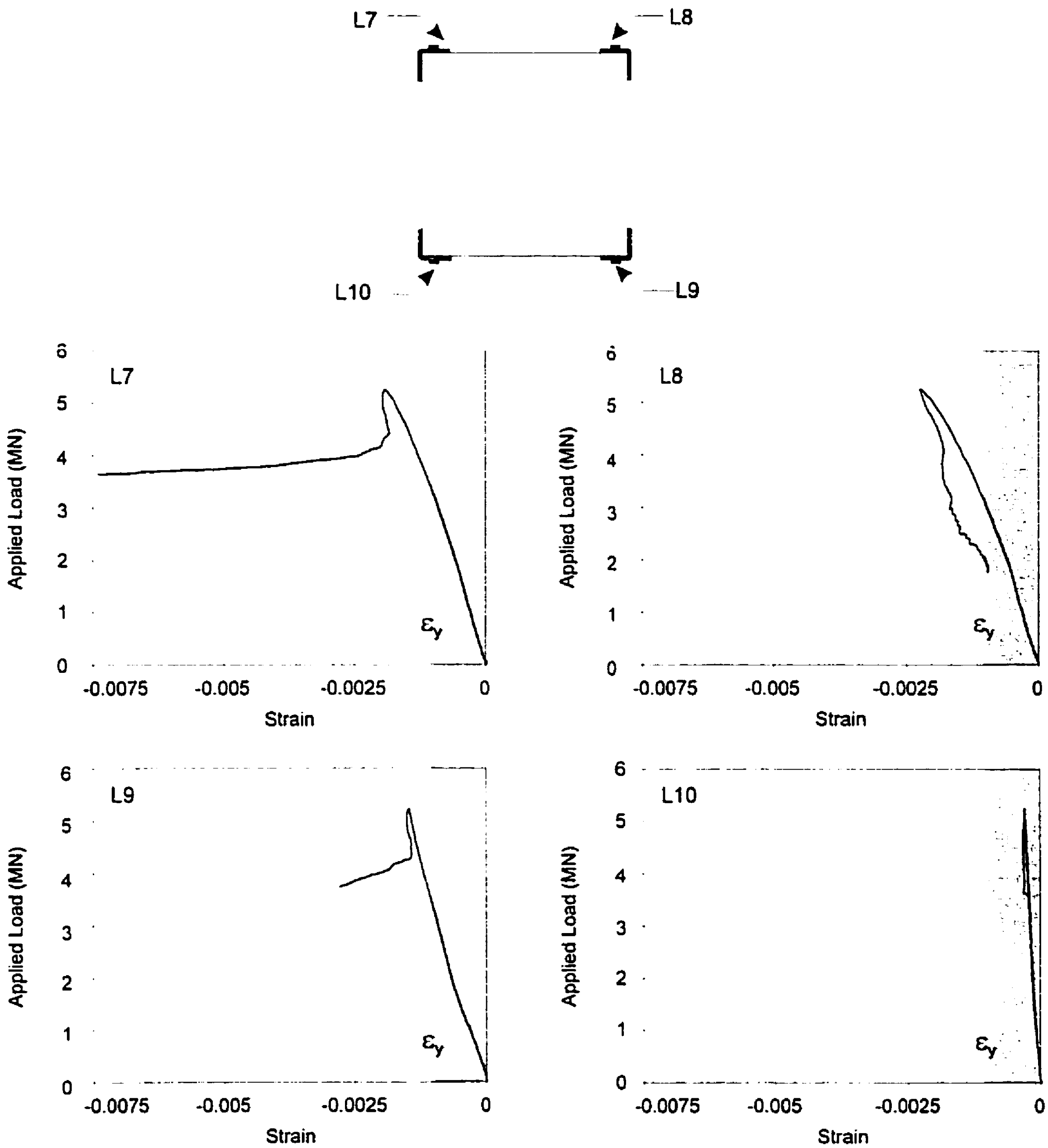

Figure 4.15: Measured strains in the added corner angles of Specimen RC2

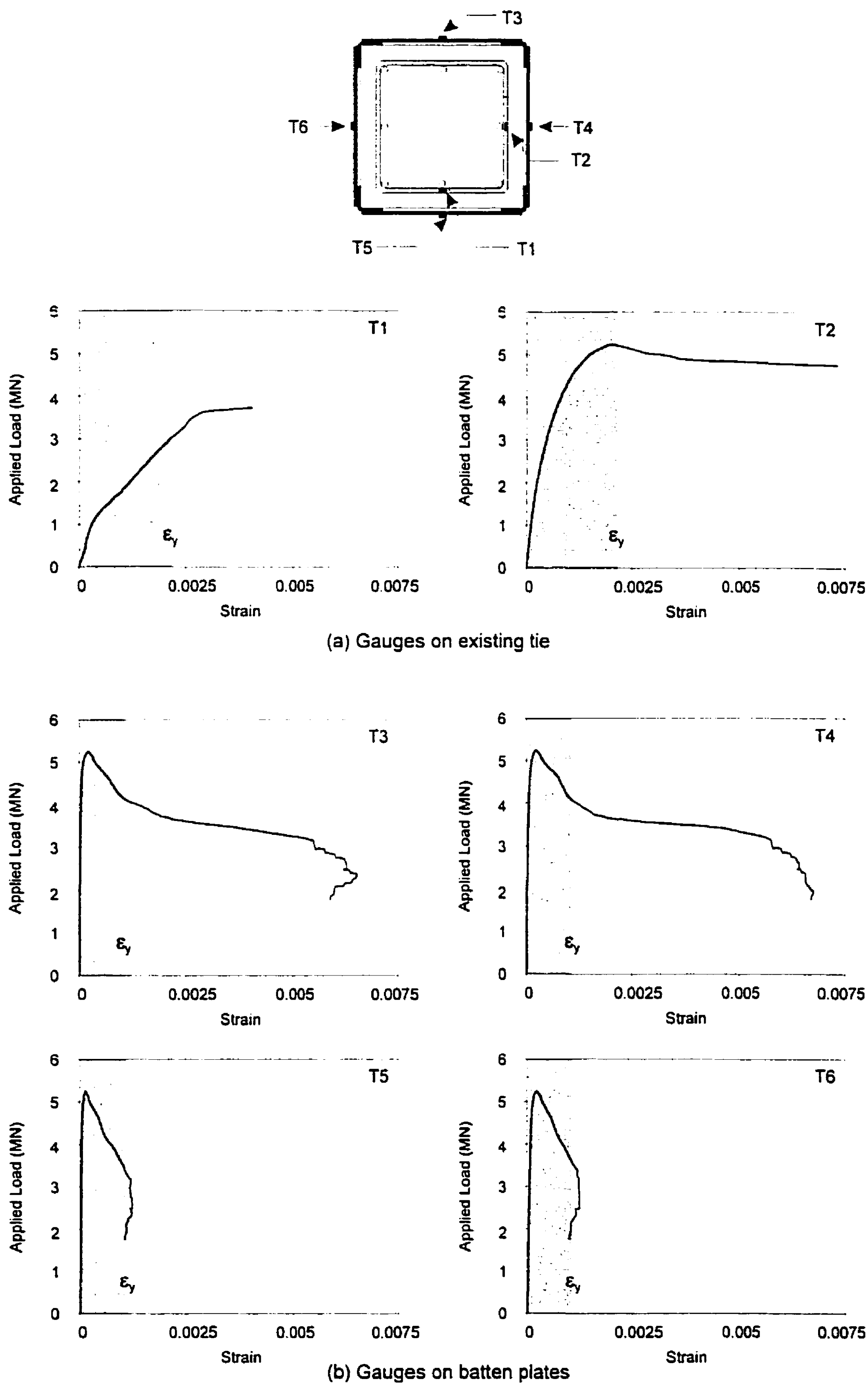

Figure 4.16: Measured strains in transverse reinforcement of Specimen RC2

4.2 Comparison of Column Responses before and after Retrofit

The load deflection responses of the three column specimens are compared in Fig. 4.17 and some of the important response parameters are summarised in Table 4.1.

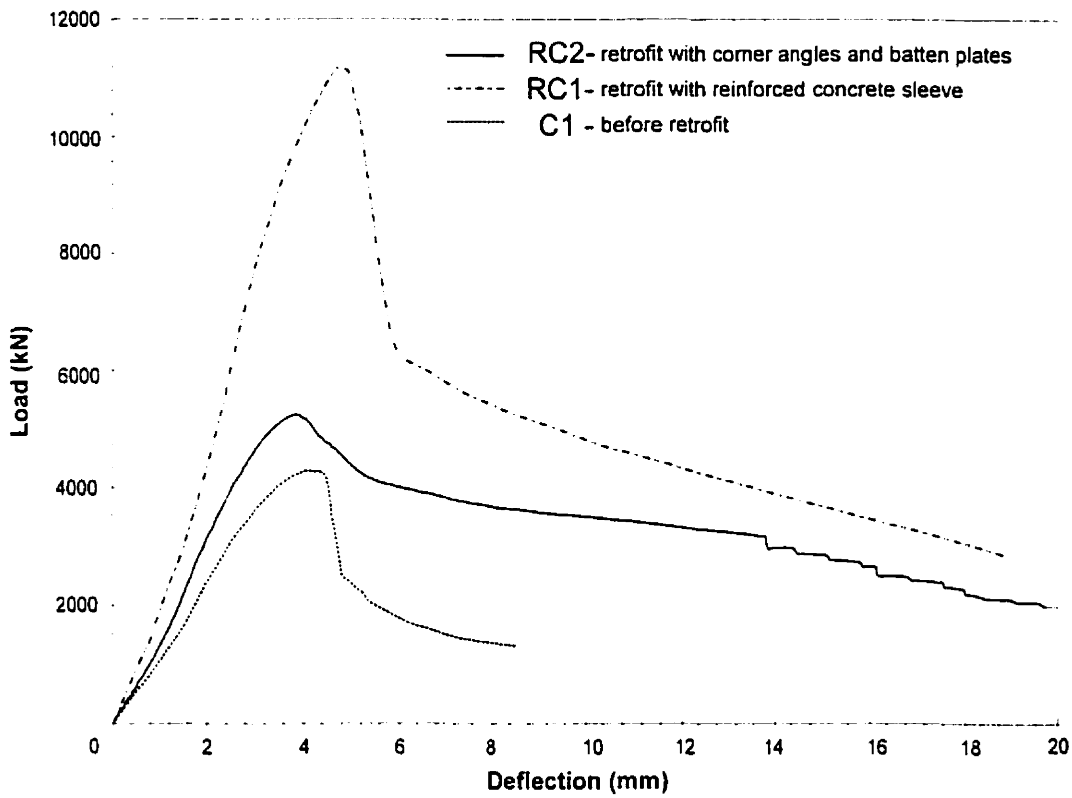

Figure 4.17: Comparsion of load versus deflection responses

The unretrofit Specimen, column C1, displayed a very brittle post-peak load deflection response. This was due primarily to the deficient detailing and design of the transverse reinforcement. The failure was characterised by: severe spalling of the concrete cover, loss of concrete core between column ties and buckling of the longitudinal bars.

Specimen RC1, which consisted of a reinforced concrete sleeve cast around the unretrofit column, reached a compressive resistance which was 2.6 times that of column C1. In addition, the stiffness was 2.3 times that of Specimen C1. However, the post peak response of this specimen is very similar to that of the unretrofit column C1.

Specimen RC2, utilised vertical steel corner angles and batten plates to strengthen as well as improve the confinement characteristics of a companion to column Specimen, C1. This retrofitted specimen experienced an increase in compressive resistance and stiffness, as well as exhibiting a more ductile post-peak response. The retrofitted Specimen, RC2 showed an increase of 20% in the compressive resistance and a 31% increase in loading stiffness. Specimen RC2 demonstrated the ability to sustain significant compressive loads after the peak load had been reached, dropping initially by only 21% instead of 50% (C1 and RC1) of the peak load. Significant concrete crushing was observed over nearly the full height of the column, whereas C1 and RC1 displayed very localised spalling and crushing failures. The appearance of the three column specimens at the end of the testing is shown in Fig. 4.18.

Table 4.1: Comparison of key response parameters

Specimen	Specimen Description	Peak load (kN)	Δ_{peak} (mm)	k_{peak} (MN/mm)
C1	Column before retrofit	4369	4.25	1.03
RC1	Retrofit with a reinforced concrete sleeve	11270	4.78	2.36
RC2	Retrofit with steel corner angles and welded batten plates	5240	3.87	1.35

4.3 Predicted Response of Column Specimens

The longitudinal strains were measured using four full height LVDTs placed at the four corners of each specimen The experimental test results along with predicted responses for all three specimens will be discussed in the following section. The predictions were made using a beta version of program RESPONSE-2000 (Bentz and Collins, 1998). The experimental responses have been modified to remove the "seating" deformations described in Section 4.1.

For all of the predictions, the in-situ concrete was assumed to peak at a stress of 0.9 f_c' and the stress-strain relationship was assumed to have the same peak stress as the cylinder test.

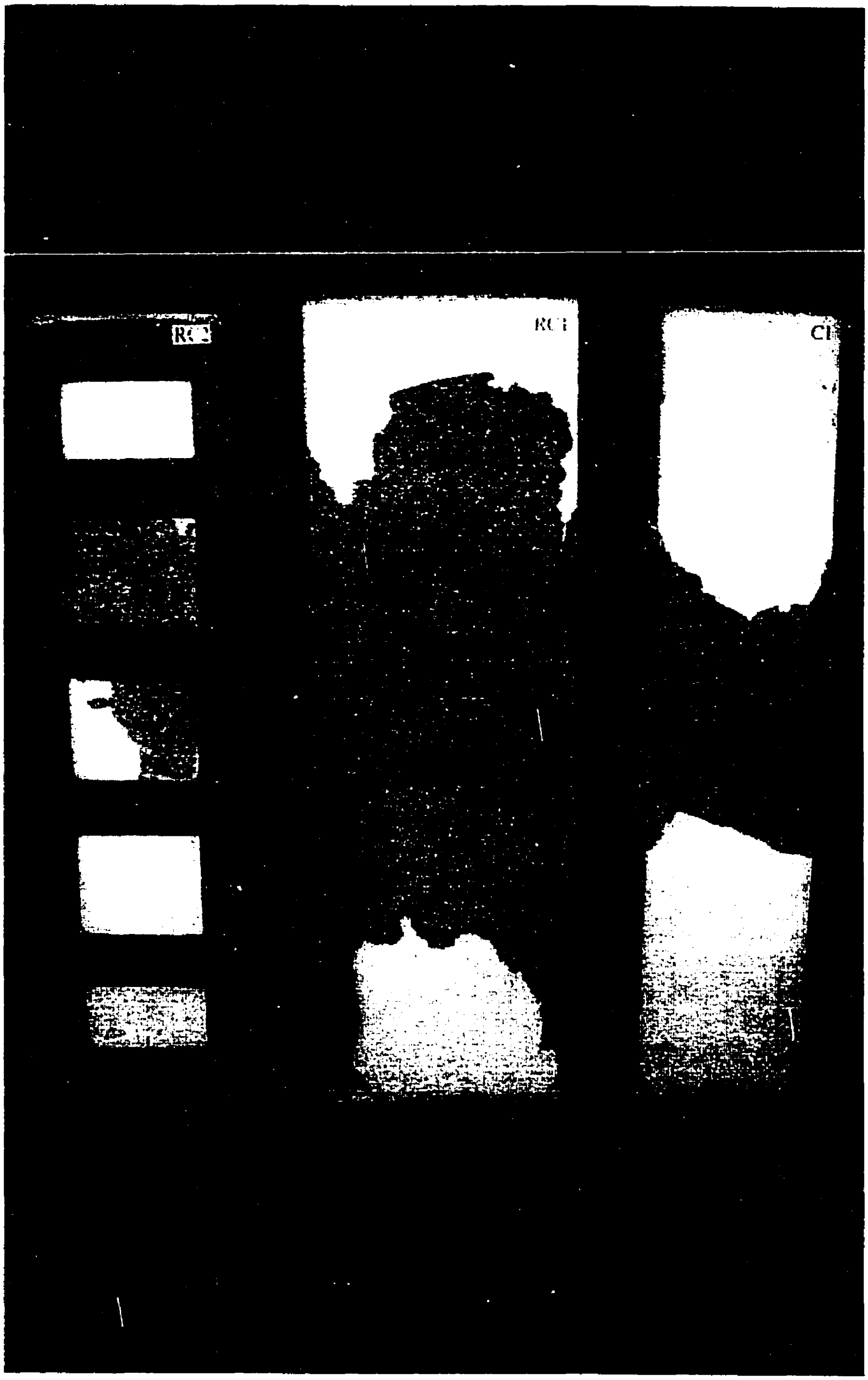

Figure 4.18: A comparison of all three specimens

4.3.1 Specimen C1

A comparison of the predicted response and the experimental response of Specimen C1, is shown in Fig. 4.19.

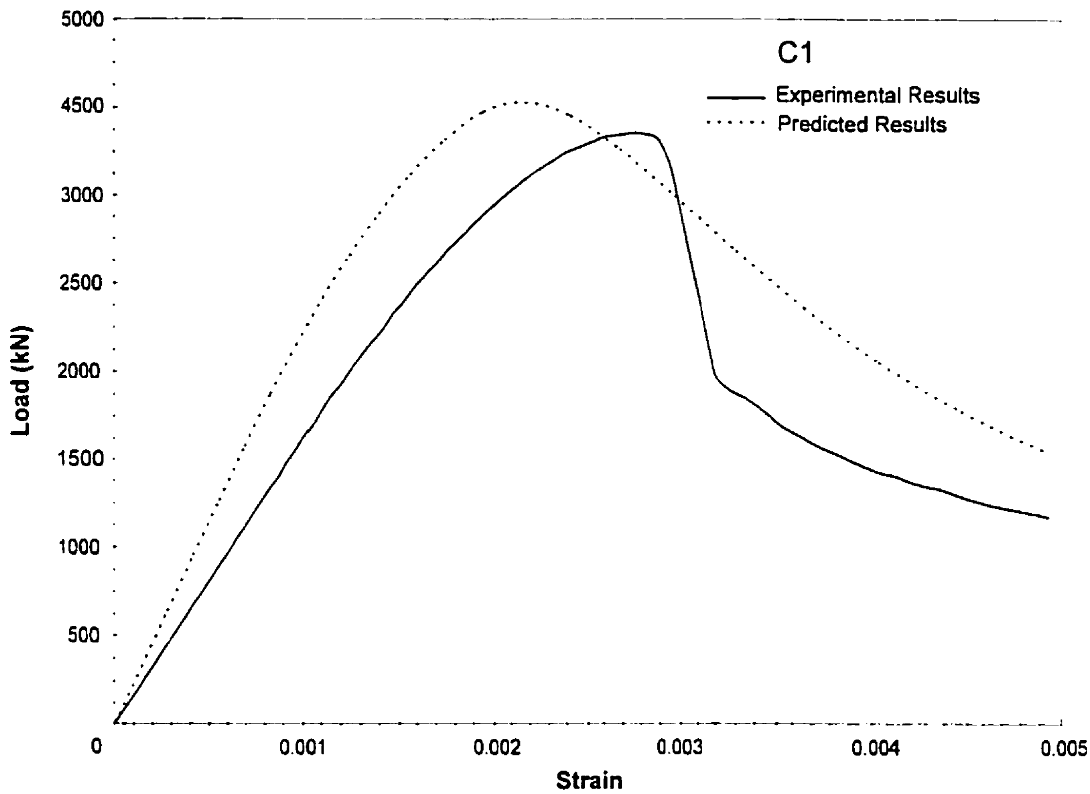

Figure 4.19: Load versus Strain Response for Specimen C1

Due to the large tie spacing, the core confinement enhancement in Specimen C1, was negligible, and therefore ignored. As shown in Fig. 4.19, the peak load reached during the test corresponds to the calculated predicted response using RESPONSE-2000 (Bentz and Collins, 1998). In addition, the predictions took into account the shrinkage strains in the concrete before testing started. A shrinkage strain of -0.309×10^{-3} was used (see Fig. 3.14), corresponding to an age of 180 days. However, the predicted response demonstrated a stiffer behaviour in comparison to the experimental test results. This can be attributed to the possibility that a small eccentricity may have been present during the testing of this specimen.

4.3.2 Specimen RC1

A comparison of the predicted response and the actual test results for column Specimen RC1 is shown in Fig 4.20.

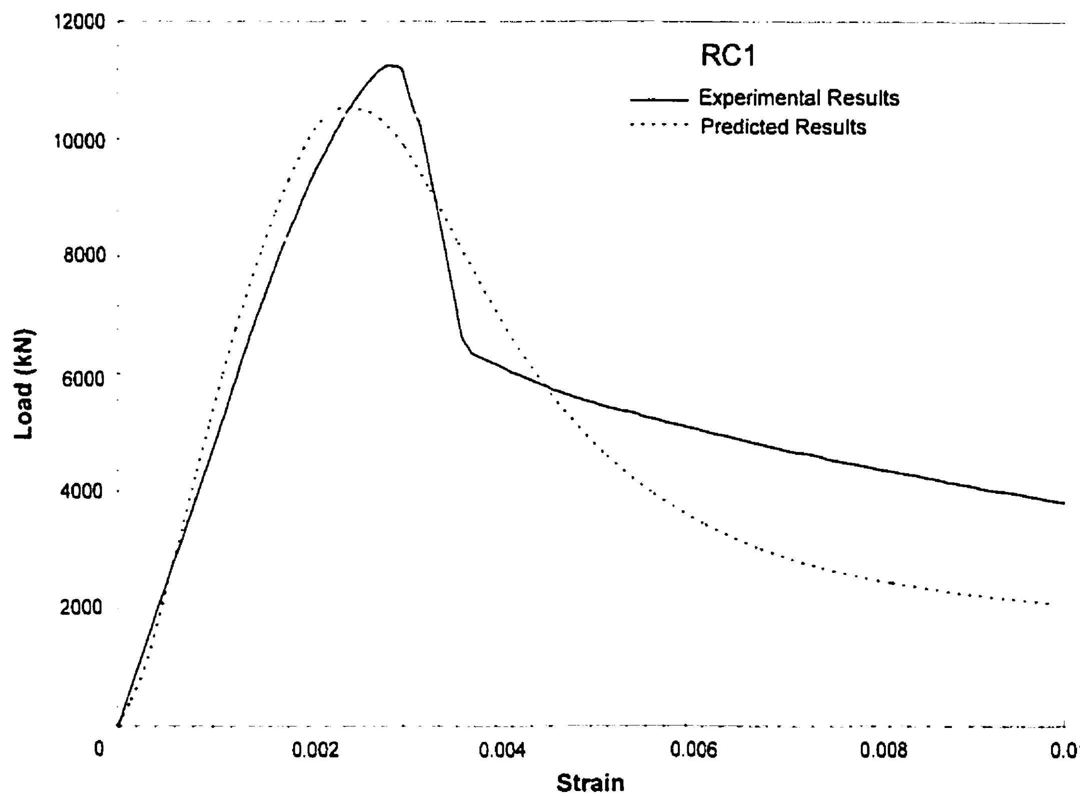

Figure 4.20: Load versus Strain Response for Specimen RC1

The predicted response does not include any confinement enhancement of the core concrete due to the large hoop spacing and details of the added reinforcement (200 mm). The shrinkage of the concrete prior to the addition of the reinforced concrete sleeve and the shrinkage of the retrofit concrete were accounted for in the predicted response. A shrinkage strain of -0.280×10^{-3} was measured in the shrinkage beam specimens of the original concrete on the day the reinforced concrete sleeve was cast. To account for the differential shrinkage between the new and the existing concrete, an initial strain of -0.25×10^{-3} was used for the unretrofit column concrete, while a shrinkage strain of -0.316×10^{-3} (see Fig. 3.14) corresponding to an age of 180 days was used for the added reinforced concrete sleeve. It is clear from Fig. 4.20 that the test results of Specimen RC1 were slightly less stiff than the predicted response.

4.3.3 Specimen RC2

The predicted of Specimen RC2 is compared to the experimental response in Fig. 4.21.

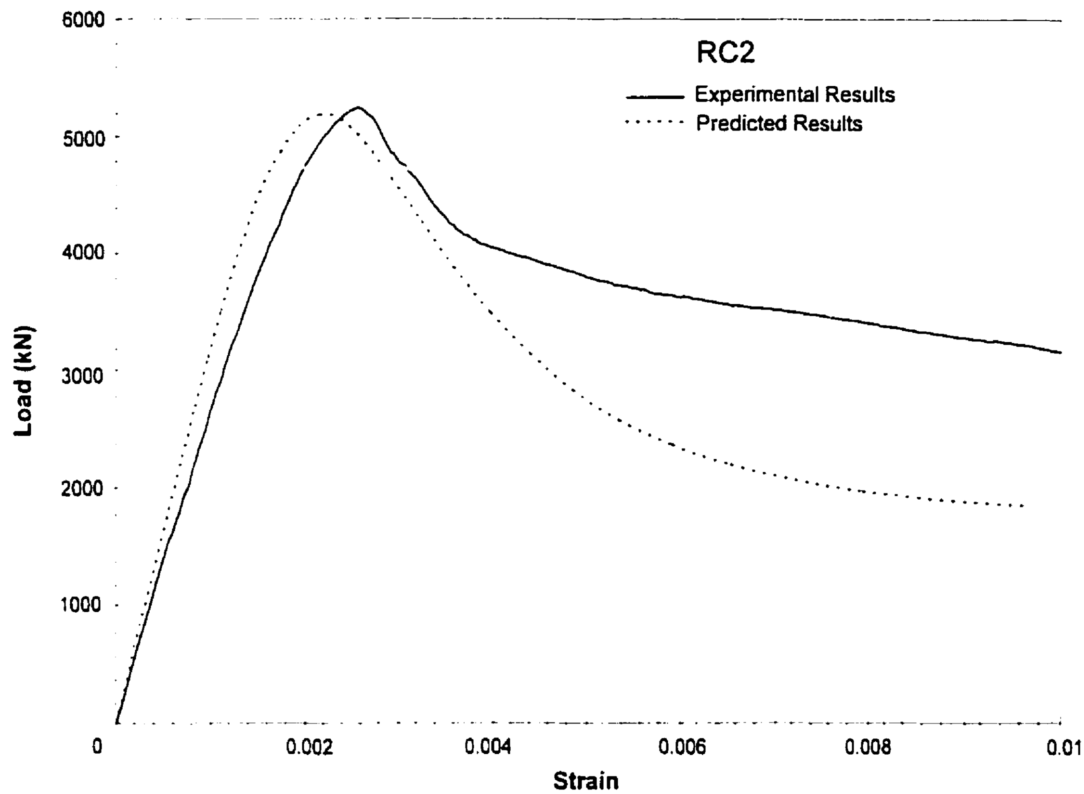

Figure 4.21: Load versus Strain Response for Specimen RC2

The predicted curve was calculated without considering any core confinement due to the small surface area in which the vertical steel angles are in contact with the column. In addition the shrinkage strains in the concrete before testing started were accounted for in the predicted response. A shrinkage strain of -0.309×10^{-3} was used (see Fig. 3.14), corresponding to an age of 180 days. This specimen showed a much more ductile response than the other two specimens, due to the confinement provided by the batten plates (see Section 4.1).

CHAPTER 5

EXPERIMENTAL RESULTS OF BEAM-COLUMN-SLAB SUBASSEMBLAGE TESTS

This chapter presents a description of the experimental results obtained from the testing of Specimens S1, RS1 and RS2. It is noted that Specimens S1 and RS1 were tested by Castele (1988), while Specimen RS2 was constructed and tested in this research program and will be compared with the results of the other two specimens. The reversed cyclic loading was simulated by the application of vertical loads at the end of the main beam at a distance of 2000 mm from the centre of the column. The lever arm for determining the maximum moment in the beam is 1800 mm for Specimens S1 and RS2 and 1700 mm for Specimen RS1. For determining the loading on the beam, the effects of the self weight of the beam, slab and the loading apparatus were added to applied loads. The additional moments at the column faces were 22.8 kNm for Specimens S1 and RS1 and 22.1 kNm for Specimen RS2.

The response of the unretrofitted Specimen S1, having a weak column and strong beam and also having deficient detailing in the column and joint region will be discussed first in order to provide a basis of comparison of the responses of the retrofit Specimens, RS1 and RS2.

5.1 Specimen S1

Specimen S1 was tested at McGill University by D. Castele (1988). It was designed and detailed according to the 1984 CSA and 1985 NBCC codes for nominal ductility. Specimen S1 is the basis for both column strengthening techniques used in Specimens RS1 and RS2.

5.1.1 Load-Deflection Response

The load deflection response for Specimen S1 is shown in Fig. 5.1. The second positive half cycle reached a peak load of 187 kN corresponding to a moment of -259.4 kNm with a downwards tip deflection of 14 mm. Similarly in the negative loading portion of this cycle, yielding of the bottom longitudinal beam bars occurred at an applied load of -102 kN (moment of 206 kNm) with an upwards tip deflection of -5.0 mm. General yielding in the positive loading direction increased to 215 kN with a corresponding tip deflection, Δ_y^+ of 25 mm. In the negative loading direction, general yielding was reached with an applied load of -154 kN with an upwards tip deflection, Δ_y^- of -18 mm. Specimen S1 reached a peak positive applied load of 226 kN in cycle 4A corresponding to a moment of -430 kNm at the column face. The maximum negative load reached was 163 kN corresponding to a moment of 271 kNm, in the fourth loading cycle.

The maximum deflection in the positive direction was 69 mm representing a displacement ductility factor of 2.7. The corresponding load for this peak deflection was 91% of the load at general yield. In the negative loading direction, a maximum upward tip deflection of -29 mm occurred at a load of -163 kN. This corresponds to a displacement of 1.6 times the deflection at general yielding.

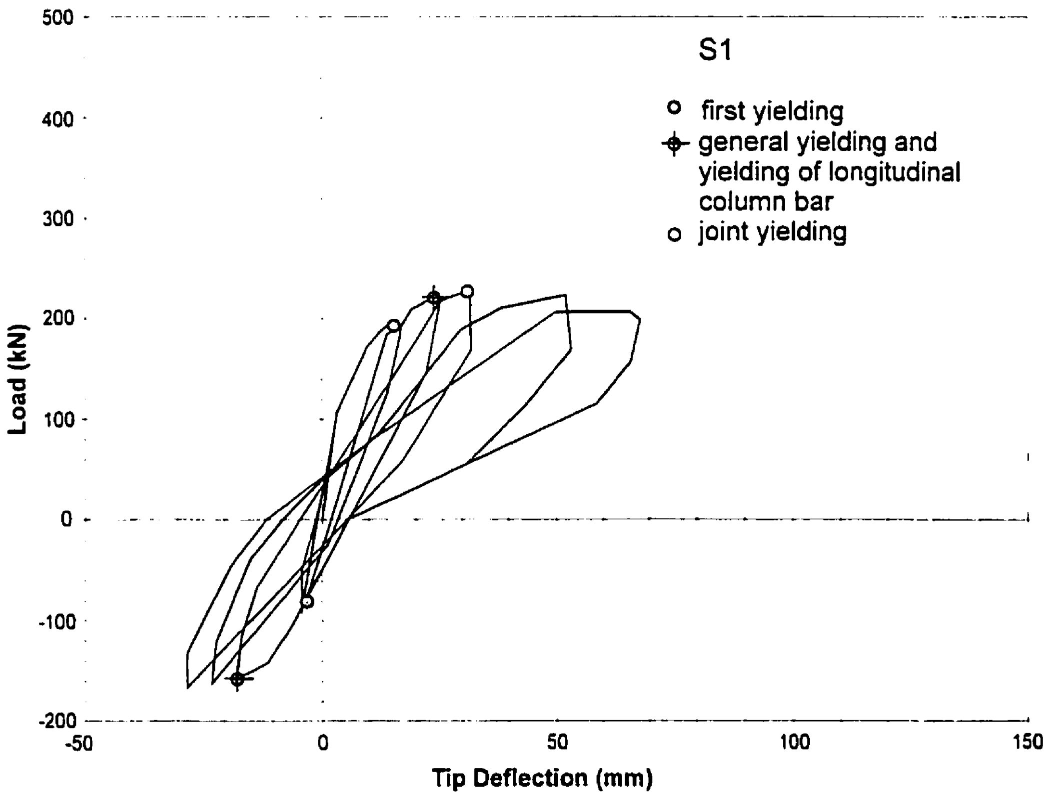

Figure 5.1: Load versus tip deflection response for Specimen S1

5.1.2 Beam Behaviour

The first flexural cracks in the main beam occurred at the column face at an applied load of 88 kN. By the end of the second cycle, cracking had extended nearly 1100 mm (2*d*) from the face of the column. These cracks were vertical near the top of the beam and as they extended into the depth of the beam they became more inclined. These diagonal cracking patterns were due to the shear and moment developed in the beam. In the third cycle, fanning of the shear cracks was observed near the joint region for both loading directions. It was in the negative half-cycles that larger cracks were observed, reaching a maximum crack width of 3.0 mm during the fifth cycle. Although flexural yielding occurred in the beam, the response of the beam was limited by general yielding of the column and yielding of the joint shear reinforcement. The shear cracks remained small and well distributed along the length of the beam. No beam stirrups yielded nor did any concrete spalling occur in the beam compression zone. Fig. 5.2 shows the beam at maximum positive tip deflection.

The measured curvatures along the length of the beam were very small throughout the test with a fairly linear distribution. This is shown for several key load stages in Fig. 5.3. The curvature at general yielding was 6.7×10^{-3} rad/m at the joint face. This value further increased to 10.0×10^{-3} rad/m by the end of the test. These small curvatures represent very little participation from the main beam in the response of the specimen. The shear strain in the beam was obtained using the mechanical targets placed in the form of rosettes along the length of the beam.

The shear strains in the beam are shown in Fig. 5.3 at certain key loads. The largest values of shear strain were found to be in close proximity of the joint region. The measured shear strains for this specimen have considerable scatter due to the discrete nature of the cracking with some of the cracks not passing through the rosettes. The largest value of shear strain was 1.2×10^{-3} rad in cycle 5A at a load of 215 kN.

5.1.3 Slab Behaviour

The strain distribution of the longitudinal slab bars over the width of the slab is shown in Fig. 5.4. The measured strains were relatively small. It was noted that the inner west slab bar was the first to yield during the second loading stage of the test. In the next cycle, the middle set of reinforcing slab bars yielded. As can be seen from Fig. 5.4 the outermost bars did not reach yield. Therefore, only bars within a distance of $4h_f$ from the beam face exceeded yield strain. The largest recorded strain was $1.8\varepsilon_y$, significantly less than the strain hardening value of $12.8\varepsilon_y$. The slab strain distribution is influenced by both shear lag effects and the torsional behaviour of the spandrel beams. In order to achieve large strains in the slab bars, the torsional resistance of the spandrel beam must be sufficient.

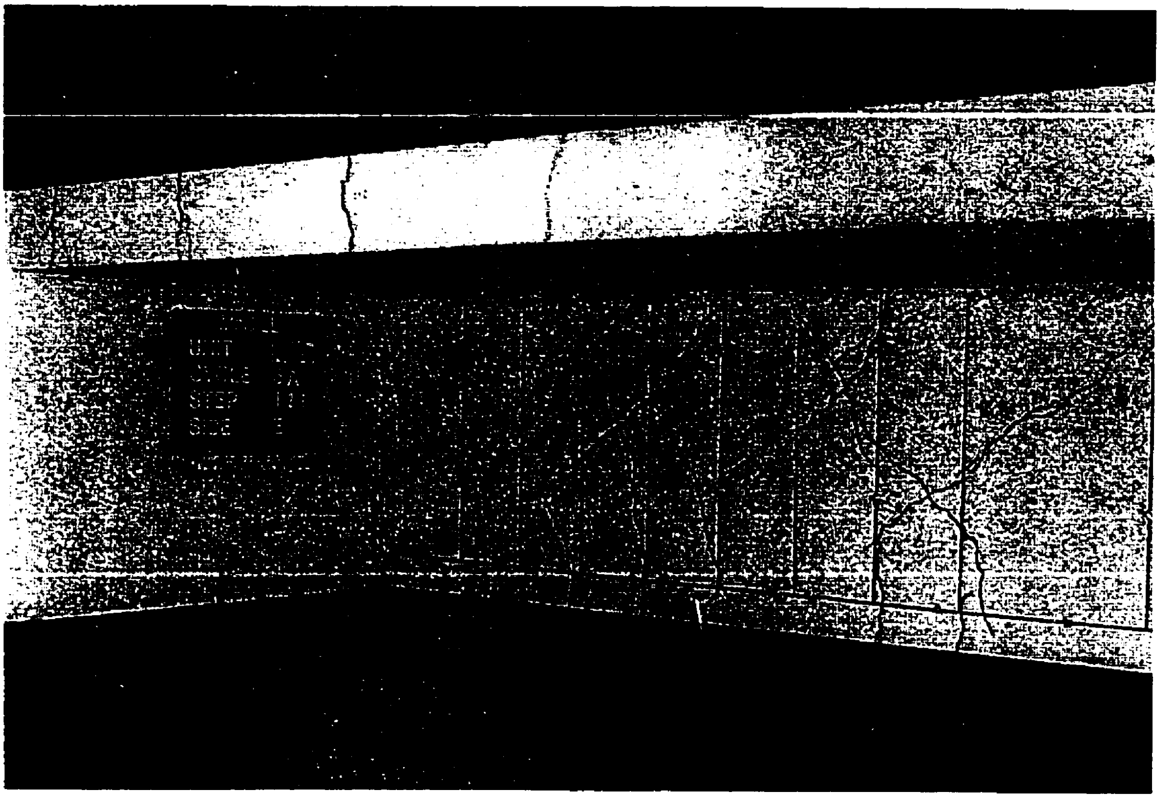

Fig. 5.2: Specimen S1 at maximum tip deflection

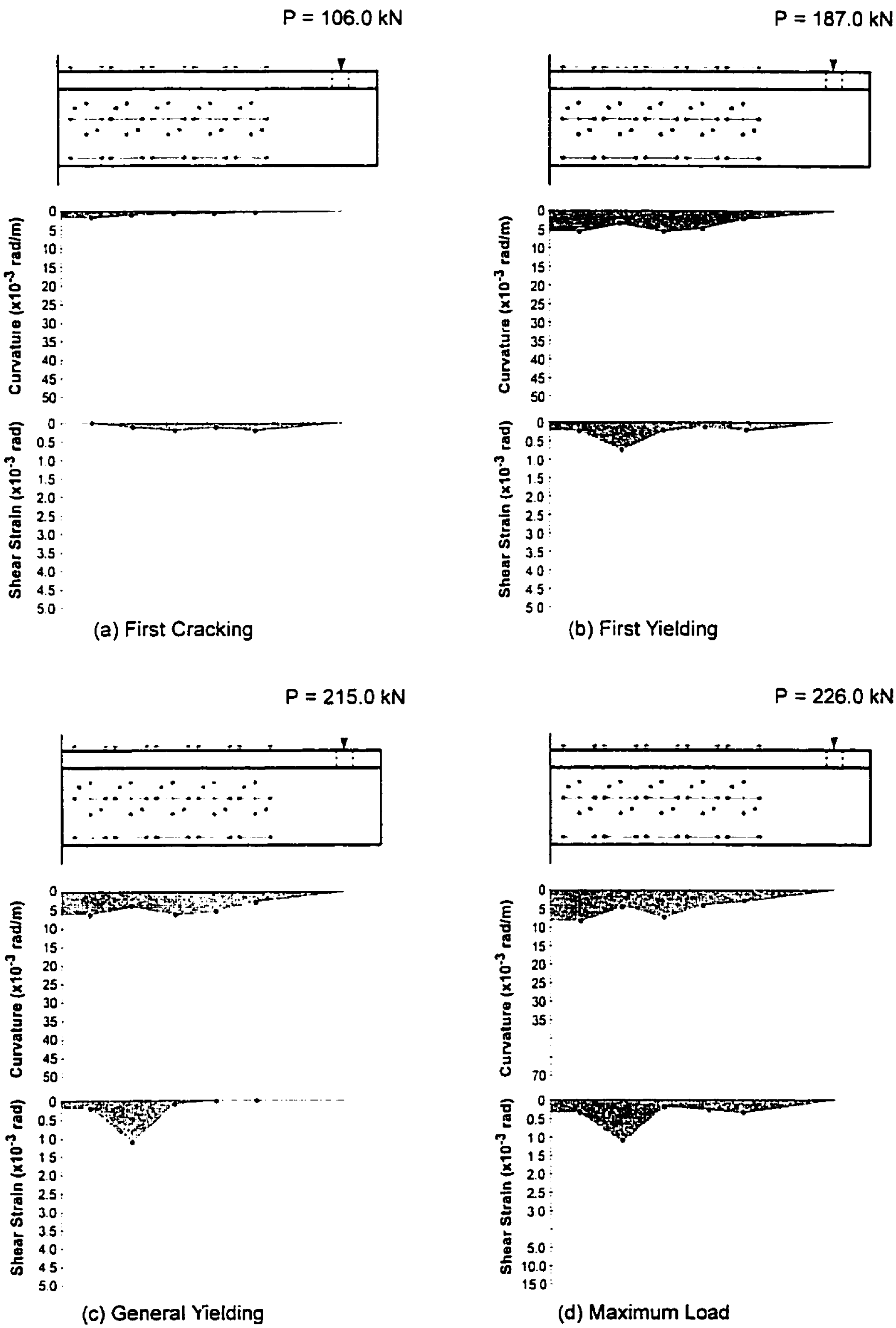

Figure 5.3: Curvature and shear strain plots for Specimen S1

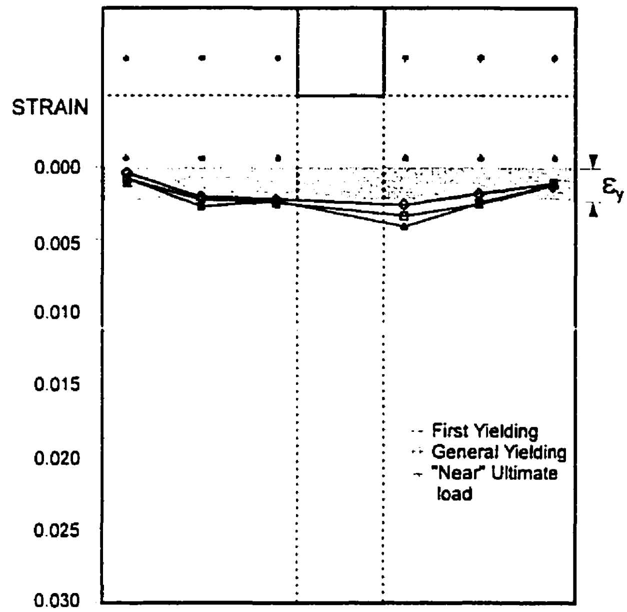

Figure 5.4: Distribution of strain in slab longitudinal bars for Specimen S1

5.1.4 Spandrel Beam Behaviour

Torsional cracking of the spandrel beam occurred during the first cycle of loading. Full depth torsional cracks were present when general yielding occurred in the main beam in the positive loading direction. The torsional cracks began at the sides of the column and propagated downward at approximately a 45° angle over the entire depth of the beam. As the loading progressed, cracks formed along the column-slab interface. At the maximum positive applied load, some spalling of the back cover of the spandrel beam was observed, with some cracks exceeding 2.5 mm in width. By the fifth cycle, major torsional distress was apparent, with crack widths measuring larger than 4.0 mm. Near the end of the test, a significant portion of the back concrete cover of the spandrel beam was lost due to spalling. In addition large cracks passed through the joint region (see Fig. 5.5). It was clear that from such distress, that the spandrel beam had yielded in torsion.

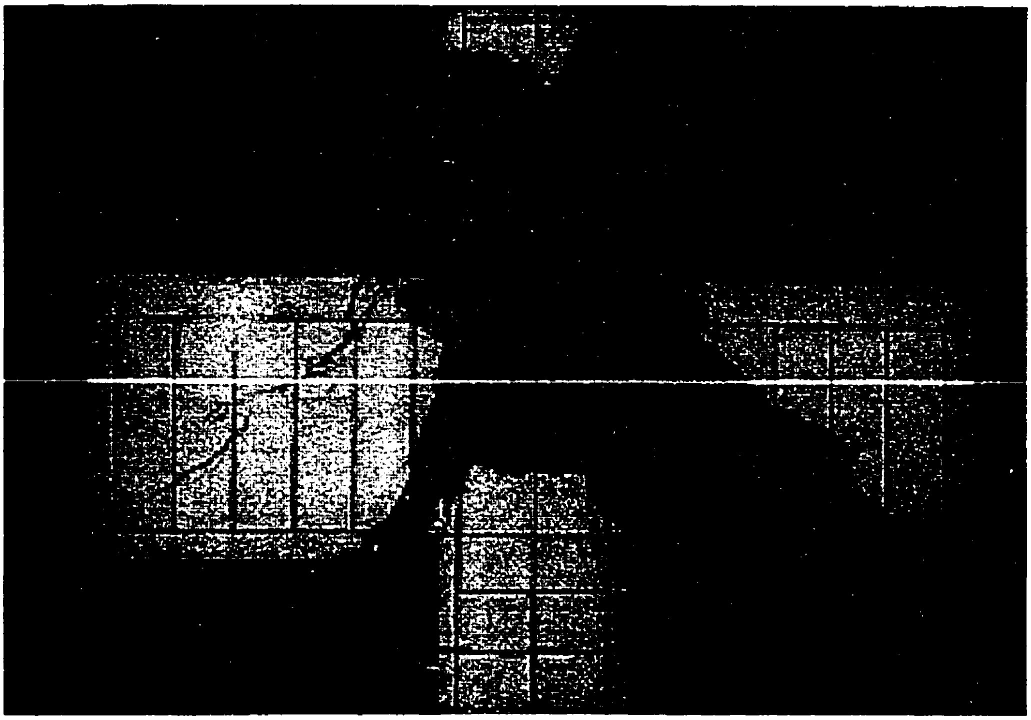

Fig. 5.5: Distress in Spandrel beam of Specimen S1 at end of test

5.1.5 Column Behaviour

Hairline flexural cracks first appeared on the north face of the top column as early as the second loading cycle. By the third loading cycle, these cracks had extended into the column core and became inclined toward the joint region. A small vertical crack extending 300 mm up from the slab level was observed on the east column face at the location of the back row of the column vertical bars. By the end of the test, this crack extended to a height of 600 mm above the slab surface having a maximum width of 6.0 mm, clearly exposing the vertical reinforcing bars (see Fig. 5.6). From the strains measured from the electrical resistance strain gauges, yielding of the column vertical bars first occurred at the slab interface. At the peak load of 226 kN in the fourth cycle, yielding of the column bars had progressed 100 mm above the level of the slab with a second vertical crack appearing at the centre of the east column face. Severe spalling of the concrete cover on the south face of the top column was evident by the fifth cycle. By the end of the test, the back cover had almost completely separated from the concrete core. A 3.0 mm wide crack was detected at the north-face column slab interface. Cracking patterns were similar in the bottom column near the joint region due to upward loading, although distress was not as severe.

Significant rotations of the top column were observed at the joint face. The curvature of the column at general yield was 6.8×10^{-3} rad/m increasing sharply to 42×10^{-3} rad/m near the end of the test. It is clear that the large inelastic deformations that took place in the column limited the beam response, resulting in an undesirable behaviour and reduced ductility.

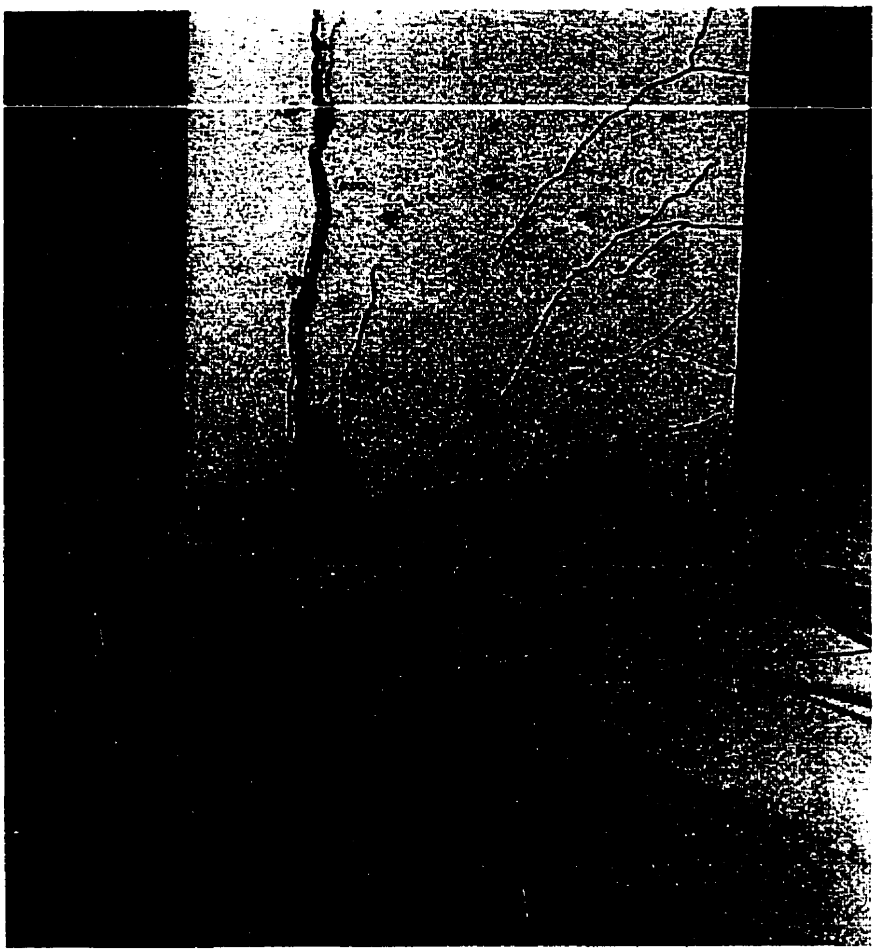

Fig. 5.6: Distress in top column of Specimen S1 at maximum tip deflection.

5.1.6 Joint Behaviour

The purpose of a well designed joint region is to provide proper anchorage for the beam longitudinal reinforcement, to confine the concrete core and to resist shear in the joint. The response of Specimen S1 to lateral loading did not reflect adequate joint design. By the peak load of 226 kN in cycle 4A, one of the two joint ties had reached yield. The second joint tie yielded in the fifth cycle, decreasing the load carrying capacity by 11%.

Torsional cracks in the spandrel beam and shear cracks from the top column in the fourth cycle had extended in to the joint core. This caused the spalling of the back joint cover in the fifth cycle.

To measure the joint distortion and bond slip, horizontal dial gauges were used to measure the relative horizontal movement between the top surface of the slab and the column. Significant relative movements were measured, indicating that there was severe joint distress.

5.2 Specimen RS1

Specimen RS1 was tested at McGill University by D. Castele (1988). The column was retrofit with a reinforced concrete sleeve to increase its column capacity and therefore ensuring the proper hierarchy of yielding of the main beam before the column. The purpose of Specimen RS1 was to compare the improved response with the response of the poorly detailed Specimen S1.

5.2.1 Load-Deflection Response

The applied load versus tip deflection response of Specimen RS1 is shown in Fig. 5.7. First flexural yielding occurred in the second positive loading cycle at a peak applied load of 173 kN and a corresponding tip deflection of 6.0 mm. Similarly in the second negative loading cycle, the peak load reached was -101 kN with a corresponding -3.0 mm upwards deflection. At the stage of general yielding in cycle 3A, a peak applied load of 349 kN was reached resulting in a downwards tip deflection, Δ_y^+ of 27 mm. In the negative loading direction of the third cycle, an applied load of -130 kN was reached causing an upwards tip deflection, Δ_y^- of -7.0 mm and general yielding under negative loading. The maximum applied load of 417 kN, corresponding to a negative bending moment of 732 kNm at the column face, was reached in the sixth positive loading cycle. The tip deflection reached for this loading was 73 mm.

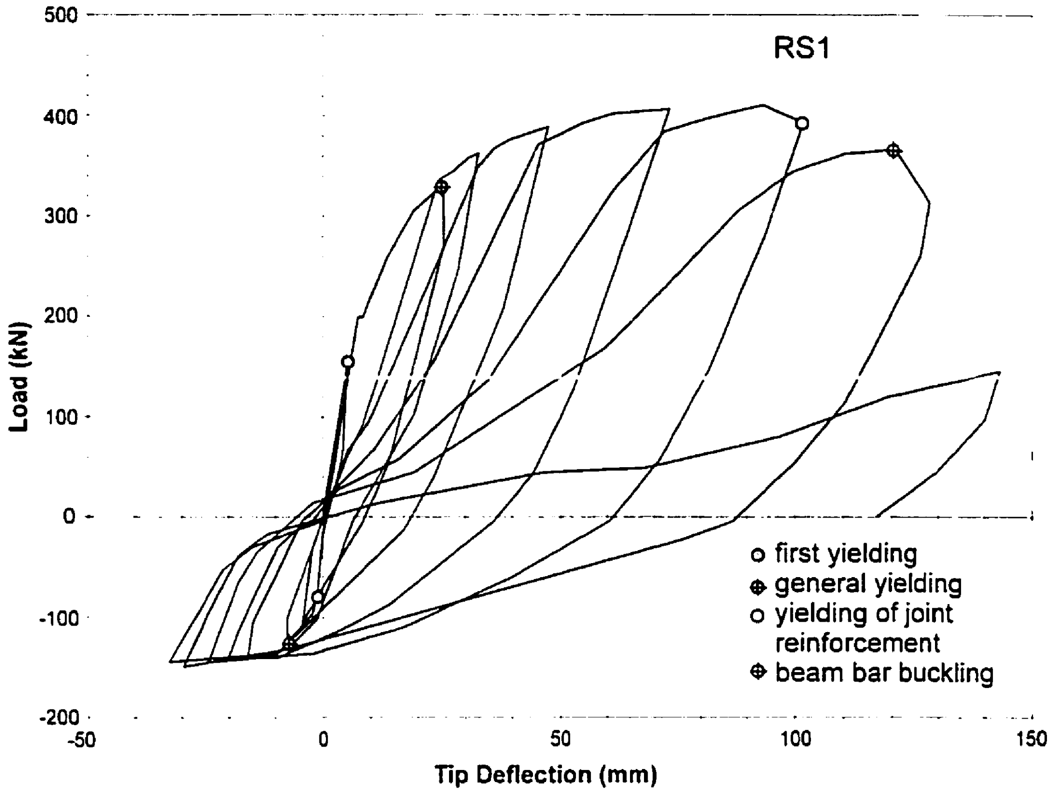

Figure 5.7: Load versus tip deflection response for specimen RS1

The peak deflection achieved in the positive loading direction was 144 mm, representing a displacement ductility of 5.3. However, due to the severe buckling of the longitudinal beam bars, in combination with the loss of concrete within the beam core due to severe spalling and crushing, the load carrying capacity had dropped to 149 kN.

In the negative loading direction, a peak load of -145 kN was reached with an upwards tip deflection of -29 mm. The peak upwards tip deflection reached was -33 mm with the load remaining constant at -144 kN. The hysteresis curves remained very stable in the negative loading direction, and it is believed that this specimen still contained some strength and ductility in this direction.

5.2.2 Beam Behaviour

During the first loading cycle, the first flexural cracks appeared at a distance of 50 mm from the column face at the applied load of 80 kN. The peak applied load for the first cycle in the positive direction was 95 kN equivalent to a moment at the column face of -184 kNm. The tip deflection of the beam was 1.9 mm downwards. By the third loading cycle, the flexural cracks had propagated through the entire depth of the beam, with the cracks being inclined toward the compression zone at the column face. The cracks were evenly spaced at 260 mm over a length of $2d$. In the fourth loading cycle, slight spalling was detected at the bottom of the beam near the column face as the compression zone started to crush. At the peak positive load in loading cycle 6A, well distributed shear cracks extended the full depth of the main beam and fanning of the compressive struts was observed near the joint region. During this loading cycle, crack widths had reached a maximum width of 3.0 mm, while strain readings had confirmed that several beam stirrups had yielded.

In the eighth positive loading cycle, the bottom beam cover was lost over a distance of 300 mm from the column face. This is due to the buckling of the bottom longitudinal beam bars. The maximum attainable load had dropped significantly, reaching only 43% of the load reached at general yielding. This was due mainly to the fact that nearly one-third of the concrete beam core was missing. The condition of the beam at key load stages is shown in Fig. 5.8, whereas Fig. 5.9 reveals the buckling of the bottom longitudinal bars near the end of the testing.

The curvature was measured along the length of the beam using mechanical targets which were monitored throughout the duration of the test. Shown in Fig. 5.10, is the curvature distribution along the length of the beam at various load stages. From this figure it can be seen that once general yielding had been reached, very large curvatures were recorded near the joint face during positive loading. Outside of this region, the curvatures were much smaller and varied linearly towards the end of the beam. At the joint face, curvature readings ranged from 15.1×10^{-3} rad/m at first yielding, to 71×10^{-3} rad/m at a displacement ductility of 3.8. It was apparent that the length of the plastic hinge extended at least 400 mm from the joint face.

The distribution of shear strain along the length of the main beam is also presented in Fig. 5.10. The strains appeared to increase linearly from the point of load application to the face of the column. The maximum shear strain recorded was 14.9×10^{-3} rad in cycle 7A at a displacement ductility of 3.8. It is noted that the majority of shear cracking did not pass through the strain rosettes for this specimen and therefore the shear strains would be considerably larger than the values given above.

5.2.3 Slab Behaviour

The distribution of longitudinal strain in the slab reinforcement is shown in Fig. 5.11. We see that in the second cycle, all slab bars remained elastic. It is not until the third cycle that the inner four slab bars have reached yield. By the fourth cycle however, all slab longitudinal reinforcement had reached yield. Near the end of the test, it was determined that some bars had even reached strain hardening, this was further confirmed by the fracture of the west inner slab bar. Extremely large cracks were detected across the full width of the slab at the locations of the transverse slab bars. The largest crack resulted in a 9.0 mm separation which was recorded at the front column face during the seventh cycle. The large strain measurements indicate that the full width of the slab had participated in the moment resisting response of this specimen.

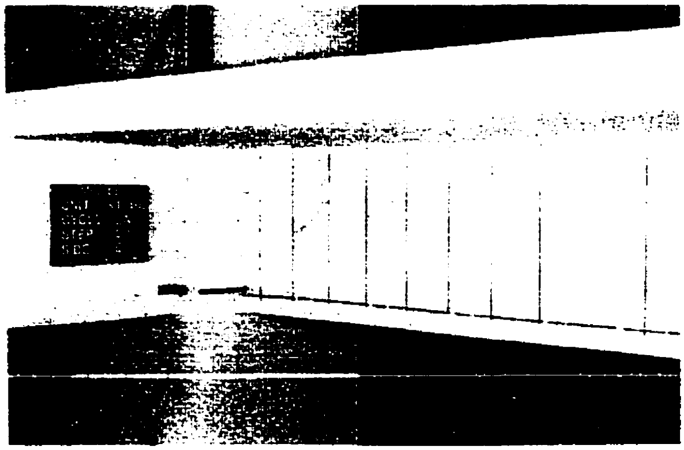

(a) First yielding, P = 173 kN

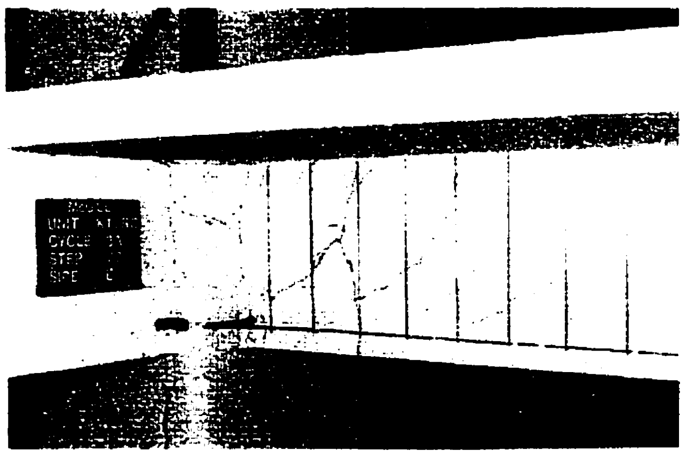

(b) General yielding, P = 349 kN

(c) Near end of test, P = 375 kN

Figure 5.8: Beam behaviour of Specimen RS1 at various stages of testing

Fig. 5.9: Buckling of bottom longitudinal beam bars of Specimen RS1

5.2.4 Spandrel Beam Behaviour

The column strengthening technique used on Specimen RS1 decreased the length of each spandrel beam by 100 mm. As a result fewer slab longitudinal reinforcing bars were anchored into the top of the spandrel beam, thus reducing the applied torsion on the spandrel beams. Torsional distress was less severe in this specimen. However, by the peak positive load of cycle 6A, torsional cracks had reached widths of 2.5 mm which extended the full depth of the spandrel beam. This indicated that some of the torsional reinforcement had reached yield. Only slight spalling of the back concrete cover of the spandrel beam was observed around the inclined cracks.

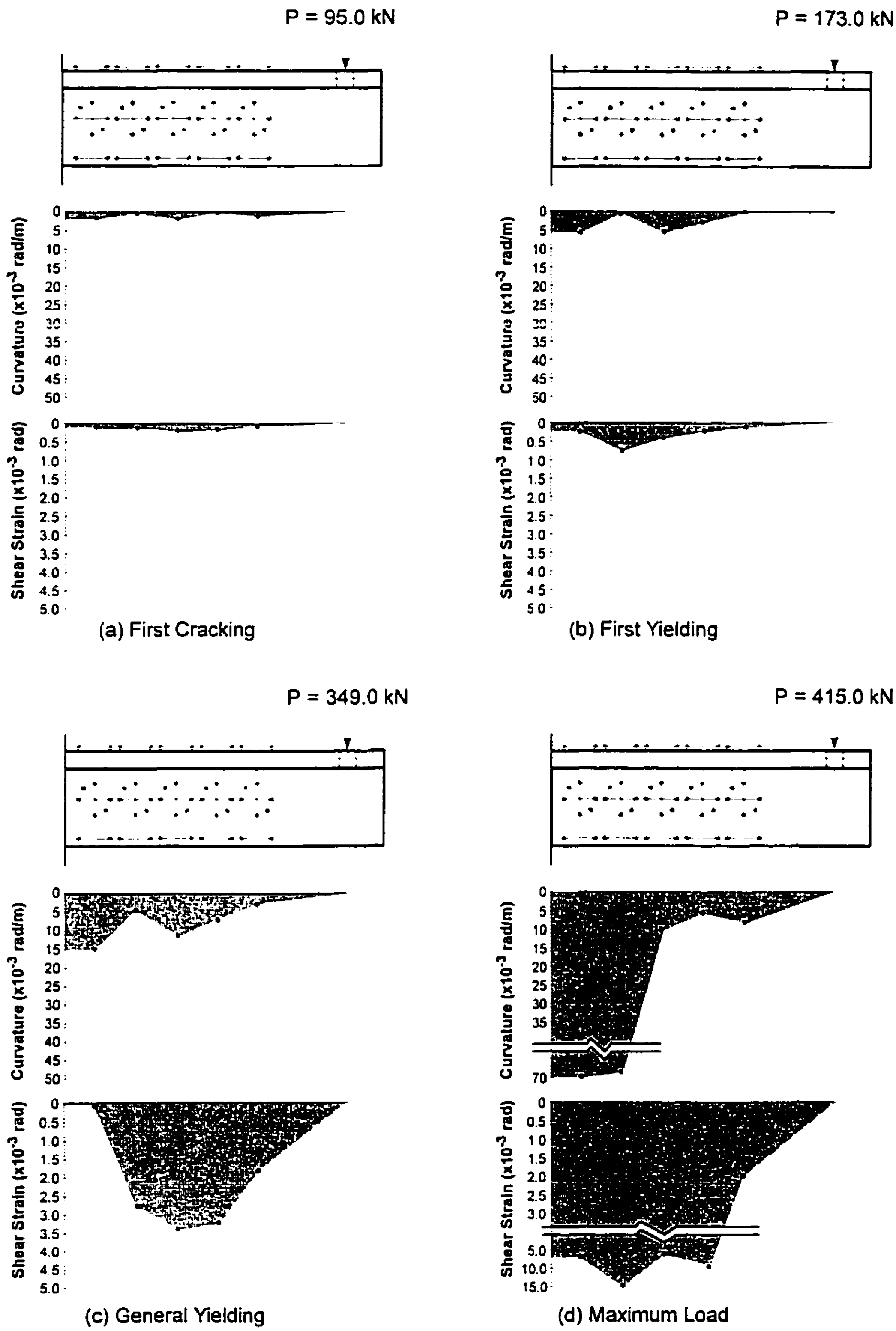

Figure 5.10: Curvature and shear strain plots for Specimen RS1

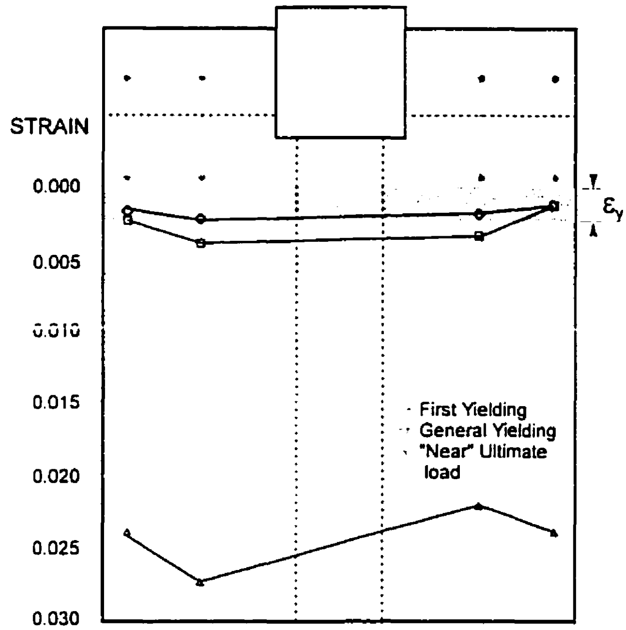

Figure 5.11: Distribution of strain in slab longitudinal bars for Specimen RS1

5.2.5 Column Behaviour

The strengthened column remained essentially elastic for the duration of the test. Hairline shrinkage cracks were observed in the new concrete at the locations of the added hoops, these shrinkage cracks did not appear to open during the test. The strains from the electrical resistance strain gauges, indicated that the original column vertical bars, as well as the added vertical bars, were well bellow yield. At the peak load of 417 kN, corresponding to a negative bending moment of 732 kNm at the column face, a strain of 0.0013 or 60% of the yield strain in the No. 30 added vertical bars was measured. Very minute splitting and diagonal shear cracks were observed on the front face of the lower column during the latter stages of the test. These cracks, which never exceeded 0.2 mm in width, were thought to be caused by the spreading of the load into the enlarged column.

Column curvatures were well controlled in Specimen RS1, with a maximum curvature recorded in the top column of 5.0×10^{-3} rad/m in the seventh or peak loading cycle. No significant flexural cracking was observed in the column. It became quite evident that the strengthening of the column inhibited inelastic actions in the column and permitted the development of flexural hinging in the main beam.

5.2.6 Joint Behaviour

The joint response was significantly improved due to the strengthening technique chosen. The electrical resistance strain gauges on the joint ties indicated that both the original ties and added ties had reached yield strains as the applied load reached 415 kN. The placement of the additional ties proved to be effective in resisting joint shears from this type of loading. Near the end of the test, slight splitting cracks were observed on the south face of the joint concrete cover. These cracks extended into the top column cover, but remained less than 0.1 mm in width.

Slight separation of the new and old concrete was detected in the joint region where the No. 30 added longitudinal reinforcement passed though the slab. This was the only indication of any loss of bond between the new and the existing concrete.

Dial gauges which were used to measure the relative movement of the slab with respect to the column, as well as measuring the bond slip, revealed significant joint deformation in Specimen RS1 near the end of the test. However, the increased column and joint region delayed the occurrence of yielding in the joint until well after general yielding of the beam.

5.3 Specimen RS2

Specimen RS2 is the beam-column-slab subassemblage which had a column which was retrofit by adding vertical corner angles and welding batten plates to these angles.

5.3.1 Load-Deflection response

The beginning of each cycle began with the application of a downward or positive load, to cause negative bending moments in the main beam. This positive portion of the cycle is referred to as half cycle "A", whereas the negative portion of the cycle is known as half cycle "B". The applied load versus deflection response for RS2 is shown in Fig. 5.12. The peak loads for each half cycle with corresponding tip deflections are summarised in Table 5.1.

The appearance of the first cracks were observed at a positive applied load of 118.1 kN. This load corresponded to a tip deflection of 3.6 mm and a cracking moment, M_{cr}^{-} of 235 kNm. Similarly in the negative portion of the cycle, an applied load of 69.4 kN caused the first cracks to appear, with a downward tip deflection of 2.3 mm and a cracking moment, M_{cr}^{+} of 103 kNm. The peak load of the first cycle was chosen to be 1.2 M_{cr}. Therefore the peak applied load of half-cycle 1A was 141.7 kN, with a tip deflection of 5.0 mm and a negative bending moment of 277 kNm. In half-cycle 1B, the peak applied load was -86 kN, resulting in an upward tip deflection of -3.9 mm and a bending moment of 133 kNm.

The next loading cycle (2A-2B) corresponded to the first yielding of the longitudinal steel in the main beam. This was determined by closely monitoring the steel strains provided by the strain gauges glued to the reinforcing bars. In the positive loading direction, first yield occurred at an applied load of 237.8 kN corresponding to a negative bending moment of 450 kNm. The yielding of the bottom bars occurred at a negative load of 100.9 kN and a positive bending moment of 159.5 kNm.

The peak load of the third cycle was determined by the general yield of the beam longitudinal bars. In cycle 3A, this occurred at a load of 251.8 kN causing a tip deflection, Δ_y^{+} of 21.4 mm and a bending moment at the face of the column of -475 kNm. An upwards load of -114.3 kN was required to achieve general yielding in the negative loading direction. This resulted in a deflection of Δ_y^{-} = -5.9 mm and a bending moment of 184 kNm. The peaks of the remaining cycles were chosen as multiples of the yield deflections (Δ_y) that occurred in the third cycle.

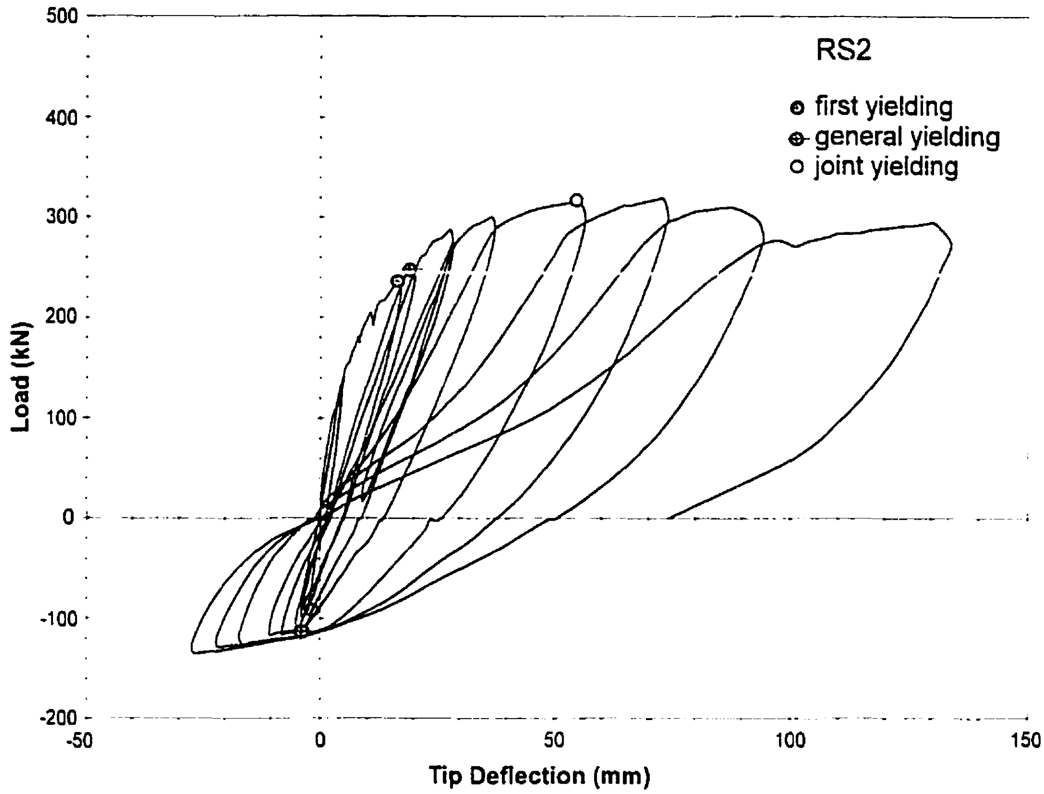

Figure 5.12: Load versus tip deflection response for Specimen RS2

In the positive direction, the maximum load was reached in the seventh cycle at a deflection of 80.4 mm ($4\Delta_y^+$). The peak load during this stage was 318.5 kN, equivalent to a negative bending moment of 595 kNm at the face of the column. In the negative direction, the peak applied load of -134.9 kN occurred in the eighth cycle at a deflection of -29.3 mm ($5\Delta_y^-$) The corresponding bending moment for this load was 220 kNm.

The maximum ductility levels reached in the test were $7\Delta_y^+$ (136.4 mm) in the positive loading direction and $5\Delta_y^-$ (-29.3 mm) in the negative loading direction. The test was stopped at the end of half-cycle 9A due to the limitations of the travel of the loading rams, even though the applied loads in the negative cycle were consistently increasing with increasing tip deflection. The hysteretic loops show good energy dissipation although some signs of pinching occur during and after the fifth loading cycle.

Table 5.1: Applied loads and tip deflections at cycle peaks for Specimen RS2

Cycle	Cycle Description	Applied Load (kN)	Tip Deflection (mm)
1A	1.2 M_{cr}	141.7	5.0
1B		-86.0	-3.9
2A	First Yield	237.8	18.0
2B		-100.9	-4.4
3A	General Yield	252.8	21.4
3B		-114.3	-5.9
4A	$1.5\Delta_y^+$	286.7	30.8
4B	$1.5\Delta_y^-$	-116.3	-8.4
5A	$2\Delta_y^+$	300.1	40.2
5B	$2\Delta_y^-$	-117.0	-11.2
6A	$3\Delta_y^+$	317.4	60.3
6B	$3\Delta_y^-$	-126.0	-17.8
7A	$4\Delta_y^+$	318.5	80.4
7B	$4\Delta_y^-$	-128.2	-24.8
8A	$5\Delta_y^+$	309.7	94.7
8B	$5\Delta_y^-$	-134.9	-29.3
9A	$7\Delta_y^+$	294.2	136.4

5.3.2 Beam Behaviour

First cracking of the slab and main beam occurred in cycle 1A. The slab experienced cracking over its entire width, with crack widths ranging from 0.08 to 0.15 mm. Two cracks measuring 0.08 mm in width extended from the bottom surface of the slab to mid-height of the beam. The cracks were located at distances of 55 mm and 300 mm from the face of the spandrel beam corresponding to the location of U-stirrups in the beam. Two additional cracks were detected in half cycle 1B and were also located at the positions of U-stirrups. These cracks, measuring 0.08 mm in width, began at the bottom of the beam and propagated to midheight of the beam.

In cycle 2A, aside from the lengthening and widening of the existing cracks, two new cracks formed in the beam. These new cracks were more inclined, and were due to the combined effects of bending and shear. The maximum flexural crack width was found to be 0.3 mm, located 55 mm away from the face of the spandrel beam. In the second negative half cycle, four new cracks were detected. Once again, these cracks, ranging in size of 0.08 mm to 0.5 mm, were formed directly over the location of the transverse beam reinforcement. In subsequent cycles, a number of new flexure and shear cracks formed with existing cracks increasing in size and width. The crack pattern at the end of the third cycle is shown in Fig. 5.13.

At the maximum positive load (peak of cycle 7A), the largest crack was 5.0 mm in width located at the stirrup closest to the column face. Some concrete crushing occurred at the bottom of the beam at the interface of the beam and the lower column as shown in Fig. 5.14. During the peak negative loading (8B), cracks had reached a maximum width of 10 mm at the mid height of the beam located 55 mm from the face of the column. In spite of the very large cracks, together with the spalling and crushing at the bottom surface of the beam, the beam was still able to carry 92% of the peak load reached during testing.

The curvature and shear strain distributions along the length of beam are plotted in Fig. 5.15. The maximum curvature and shear strain at yield in the positive direction was 3.65×10^{-3} rad/m and 0.48×10^{-3} rad respectively. The maximum recorded curvature occurred in the positive peak of the ninth cycle with a curvature of 38.01×10^{-3} rad/m. Similarly, the maximum shear strain was recorded to be 2.52×10^{-3} rad in half cycle, 7A, which corresponds to the maximum positive applied loading cycle. Due to the discrete nature of the cracks that formed, many of the cracks missed the gauge lengths of the mechanical targets glued to the concrete surface. Because of this, some of the curvatures and shear strains determined from the strain rosettes, readings have low values.

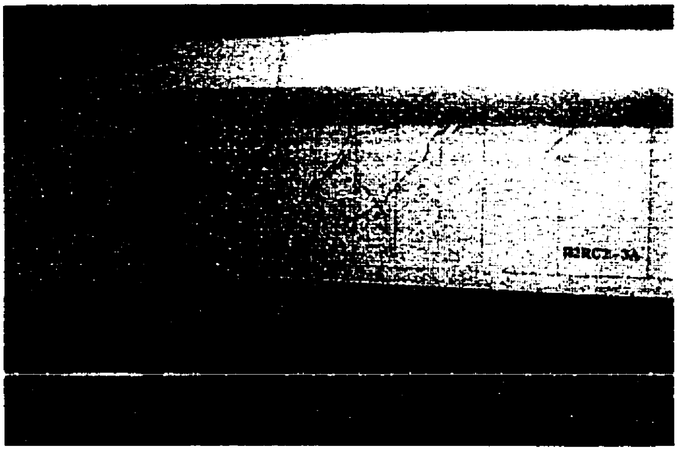

(a) General yielding, P = 252.8 kN

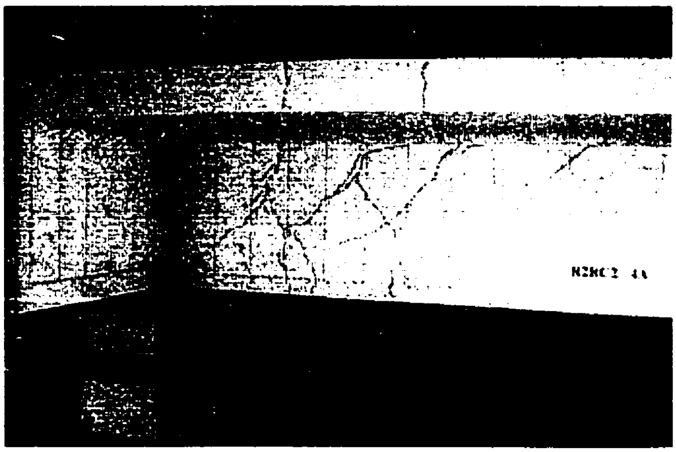

(b) $1.5\Delta_y^*$, P = 286.7 kN

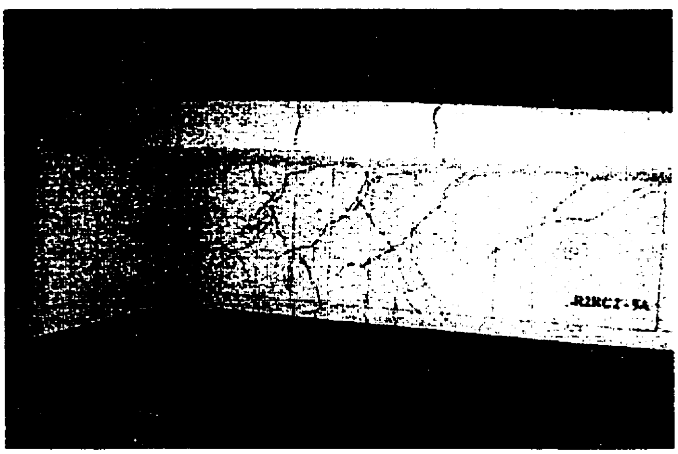

(c) Maximum deflection, P = 294.2 kN

Figure 5.13: Beam behaviour of Specimen RS2 at various stages of testing

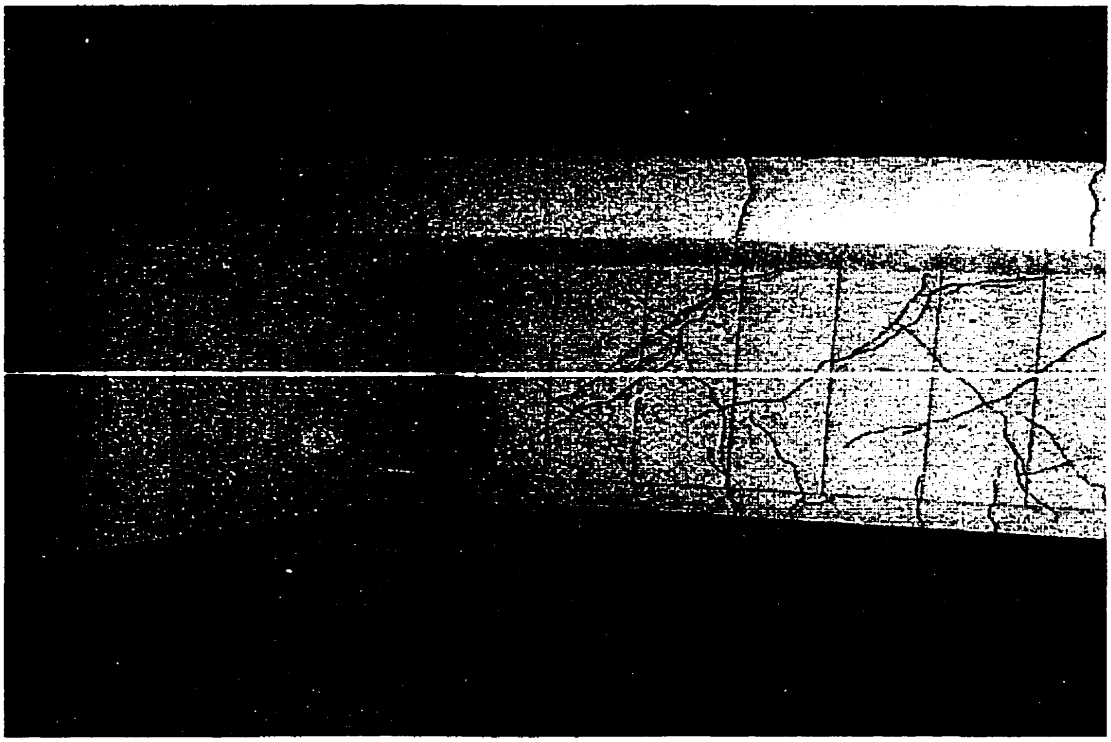

Fig. 5.14: Distress in Beam at column interface of Specimen RS2

5.3.3 Slab Behaviour

First cracking occurred during the first positive half-cycle, with further cracks occurring in subsequent positive half cycles. The two cracks that formed in cycle 1A, extended over the entire width of the slab and had crack widths ranging from 0.08 to 0.15 mm. These cracks formed directly over transverse reinforcing bars in the slab.

In the next positive half cycle, 2A, two additional cracks extending the full width of the slab were formed. The four cracks all coincided with the location of the slab bars and ranged in size from 0.08 to 0.3 mm.

Torsional cracks on the top surface of the slab immediately over the spandrel beam occurred in the third positive half-cycle. These small cracks (0.08 mm width) started from the east and west faces of the column and propagated to the external face of the spandrel beam. This can be seen in Fig. 5.16. In the final cycle, 9A, the cracks caused by torsion had increased to a maximum width of 10 mm.

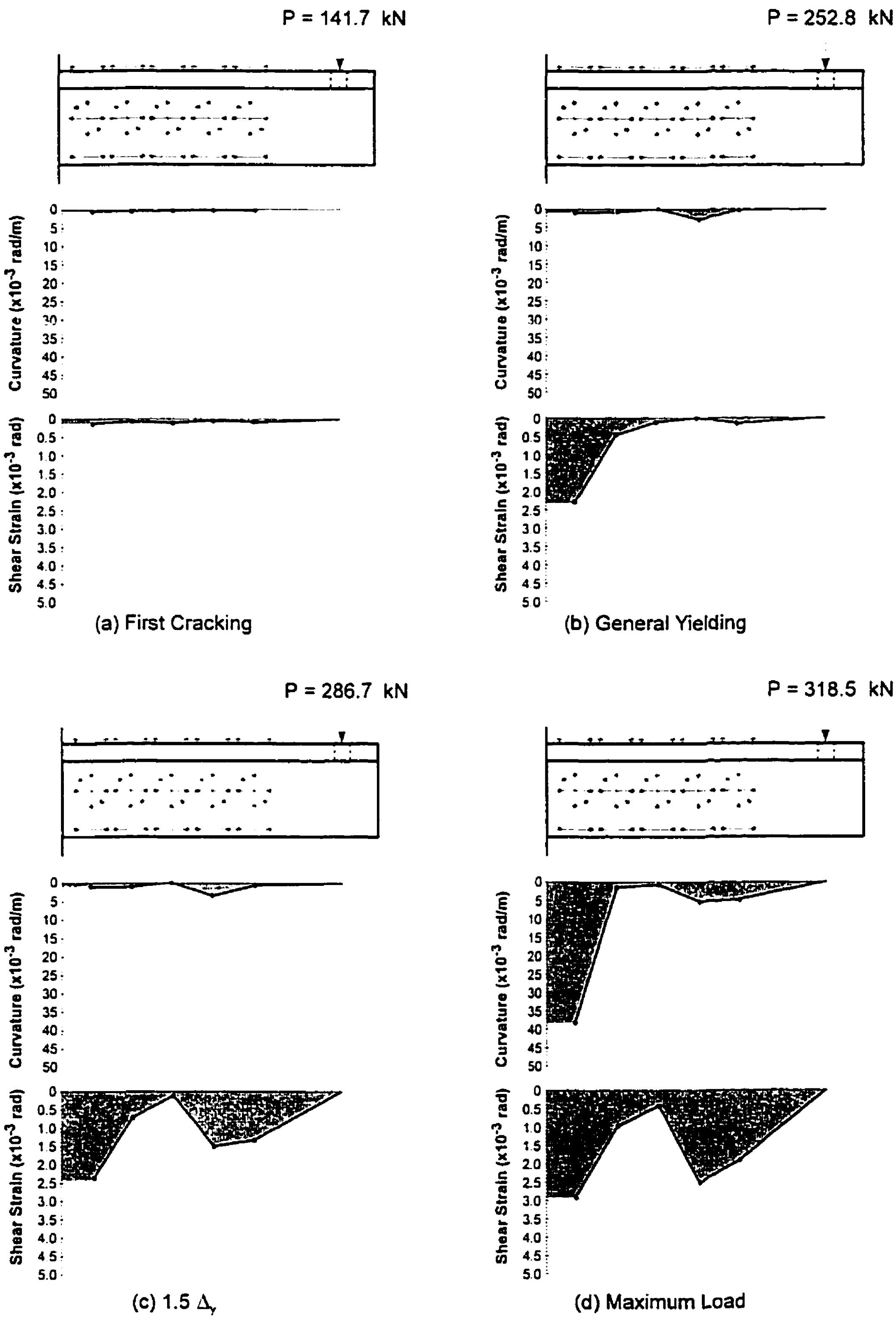

Figure 5.15: Curvature and shear strain plots for Specimen RS2

In the fourth cycle, cracks were formed around the loading beam. Also shown in Fig. 5.16, is the slab cracking pattern during the eighth cycle, where the crack at the face of the column had reached its maximum width of 8.0 mm.

Figure 5.17 shows the strain distribution in the longitudinal slab reinforcement for Specimen RS2. These measurements were taken from the two rows of mechanical targets which were glued to the slab top surface (gauge length of 200 mm). The shaded area on the plots represents the yield strain of the No. 10 longitudinal slab bars (ε_y = 0.00215). In row #1, it is interesting to note that at yield, only the four inner pairs of slab bars had reached yield, corresponding to the effective slab width in the CSA Standard. However, in the subsequent cycles, all 6 slab bar pairs reached yield. The values obtained from row #2 are not representative of the maximum strain in the longitudinal slab reinforcement because the cracks formed just outside of the gauge length (compare Fig. 5.16 and Fig. 5.17).

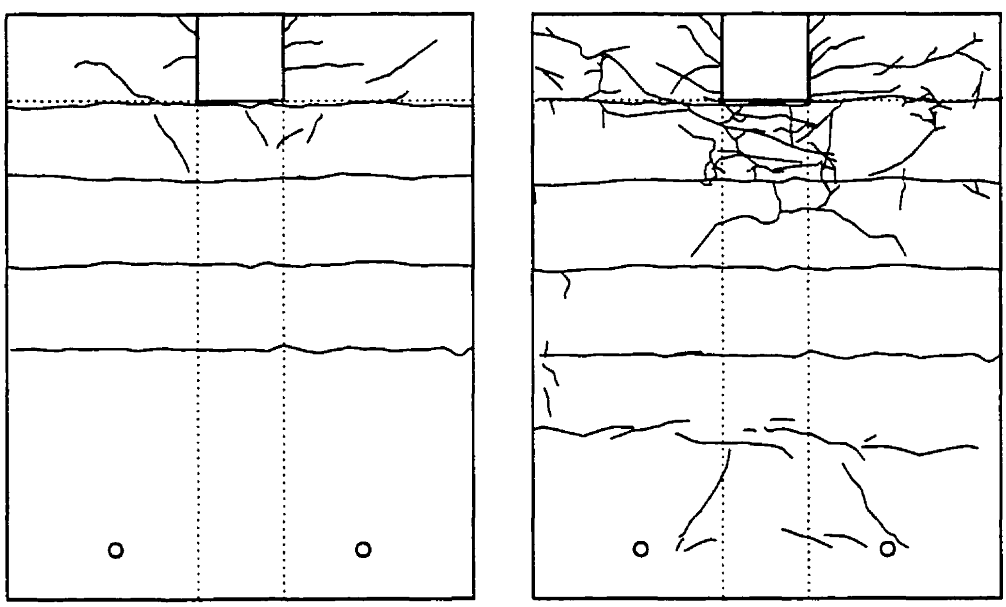

(a) Cycle 3A (b) Cycle 8A

Figure 5.16: Crack patterns in slab of Specimen RS2

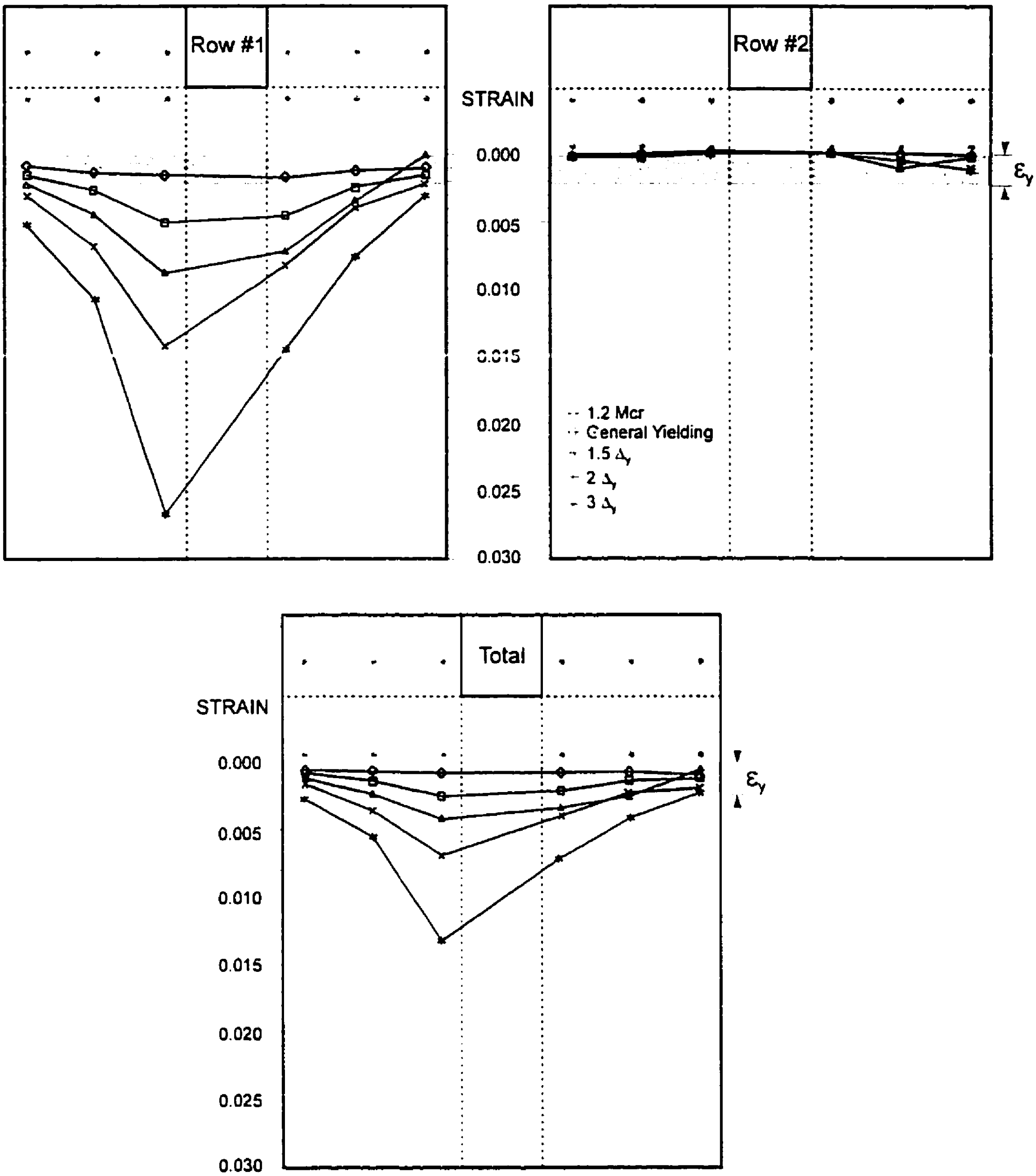

Figure 5.17: Distribution of strain in slab longitudinal bars for Specimen RS2

5.3.4 Spandrel Beam Behaviour

The first signs of distress in the spandrel beam occurred in the first cycle. Two torsional cracks extended from the top column-spandrel beam interface and propagated downwards at a 45° angle into the spandrel beam. Two vertical splitting cracks were also apparent, in the joint region of the spandrel beam. All cracks at this loading stage were less than 0.08 mm. No new cracks formed when the specimen was loaded in the negative direction during cycle 1B. However, during the second positive cycle, several additional torsional cracks on both sides of the column had formed, extending almost the entire depth of the spandrel beam. These cracks widths varied from 0.08 to 0.4 mm. Four new splitting cracks occurred on the outside face of the joint, lining up with the vertical bars in the column.

By the fifth positive loading cycle, cracks had started to form on the north face of the spandrel beam just under the level of the slab. During the eighth cycle, crushing of the column and spandrel beam were evident. At this stage, lateral movement between the ends of the spandrel beam and the joint region was 9.0 mm. By the final loading stage, extensive crushing, spalling and cracking had occurred as shown in Fig. 5.18.

Fig. 5.19 shows the torque versus twist response of the spandrel beam of Specimen RS2. The applied torque was determined from the calculated forces in the slab bars corresponding to strains measured in the slab bars. These forces were then multiplied by their eccentricity about the centre of rotation of the spandrel beam to obtain the applied torques. A more detailed description of these calculations are given in Section 6.5.

Fig. 5.18: Distress in Spandrel beam of Specimen RS2

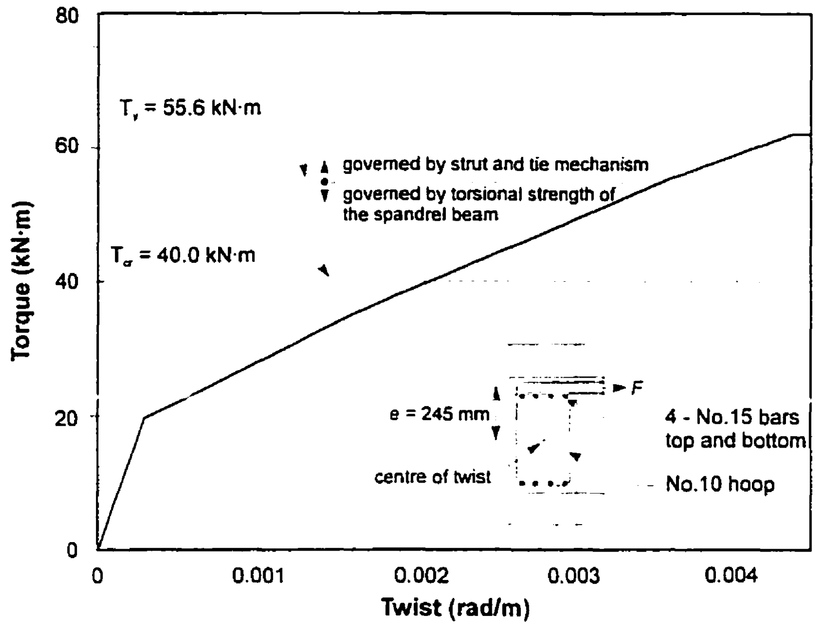

Figure 5.19: Torsional response of spandrel beam for Specimen RS2

5.3.5 Column Behaviour

The presence of batten plates immediately above and below the joint region made it impossible to observe the cracking in these critical regions. At the fourth positive cycle, a horizontal, 0.08 mm wide crack appeared on the south face of the lower column. The crack extended the entire width of the column at a location 250 mm below the bottom level of the spandrel beam. No other cracks were apparent on the exposed column faces until crushing occurred in the eighth positive cycle. Concrete crushing was evident on the south face of the upper column.

Fig. 5.20 shows the strains in the longitudinal column reinforcement at peak loads for all positive cycles during the testing of RS2. During the third cycle when general yielding of the beam occurred, the maximum tensile strain in the vertical bars in the column was about 75% of the yield strain. It can be seen that the first yielding of the column vertical reinforcement occurred in the fifth positive cycle. The two north bars in the top column reached yield in tension, whereas the bars on the south face did not yield. In the lower column, all bars remained elastic throughout the duration of the test. The smaller strains in the bottom column may be due to the higher axial load and higher compressive strength of the concrete in this region.

Figure 5.21 shows the strains experienced in the vertical steel corner angles at peak loads of the positive loading cycles. The strains the vertical angles of the steel retrofit remained quite small during the early stages of the test. During the third positive loading cycle when general yielding of the beam occurred, a maximum compressive strain equal to 698 $\mu\varepsilon$ occurred in two top south angles. At the first yielding of the column reinforcement (top north vertical bars) during the fifth cycle, a maximum compressive strain of 796 $\mu\varepsilon$ was recorded in the top south angles. Yielding of the steel angles occurred in the final cycle. The two top south angles reached 1854 $\mu\varepsilon$ in compression and the two bottom north angles experienced an increase in strain to 996 $\mu\varepsilon$ in compression, or about 60% of the yield strain. The other angles remained elastic with a maximum tensile strain of 600 microstrain. It is evident that the vertical corner angles had a significant participation in the latter cycles of loading.

The four very stiff horizontal collar angles (A_s = 2990 mm^2) above and below the joint, provided anchorage points for the vertical rods which passed through the slab. These collar angles provided significant horizontal clamping forces for the column immediately above and below the joint. A maximum tensile strain of 50 $\mu\varepsilon$ was recorded, representing approximately 1600 kN of tension. In the final cycle of loading, the weld between the vertical rod and the collar angle broke leading to a large concentrated rotation in the joint region.

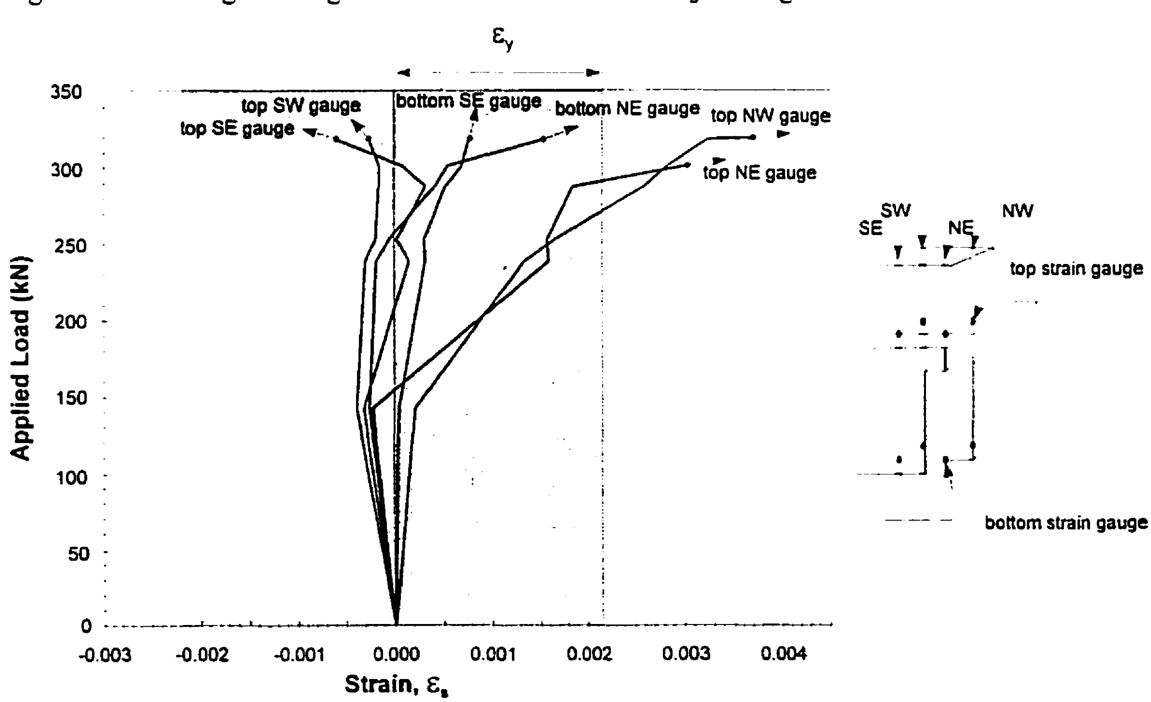

Figure 5.20: Strains in vertical column bars of Specimen RS2

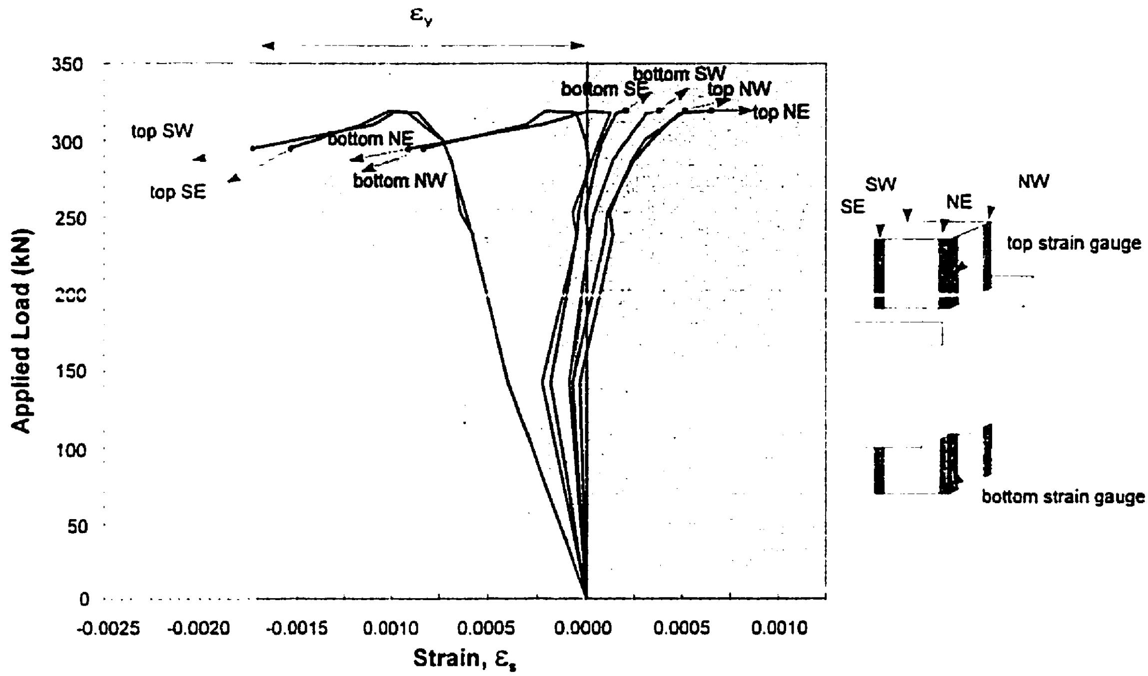

Figure 5.21: Strains in vertical steel corner angles of Specimen RS2

5.3.6 Joint Behaviour

The joint behaviour was monitored using two strain gauges glued to stirrups in the joint region. The strains at these locations are shown in Fig. 5.22. It can be seen that the first yielding of the top stirrup occurs in the fifth positive cycle. The bottom stirrup reached yield in the sixth cycle. A maximum strain of 0.011 was reached in the seventh positive cycle in the bottom stirrup.

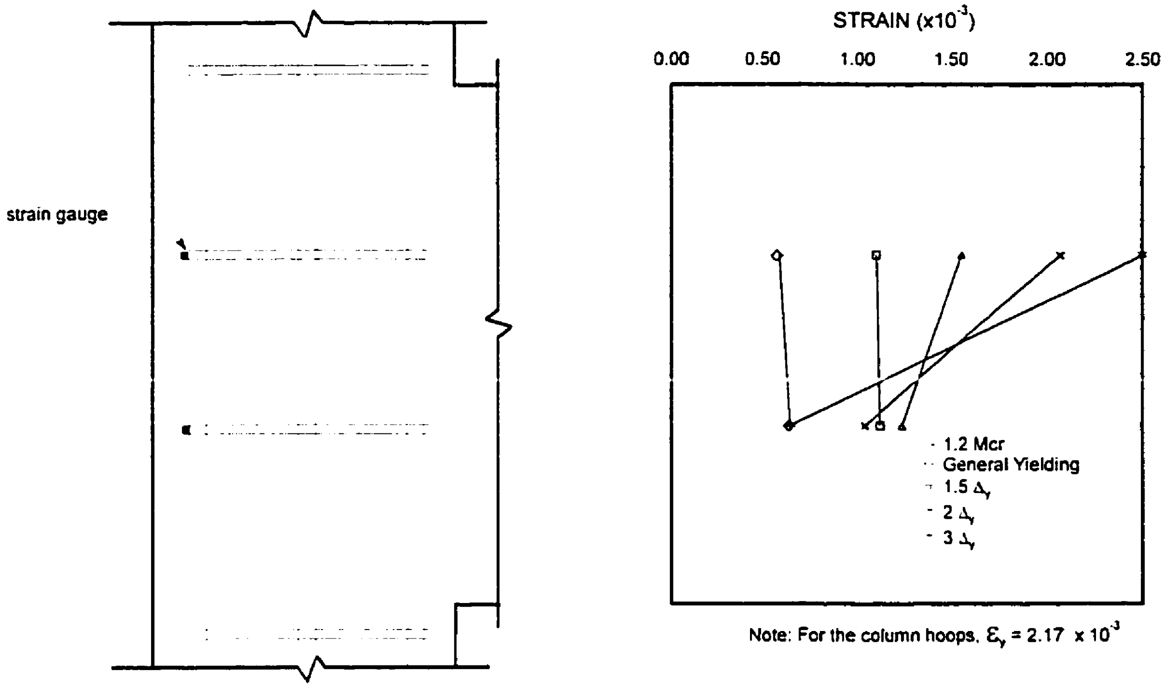

Figure 5.22: Distribution of strain in column hoops of Specimen RS2

CHAPTER 6

ANALYSIS AND COMPARISON OF SUBASSEMBLAGE TEST RESULTS

This chapter presents the analysis of the test results and compares the performance of Specimen RS2 tested in this research project with the performance of Specimens S1 and RS1, both tested by Castele (1988).

6.1 Load - Deflection Responses

Several key response parameters are summarised in Table 6.1 for Specimens S1, RS1 and RS2. The values of Δ_y and P_y correspond to the deflection and load, respectively, at general yielding of each specimen. The values of Δ_u and P_u are the deflection and load at the maximum deflection and maximum loading, respectively. The parameters k_y and k_u are the slopes which join the peak positive and negative load displacement values at general yielding and at the final loading stage, respectively. The parameter Δ_u/Δ_y is the displacement ductility, P_u/P_y indicates the ability of the specimen to maintain load after general yield and k_u/k_y provides a measure of the change in loading stiffness.

Table 6.1: Comparison of failure mode and key response parameters

Specimen	Mode of Failure	Δ_u/Δ_y	P_u/P_y	k_u/k_y
S1	Column hinging and joint yielding	2.7	1.05	0.46
RS1	Beam flexural hinging followed by buckling of beam bottom bars and joint yielding	5.3	1.19	0.12
RS2	Beam flexural hinging followed by joint yielding	6.37	1.26	0.19

The applied load versus tip deflection responses for all three specimens are shown in Fig 6.1, 6.2 and 6.3.

Figure 6.1 shows the load deflection behaviour for Specimen S1. The weak column design of this specimen greatly influenced the response under reversed cyclic loading. The column underwent severe distress, while the joint experienced significant yielding due to the lack of adequate joint shear reinforcement. This resulted in a premature failure of the specimen before flexural hinging of the main beam developed. The ability to dissipate energy of this specimen was greatly decreased due to the column and joint yielding. The maximum load was 1.05 times the general yielding load level in cycle 4A. The load carrying capacity decreased after this cycle, and the test was terminated due to the severe column and joint yielding.

The hysteretic response of Specimen RS1 can be seen in Fig. 6.2. This specimen was able to maintain its load carrying capacity over a large number of cycles. Significant loss in the load carrying capacity was not evident until the final cycle of the testing. The response of this specimen demonstrates excellent energy dissipation characteristics, showing only slight signs of pinching in the sixth positive loading cycle. The strengthening technique succeeded in improving the ability of the structure to dissipate energy by increasing the column strength. In the negative loading direction, the hysteresis curves remained very stable and it is believed that the specimen was able to undergo larger deflections without loss in load carrying capacity. The test was terminated due to the severe spalling and loss of the beam concrete core over a distance of 300 mm from the joint face.

Figure 6.3 shows the hysteretic response of Specimen RS2. This plot shows very stable hysteretic loops in both the positive and the negative directions, reaching peak loads greater than that obtained at general yield throughout the remainder of the test sequence. However, signs of pinching were evident by the fifth positive loading cycle. In the negative loading direction, loads were constantly increasing with increasing deflection. The test was stopped after both welds broke in the attachment of the added vertical reinforcement to the steel collar angles just above the slab.

A comparison of the load-deflection envelopes for the three specimens is shown in Fig. 6.4. It is clear that the two different retrofit techniques provided significant improvements in both strength and ductility. The larger load-deflection envelope of Specimen RS1 is due to the smaller lever arm (1700 mm) for the main beam. This decrease in lever arm creates a higher level of shear stress in the main beam, thus larger shear deformations were experienced in the main beam of Specimen RS1. Both of the retrofit specimens showed significant improvements in energy dissipation with only some pinching evident in the latter positive loading cycles.

Specimen S1 possessed very limited energy dissipation due to the excessive column rotation and joint distress leading to a premature failure of the specimen. Specimen RS1 shows a slightly larger loading stiffness that than the other two specimens, due to the larger column dimensions after retrofit and resulting shorter span of the main beam.

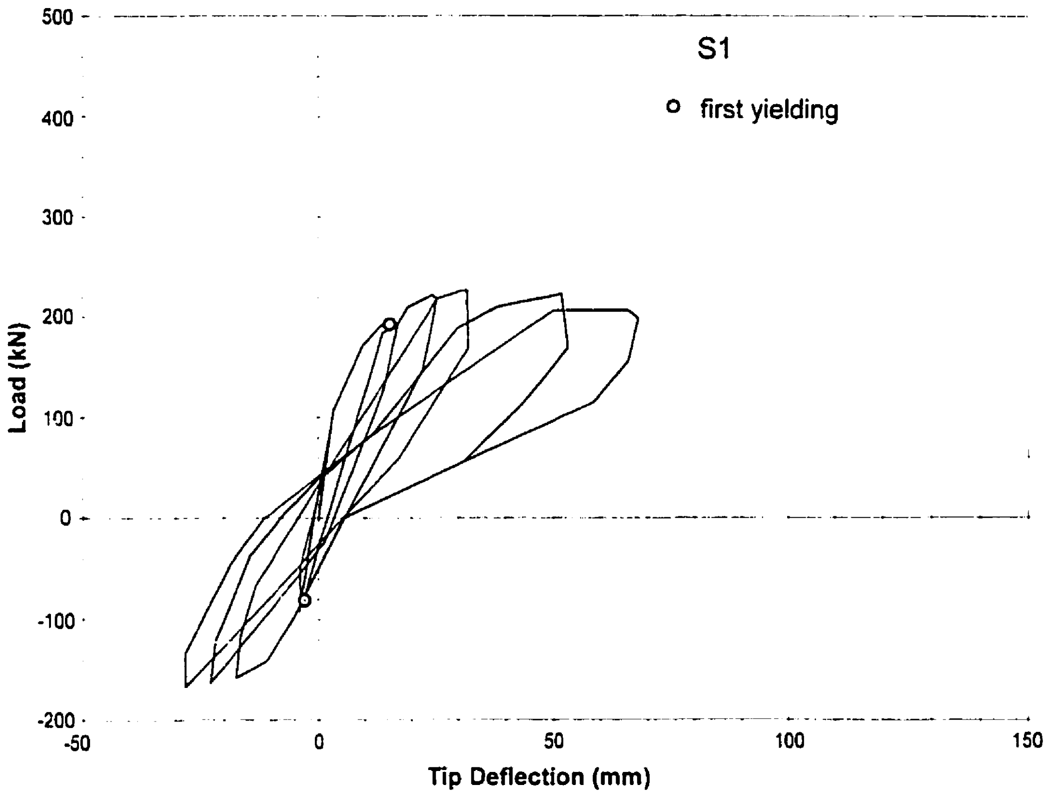

Figure 6.1: Load versus tip deflection response for Specimen S1

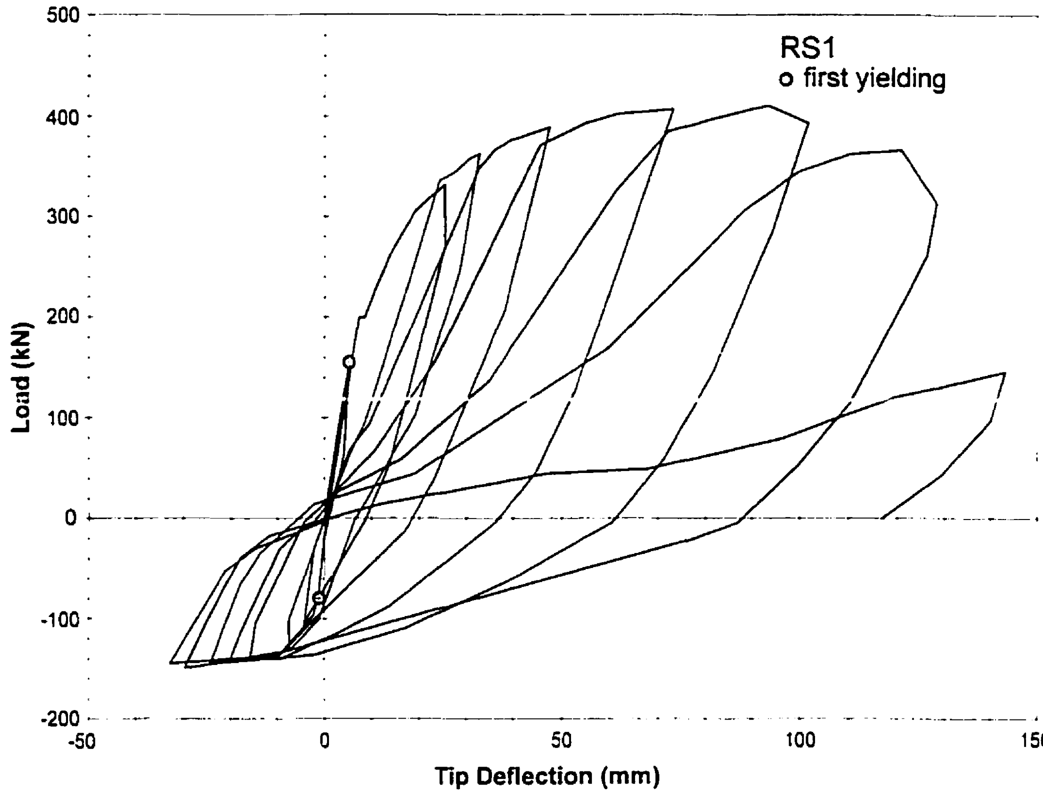

Figure 6.2: Load versus tip deflection response for Specimen RS1

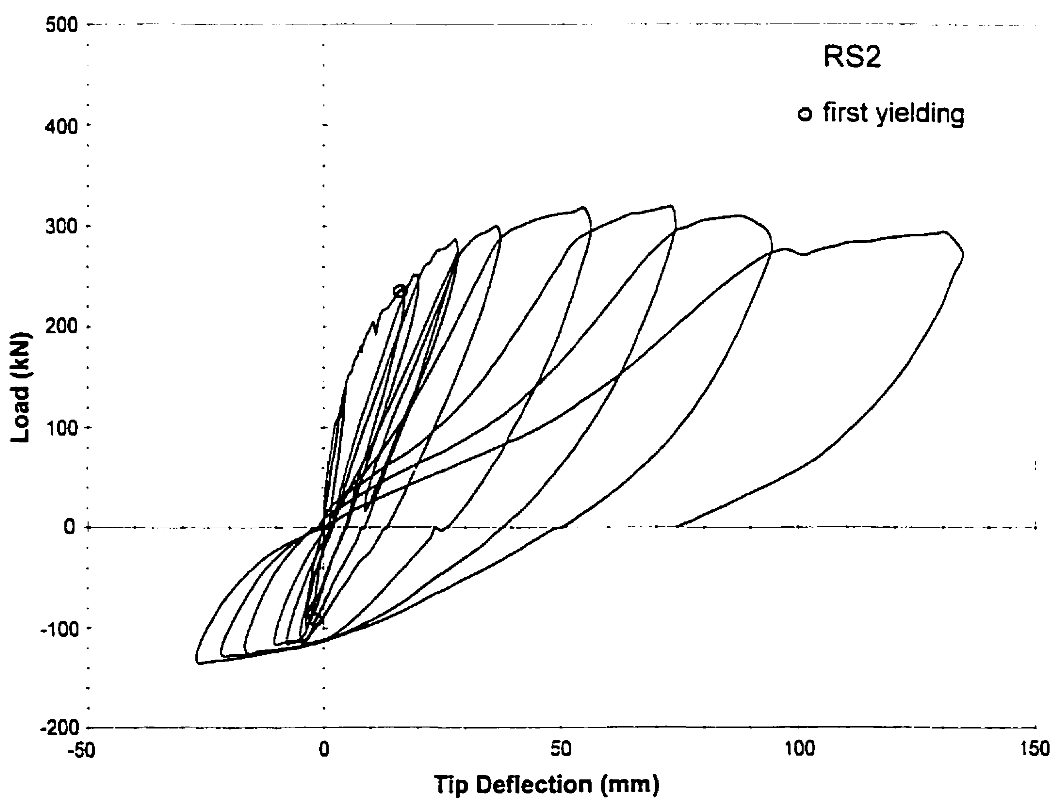

Figure 6.3: Load versus tip deflection response for Specimen RS2

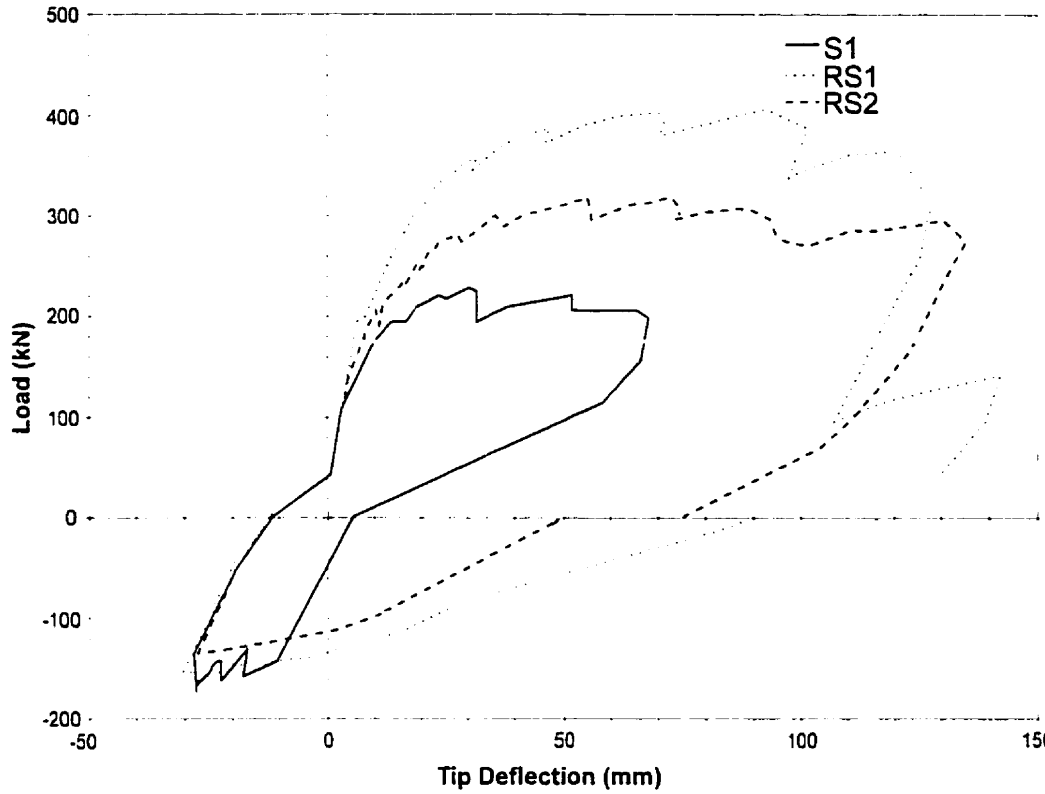

Figure 6.4: Load versus deflection envelopes for the three specimens

6.2 Tip Deflection Components

The tip deflection of the main beam is the result of the defonnations of the beam as well as the deformations of the joint. The beam deformations consist of deformations due to flexure as well as those due to shear. The joint deformation is also made up of two components, they are deformations from: shear distortion and bond slip of the bars within the joint region.

The following equation can be used to calculate the beam tip deflection from the components mentioned above:

$$\Delta_{tip} = \Delta_f + \Delta_s + \Delta_j \qquad (6\text{-}1)$$

where, Δ_{tip} is the total estimated beam tip deflection

Δ_f is the component due to beam flexure

Δ_s is the component due to beam shear

Δ_j is the component due to joint shear and bond slip

The first component Δ_f, is determined by applying the moment area theorem to the measured curvature distributions plotted in Fig. 5.3, 5.10 and 5.15. The equation is shown in Fig. 6.5, where φ is the beam curvature and x is the distance from the loading point to the centroid of a small element of area, φdx. Similarly in Fig. 6.6, the shear component Δ_s, is calculated by integrating the measured shear strains, γ, given in Fig. 5.3, 5.10 and 5.15.

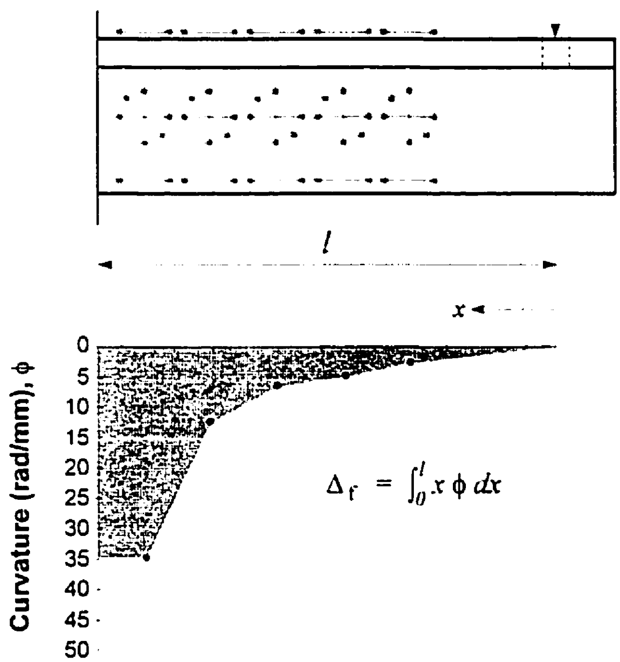

Figure 6.5: Determination of Δ_f

The displacement component caused by joint shear and bond slip is Δ_j. This is determined using the equations found in Fig. 6.7, considering the joint deformations due to shear and the joint deformations due to bond slip. The deflections and curvatures used in these calculations were obtained from the LVDT measurements recorded throughout the duration of the test.

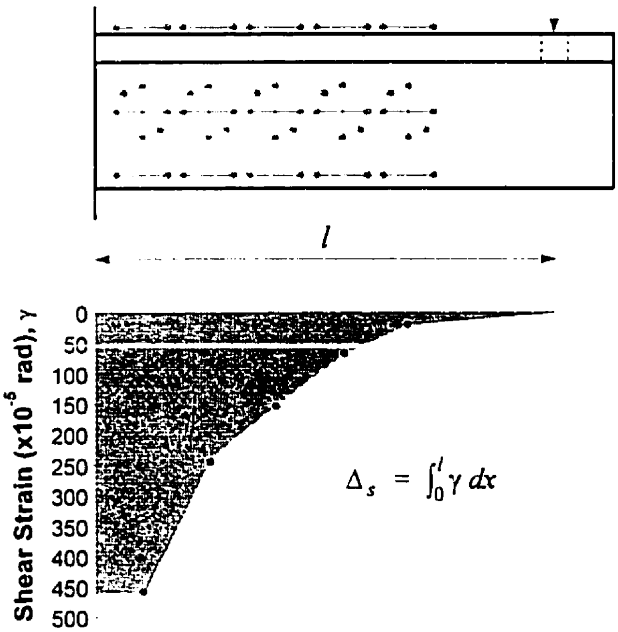

Figure 6.6: Determination of Δ_s

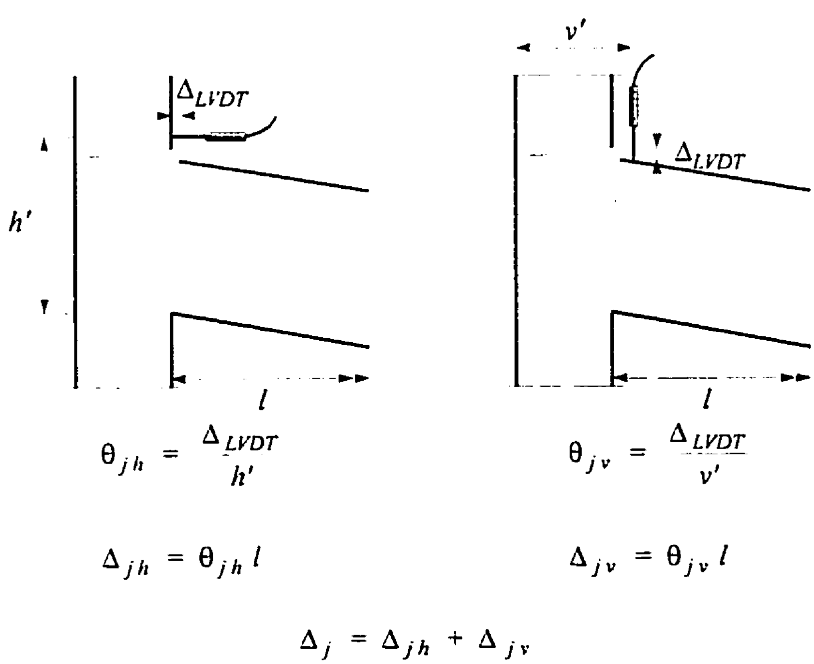

Figure 6.7: Determination of Δ_j

A comparison of the predictions and test results for Specimen S1 is shown in Fig. 6.8. The sum of the predicted tip deflection components is significantly less than those obtained from the test results. It is believed that the main reasons for this discrepancy are: local column rotations which may not have been totally removed from the measured tip deflection, as well as the fact that many of the major shear cracks did not pass through the strain rosettes on the beam. An inspection of the tip deflection components shows that the contributions from flexure remained very small after the yielding of the joint ties occurred. The yielding of the joint reinforcement, in combination with large column rotations, have limited the flexural behaviour of the main beam.

The predictions for Specimen RS1 agreed reasonably well with the actual test results, as seen in Fig. 6.9. The tip deflection due to flexure and joint distortion were similar throughout the duration of the test, representing 43% and 34% of the total deflection, respectively. Large shear strains were measured near the end of the test, representing about 11% of the total tip deflection. The results indicate that the main beam participated fully in the response of this specimen and that the column strengthening techniques proved to be effective.

The predictions for the tip deflections of Specimen RS2 are slightly less than the test results, as shown in Fig. 6.10. This is due mostly to the results obtained from the mechanical targets on this specimen which did not capture some of the cracks which occurred, leading to underestimation of the curvature and shear strains. The contributions of the joint components contributed greatly to the total tip deflection.

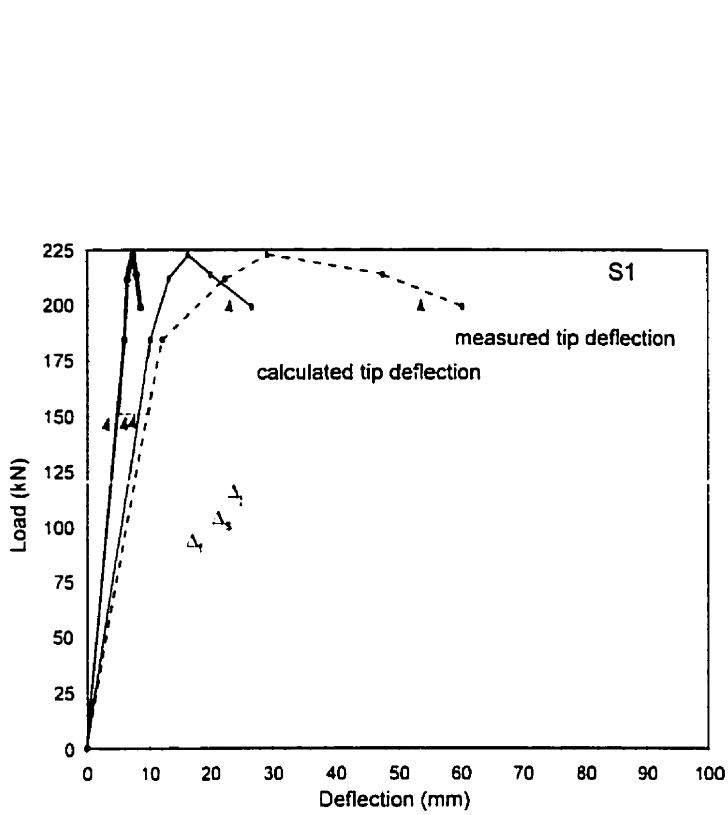

Figure 6.8: Predicted and measured tip-deflection components for Specimen S1

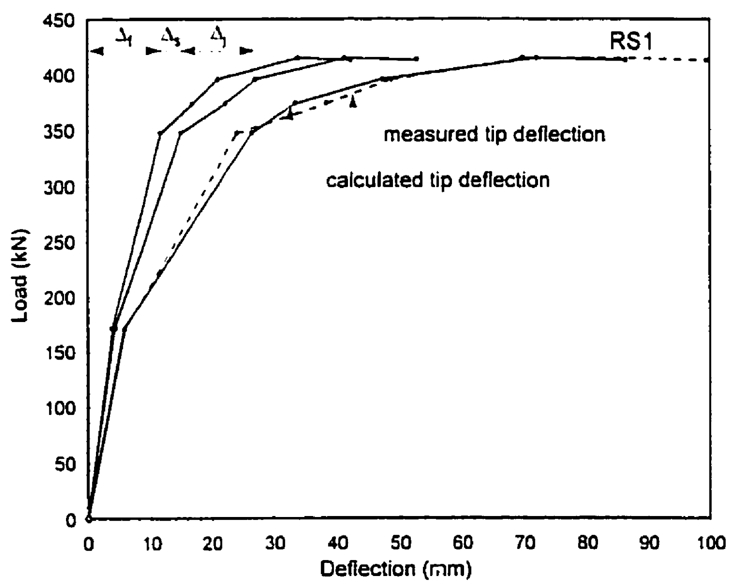

Figure 6.9: Predicted and measured tip-deflection components for Specimen RS1

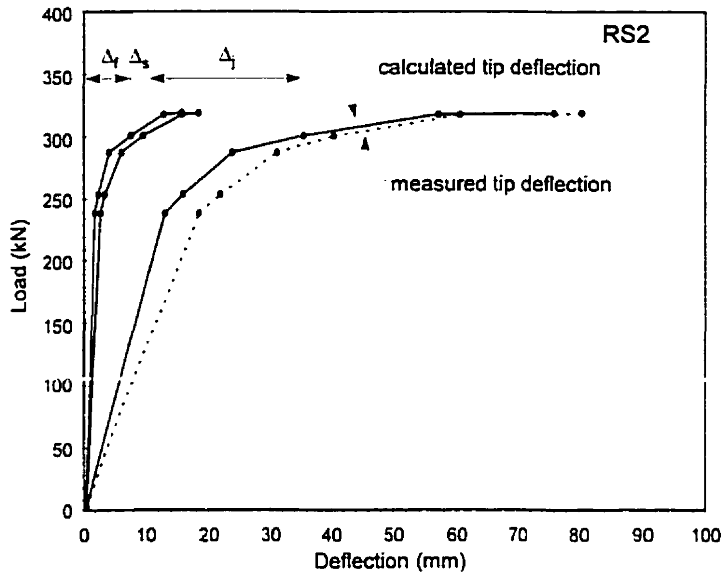

Figure 6.10: Predicted and measured tip-deflection components for Specimen RS2

6.3 Hysteretic Loading Behaviour

6.3.1 Energy Dissipation

The amount of energy dissipated under reversed cyclic loading can be calculated as the area enclosed by each loop of the load deflection curves. The cumulative energy dissipated by all three specimens is shown in Tables 6.2, 6.3 and 6.4.

The influence of the column strength on this parameter is made clear by simple comparison of the three specimens in their ability to dissipate energy. Specimen S1 was only able to dissipate 21.1 kNm of energy, whereas Specimen RS1 reached 99.1 kNm and Specimen RS2 dissipated 73.1 kNm. These values represent 5.0 and 3.5 times the amount of energy dissipated by Specimen S1. The results obtained from the two retrofit specimens show that the strengthening techniques used were successful in improving the ability of the structure to dissipate energy, as well as the beneficial effects of providing adequate column strength. It should be noted however, that the values obtained from the three tests cannot be directly compared due to the different loading histories. For example, Specimen RS2 underwent one more cycle than RS1.

Fig. 6.11 shows the plots of the cumulative energy versus ductility ratio as well as the cumulative energy versus tip deflection for each of the three specimens.

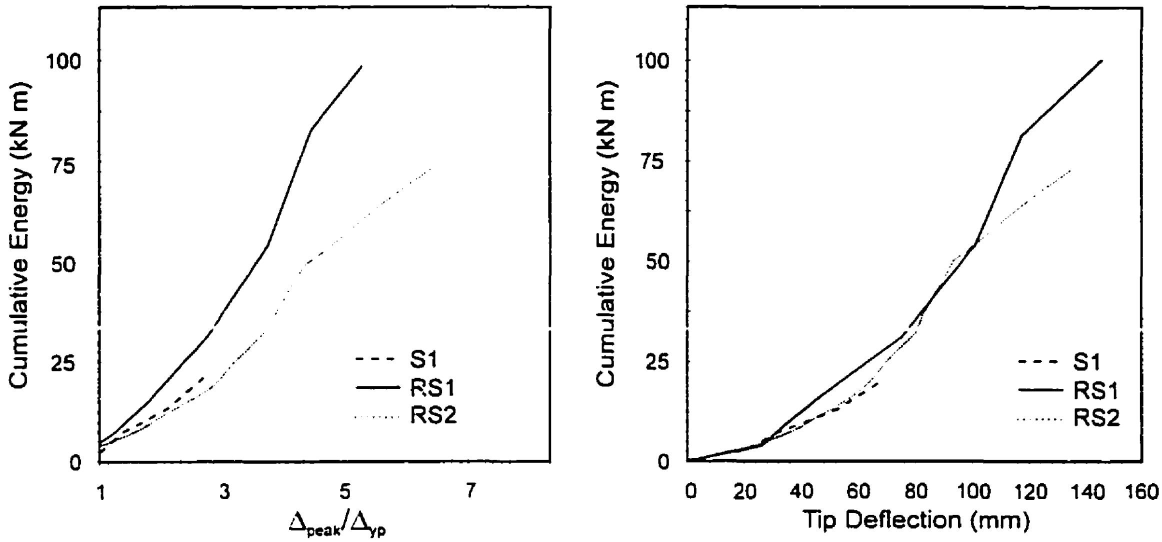

(a) Cumulative energy versus ductility ratio (b) Cumulative energy versus tip deflection

Figure 6.11: Cumulative Energy dissipation of the specimens

6.3.2 Displacement Ductility

The values of the displacement ductility can be seen in Tables 6.2, 6.3 and 6.4 for the three specimens. From a comparison of the tables, it can be seen that Specimen S1 reached a maximum ductility ratio of 2.69 while RS1 and RS2 reached maximum ductilities of 5.37 and 6.37, respectively. This parameter demonstrates the importance of column strength on the overall performance of the subassemblage.

Table 6.2: Cumulative Energy dissipation for Specimen S1

Cycle	Cycle Description	Δ_{peak}/Δ_y positive cycles	Energy Dissipated (N·m)	P_{peak}/P_y positive cycles
1A	1.2 M_{cr}	0.15	70.9	—
1B			115.6	
2A	First Yield	0.54	1039.5	—
2B			184.8	
3A	General Yield	1.00	1830.7	1.00
3B			1431.6	
4A	1.5Δ_y	1.30	2733.1	1.05
4B			1302.2	
5A	2Δ_y	2.12	5023.7	1.01
5B			1793.7	
6A	2.5Δ_y	2.69	5523.5	0.91
		Total	21049.3	

Table 6.3: Cumulative Energy dissipation for Specimen RS1

Cycle	Cycle Description	Δ_{peak}/Δ_y positive cycles	Energy Dissipated (N·m)	P_{peak}/P_y positive cycles
1A	1.2 M_{cr}	0.09	73.8	—
1B			72.5	
2A	First Yield	0.22	297.3	—
2B			141.9	
3A	General Yield	1.00	3604.4	1.00
3B			674.6	
4A	1.5Δ_y	1.27	3231.9	1.08
4B			1390.9	
5A	2Δ_y	1.80	6712.6	1.14
5B			2468.5	
6A	3Δ_y	2.74	12805.0	1.19
6B			4679.5	
7A	4Δ_y	3.78	18110.1	1.19
7B			7244.0	
8A	4.5Δ_y	4.41	21037.9	1.07
8B			8188.5	
9A	5Δ_y	5.37	8334.0	0.43
		Total	99067.4	

Table 6.4: Cumulative Energy dissipation for Specimen RS2

Cycle	Cycle Description	Δ_{peak}/Δ_y positive cycles	Energy Dissipated (N·m)	P_{peak}/P_y positive cycles
1A 1B	1.2 M_{cr}	0.23	202 116	---
2A 2B	First Yield	0..84	1023 233	---
3A 3B	General Yield	1.00	1653 209	1.00
4A 4B	$1.5\Delta_y$	1.44	2298 763	1.13
5A 5B	$2\Delta_y$	1.88	3778 1332	1.19
6A 6B	$3\Delta_y$	2.82	7768 3153	1.26
7A 7B	$4\Delta_y$	3.76	9800 4548	1.26
8A 8B	$5\Delta_y$	4.43	12357 5776	1.23
9A	$7\Delta_y$	6.37	18053	1.16
		Total	73062	

6.3.3 Damping and Stiffness

The inherent stiffness and damping of a subassemblage are described by the stiffness and hysteretic damping coefficients, α and β respectively. These factors are defined in Fig. 6.12a. The values of α and β are plotted versus ductility ratio in Fig. 6.12b and 6.12c for all three specimens. The loading stiffness coefficient, α, versus ductility ratio plots show similar stiffness degradation, although Specimen RS1 exhibits a slightly higher stiffness versus ductility ratio response. This can be attributed to the larger column dimensions for the specimen. Likewise, in the hysteretic damping coefficient, β, versus ductility ratio plots similar increase in damping as the stiffness degrades, is shown.

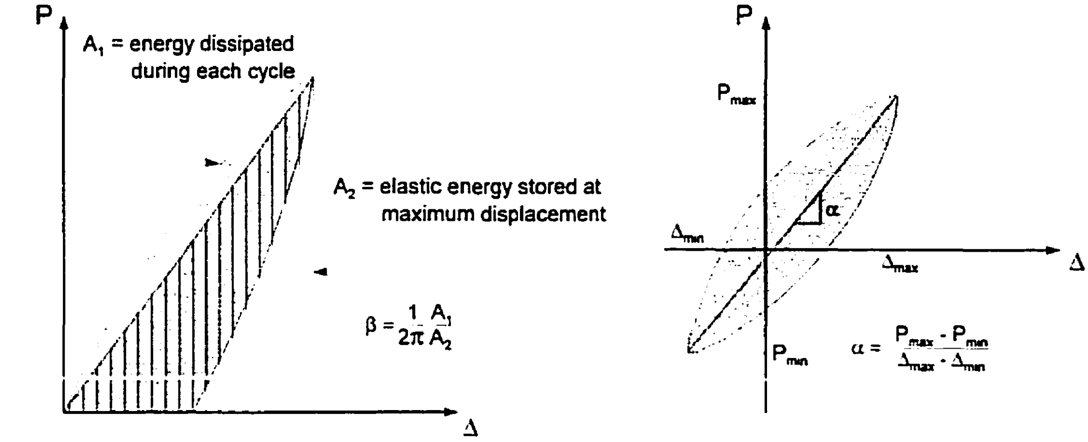

(i) Hysteretic damping coefficient, β

(ii) Loading stiffness, α

(a) Definition of damping coefficients, β and α

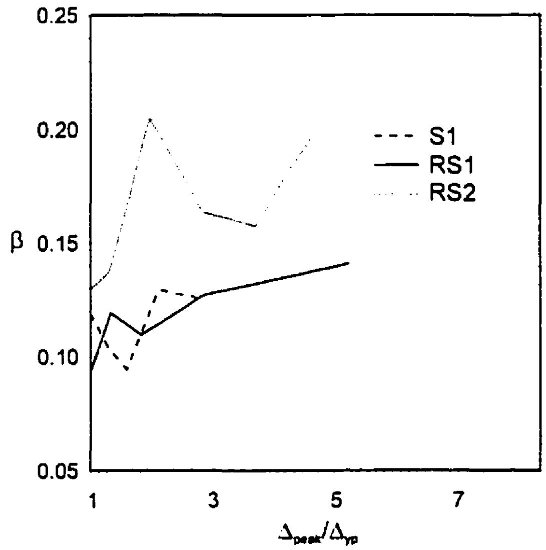

(b) Hysteretic damping of the specimens

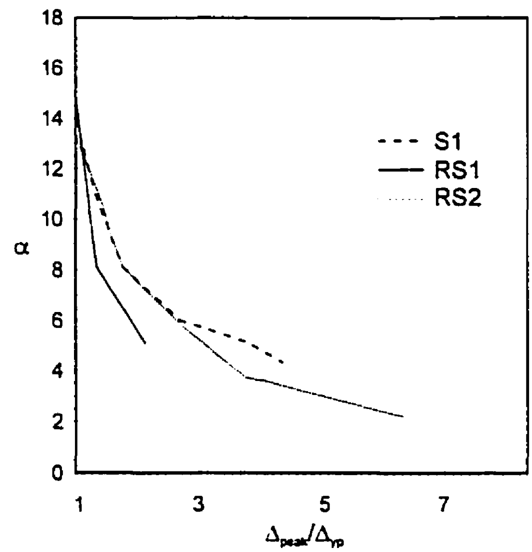

(c) Stiffness degradation of the specimens

Figure 6.12 : Hysteretic damping and stiffness degradation of the specimens

6.4 Moment - Curvature Responses and Predictions

6.4.1 Moment - Curvature Responses of the Beams

The curvature ductility of the specimens is defined as the ratio of the maximum attainable curvature before significant drop in load carrying capacity divided by the curvature at yield (φ_u/φ_y). The results of these calculations are shown in Table 6.5 for all three specimens. It is noted that for Specimen RS2, the ultimate curvature would be somewhat larger than the value given in Table 6.5 which was determined for cycle 8A since the strain measurements were not working in cycle 9A.

Table 6.5: Maximum moments and curvature ductility of the specimens

Specimen	M_{max} (kN·m)	φ_y ($x10^{-3}$ rad/m)	φ_u ($x10^{-3}$ rad/m)	φ_u/φ_y
S1	430	5.9	10.0	1.69
RS1	732	5.9	71	12.0
RS2	595	5.9	>48.6	>8.2

The effective slab width assumed in design has a significant impact on the negative bending moment-curvature responses of the beams. The moment curvature responses for the main beam, with various slab widths, were predicted using the program RESPONSE (Collins and Mitchell, 1997). It should be noted that the three specimens tested all had identical designs for the main beam. In order to determine the contribution of the slab to the moment-curvature response, five different assumptions concerning the effective cross sections were considered, including:

(i) A rectangular beam with no flanges having cross-sectional dimensions of 400 x 600 mm .

(ii) A T-beam with an effective slab width of $3h_f$ on each side of the beam. This resulted in an effective slab width, b_e = 1010 mm, with 4 No. 10 slab bars within this width.

(iii) A T-beam with an effective slab width of $4h_f$ on each side of the beam. This resulted in an effective slab width, b_e = 1230 mm, with 8 No. 10 slab bars within this width.

(iv) A T-beam including the entire width of the slab, b_e = 1900 mm, with 12 No. 10 slab bars within this width.

(v) A T-beam including the entire slab width and considering a non-linear distribution of strains across the slab.

The prediction which was produced by case (v), incorporated the shape of the actual strain distribution in the slab bars during the test at maximum load. This is shown in Fig. 6.13 and 6.14. The moment-curvature predictions for the five cases along with the actual test results for each of the three specimens are shown in Fig. 6.15, 6.16 and 6.17. It was found that for Specimens RS1 and RS2, the prediction using a constant strain distribution resulted in the best fit curve (prediction iv). However, the prediction using the variable strain over the width of the slab produces a more rounded curve than those assuming a uniform strain distribution. This can be explained by the sequential yielding of the slab bars in the tension flange. However, for the response of Specimen S1, general flexural yielding of the main beam did not occur before the specimen failed by column hinging and joint yielding. The distribution of strains in the tension flange of the beam is a function of the torsional stiffness and strength of the spandrel beam (DiFranco, 1993, Marquis, 1997). As the stiffness of the spandrel beam is increased, the strain distribution in the slab bars becomes more linear, causing the slab bars to yield simultaneously. This is the assumption made for cases (ii) to (iv). It is interesting to note that the best prediction to the actual test results are cases (iv) and (v). This suggests that the effective flange with of $3h_f$ that is recommended by the 1994 CSA Standard may be underestimated.

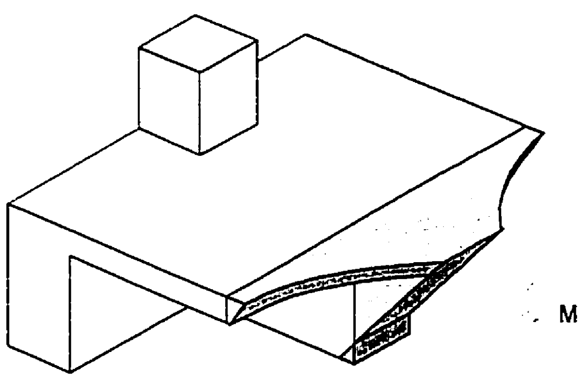

Figure 6.13 Variation of strain across the T-section

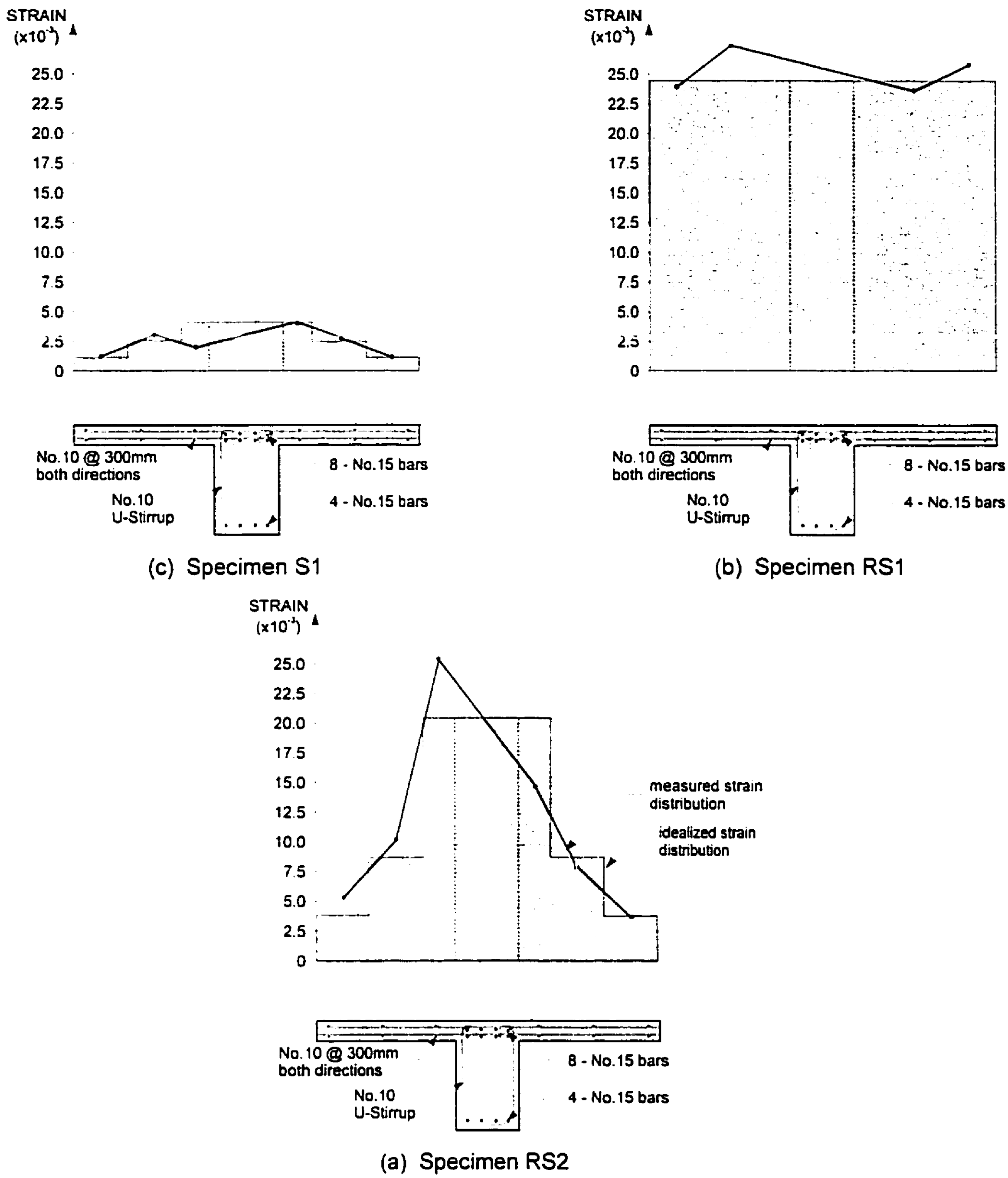

Figure 6.14: Accounting for strain variation across the flange of the T-beams

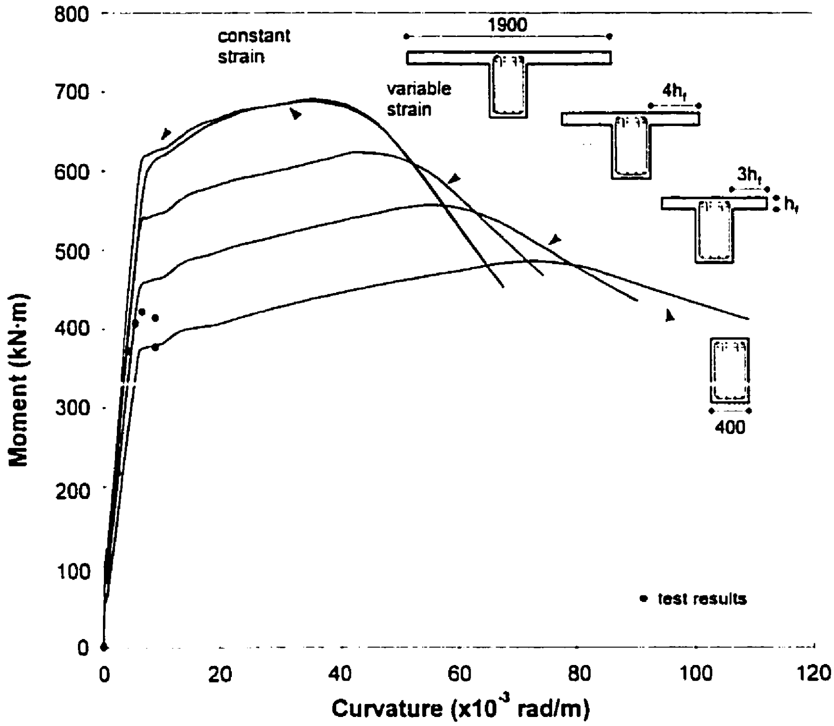

Figure 6.15: Moment-curvature responses for the beam of Specimen S1

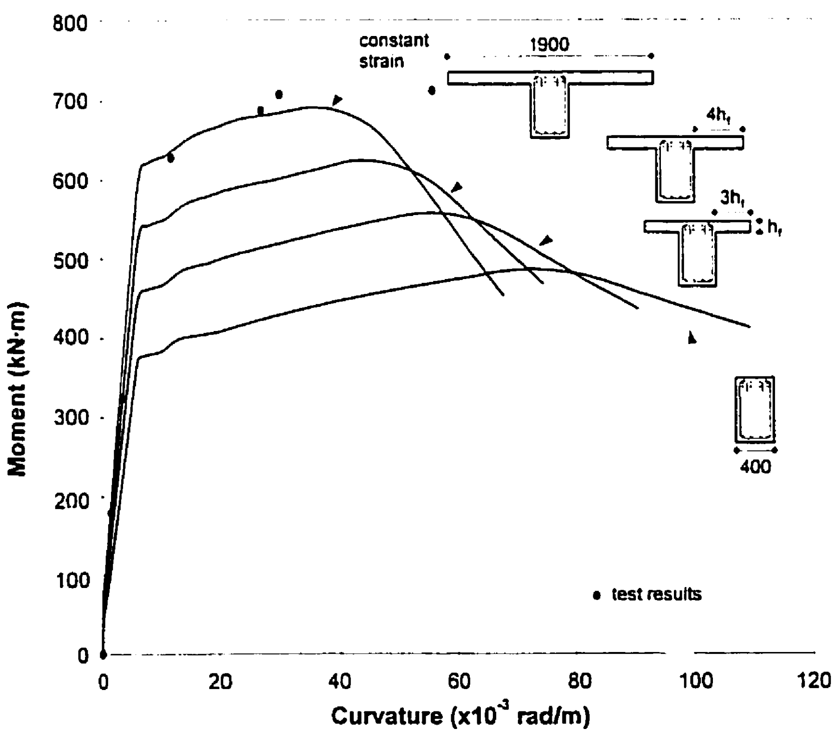

Figure 6.16: Moment-curvature responses for the beam of Specimen RS1

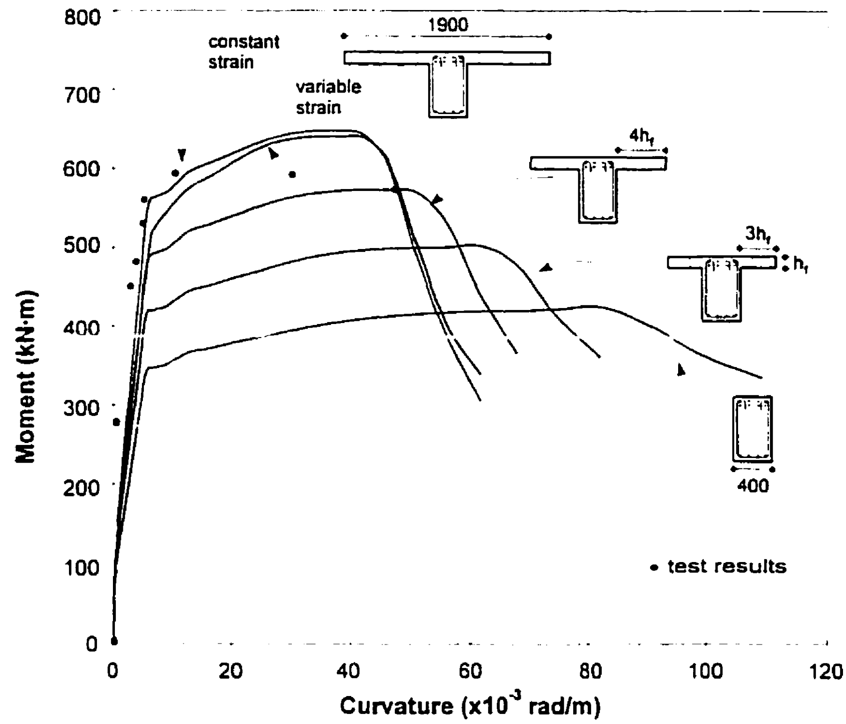

Figure 6.17: Moment-curvature responses for the beam of Specimen RS2

6.4.2 Moment - Curvature Response of the Column in Specimen RS2

The curvature of the column in Specimen RS2 was measured using two sets of LVDTs placed vertically at the north and south column-joint interface. The strain gauges placed on the column vertical steel were also used to determine the curvature of the column. The experimental results from the test are shown in Fig. 6.18, along with two predicted moment curvature responses. The first prediction was calculated considering only the original concrete column, while the second prediction takes into account the effect of the added vertical corner angles. It can be seen that the prediction including the effects of the corner angles greatly increased the ability of the column to reach greater bending moments.

The results obtained from the test initially follow the predicted curve calculated including the added vertical corner angles. At a bending moment of 230 kNm, the actual response deviates from the predicted response due to yielding of the joint, causing increased curvatures in the column close to the joint face.

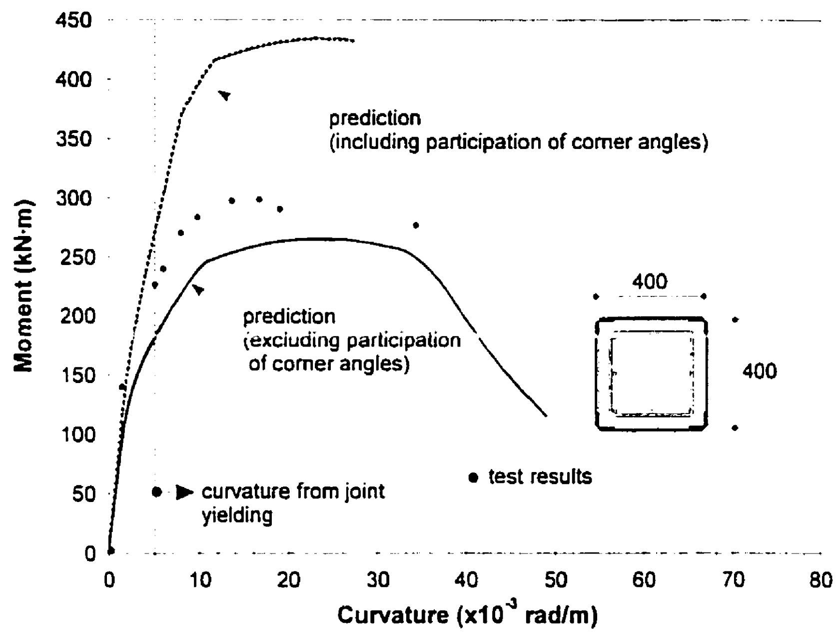

Figure 6.18: Moment-curvature response for the column of Specimen RS2

6.5 Role of the Spandrel Beam

When the main beam is subjected to negative bending moments, torsional moments are created in the spandrel beam. The torsional moments are created because each slab bar is anchored into the top of the spandrel beam. As the main beam is loaded to cause negative bending, tensile strains build up in the longitudinal slab bars, these forces are then transferred into the spandrel beam in the form of eccentrically applied shears. The eccentricity is due to the difference in the line of action of the forces in the slab bars and the centroid of the spandrel beam. The free body diagram of the subassemblage depicting the flow of forces which take place in the hinge region of the spandrel beam while the main beam is experiencing negative bending is given in Fig. 6.19. As the moments increase in the main beam, larger strains are formed in the slab bars, which in turn create greater torsional effects in the spandrel beam. However, when torsional cracking occurs in the spandrel beam, the stiffness is greatly decreased and the stiffness is further decreased upon torsional yielding. This torsional cracking and yielding of the spandrel beam limits the strains that can develop in the slab bars. Torsion in the spandrel beam also causes the side faces of the joint region to be subjected to both direct shear and torsional shear flow, demonstrating that the size and strength of the spandrel beam are of key importance in determining the strain distribution of the slab bars. As mentioned in Section 6.4.1, the greater the torsional stiffness and torsional yield moment of the spandrel beam, the more uniform the strain distribution of the slab bars across the width of the slab.

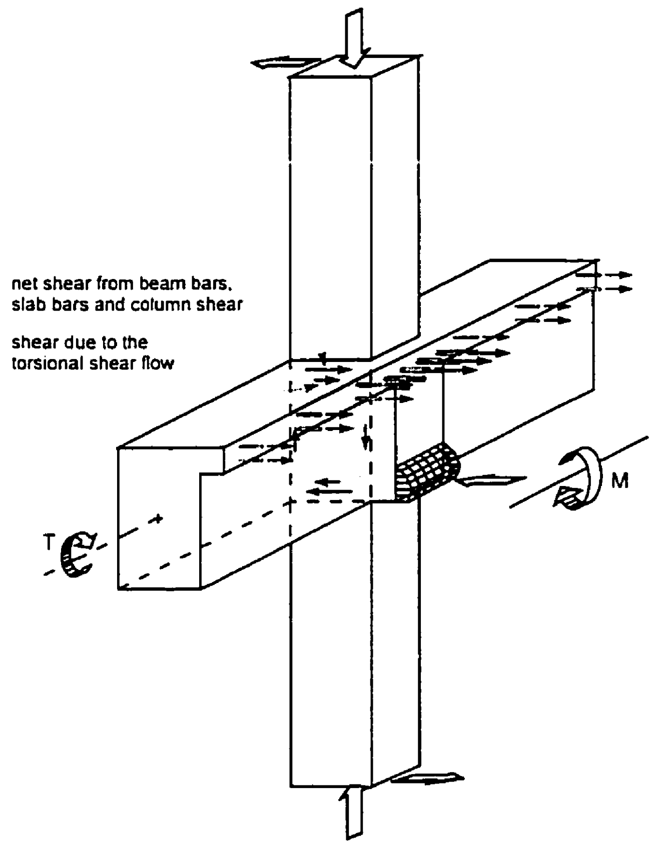

Figure 6.19: Role of spandrel beam

Figure 6.20 shows the results of the strain distributions of the slab bars for all three specimens. This figure shows that at maximum load, Specimens RS1 and RS2, both have yielding of all twelve No. 10 slab bars. However, at maximum load only the eight inner slab bars reached yield for Specimen S1. This is due to the fact that premature failure took place by column hinging and joint yielding.

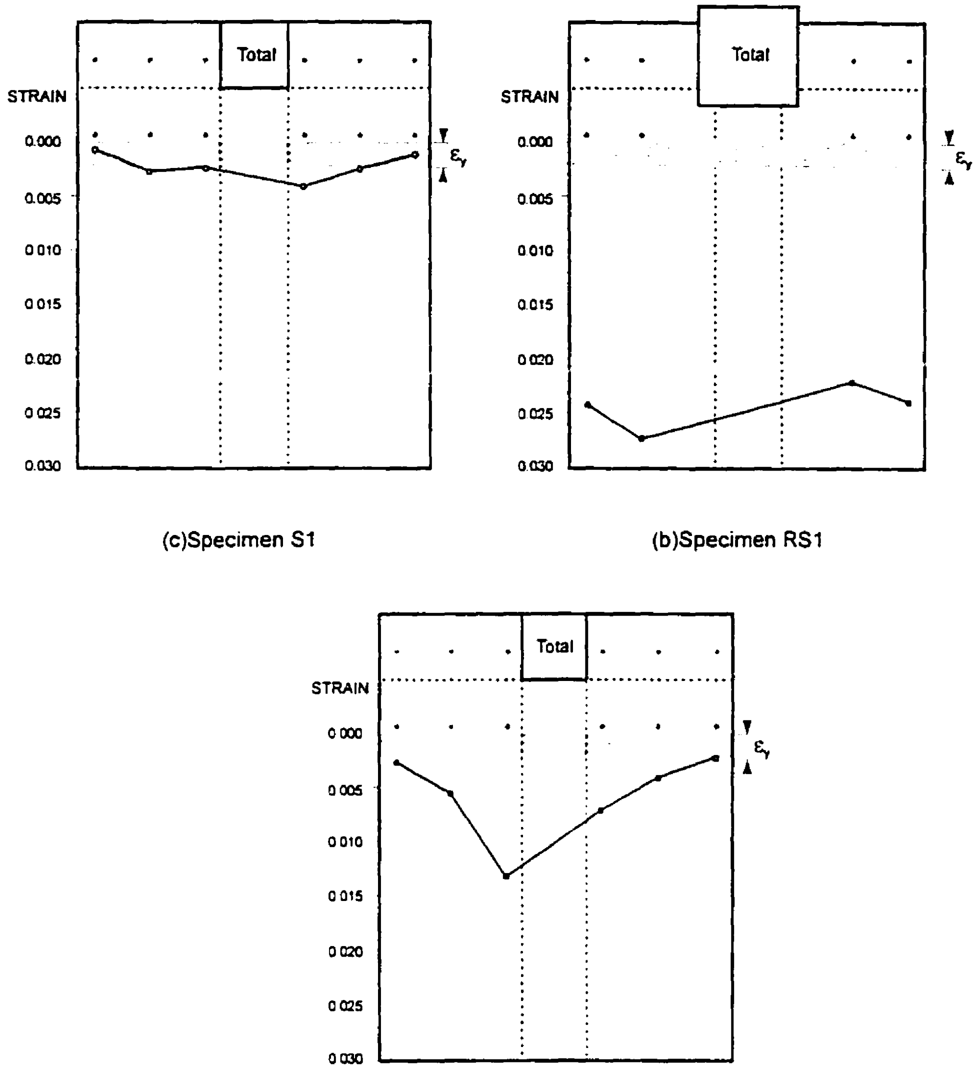

(c)Specimen S1 (b)Specimen RS1

(a) Specimen RS2

Figure 6.20: Measured strain distribution at maximum load in the slab bars at slab-spandrel beam interfaces

6.5.1 Measured and Predicted Torsional Response of the Spandrel Beams

The torsional response of the spandrel beam was measured by two pairs of LVDTs on the south face on the spandrel beam as shown in Section 3.6. Each pair consisted of one LVDT placed 100 mm from the bottom of the spandrel beam and the other placed 400 mm directly above it. One set of LVDTs were placed along the column with the other pair being placed at a distance of 775 mm away from the column, towards the east end of the spandrel beam. The rotation and horizontal deformation of the spandrel beam are shown in Fig. 6.21. These values were calculated from the results obtained from the LVDT measurements.

The rotation or twist of the spandrel beam of Specimen RS2 at peak positive loading cycles is shown in Fig. 6.21a. The values were calculated by subtracting the bottom LVDT deflection reading from the top deflection LVDT reading and dividing by the distance of 400 mm. The horizontal deformations are calculated by taking the average of the deflection of each pair of LVDTs. The horizontal deformations are shown for Specimen RS2 in Fig. 6.21b.

Shown in Fig. 6.22 is the torsional response of the spandrel beam of Specimen RS2. The torque in the spandrel beam was calculated using the measured strains in the slab bars to determine the forces in the slab steel. The sum of these slab forces were then multiplied by the eccentricity to the centre of the spandrel beam to obtain a torque. The twist in the spandrel beam was obtained by calculating the difference between the measured rotation of the column and the measured rotation determined near the tip of the spandrel beam. The measured cracking torque is approximately 19.5 kNm (see Fig. 6.22) with a corresponding twist of 0.0003 rad. The pure torsional cracking moment T_{cr}, can be calculated by the equation:

$$\begin{aligned} T_{cr} &= \frac{A_c^2}{p_c}\, 0.33\sqrt{f_c'} \qquad (6\text{-}2) \\ &= \frac{(400 \times 600)^2}{2(400+600)}\, 0.33\sqrt{43.7} = 62.8 \text{ kN}\cdot\text{m} \end{aligned}$$

where, A_c = area enclosed by outside perimeter of concrete cross section

p_c = outside perimeter of the concrete cross section

The value which is calculated using this equation is greatly overestimated due to the fact that this equation only considers the torsional effects while neglecting the shear involved. Therefore, to properly estimate the cracking torque, the interaction between shear and torsion must be accounted for as in Equation 6-3.

$$\begin{aligned} v_{cr} &= v_t + v_v \qquad (6\text{-}3) \\ 0.33\sqrt{f_c'} &= \frac{T_{cr}\, p_c}{A_c^2} + \frac{F_{cr}}{b_w\, d} \\ 0.33\sqrt{43.7} &= \frac{(F_{cr} \times e) \times 2(400+600)}{(400 \times 600)^2} + \frac{F_{cr}}{600 \times 342.5} \end{aligned}$$

where, b_w = minimum effective width in shear

d = effective depth in shear

e = eccentricity of slab bars from the centre of twist of the spandrel beam = 245 mm

F_{cr} = force in slab bars at cracking

T_{cr} = cracking torque induced by slab bars = F_{cr} x e

The solution of this equation gives a value of 40.0 kNm for the predicted cracking torque of Specimen RS2, which is double the observed cracking torque of 19.5 kNm. This difference is attributed to the small slab strain measurements recorded during the test, since the large cracks did not pass through the gauge lengths of the mechanical targets. Specimens S1 and RS1 had predicted cracking torque of 32.9 kNm and 33.1 kNm respectively.

In order to estimate the yielding level of the spandrel beam, the compression field theory will be used to determine the behaviour under shear and torsion. The pure torsional yield torque, T_y, can be calculated using the following equation (Mitchell and Collins, 1974, Collins and Mitchell, 1991):

$$T_y = \frac{2 A_o A_t f_y}{s} \cot\theta \qquad (6\text{-}4)$$

where, A_o = area enclosed by torsional shear flow path to pass through the centres of the corner bars of the spandrel beam

A_t = area of one leg of the closed hoop reinforcement

f_y = yield stress of hoop reinforcement

θ = angle of principal compression measured from the horizontal axis of the beam

s = spacing of shear or torsion reinforcement measured parallel to the longitudinal axis

This equation gives a predicted torsional yield moment, T_y, of 156.4 kNm for Specimen RS2 and 158.9 kNm for Specimens S1 and RS1. However this equation has not taken into account the interaction of shear and torsion, therefore the yield shear force in the stirrups must be determined by:

$$V_y = A_v f_y \frac{d}{s} \cot\theta \qquad (6\text{-}5)$$

where, A_v = area of shear reinforcement

d = effective depth

f_y = yield strength of reinforcement

V_y = yield force in shear

Using a linear interaction curve to combine the effects of both shear and torsion from Equation 6-4 and Equation 6-5, results in:

$$\frac{(F_y\ e)\ s}{2\ A_o\ A_t}\tan\theta + \frac{F_y\ s}{A_v\ d}\tan\theta = f_y \qquad (6\text{-}6)$$

$$\frac{(F_v \times 245) \times 125}{2\ (0.85 \times 310 \times 510) \times 100}\tan\theta + \frac{F_v \times 125}{200 \times 342.5}\tan\theta = 434.0$$

where, F_y = force in slab bars when yielding of spandrel beam occurs.

In order to determine θ, the combined shear stress for a solid section is needed and can be determined from the following expression (Mitchell and Collins, 1974 and Collins and Mitchell, 1991):

$$v = \sqrt{\left(\frac{V}{b_w\ d_v}\right)^2 + \left(\frac{T\ p_h}{A_{oh}^2}\right)^2} \qquad (6\text{-}7)$$

where, A_{oh} = area enclosed by centreline of closed transverse torsion reinforcement

b_w = minimum effective width

d_v = distance, measured perpendicular to the neutral axis, between the resultants of the tensile and compressive forces due to flexure

e = eccentricity of slab bars from the centre of twist of the spandrel beam

p_h = perimeter of the centreline of the closed transverse torsion reinforcement

T = torsion induced by slab bars = F x e

V = transverse shear = F_y

v = shear stress under combined loading

An iterative approach was used to solve for the yielding torque using both Equations 6-6 and 6-7 as well as using the limits for θ from the compression field theory. This method resulted in a predicted yielding torque of 55.6 kNm for Specimen RS2 and 56.5 kNm for both Specimens S1 and RS1. The measured torque reached at maximum load level for Specimen RS2 was 63.7 kNm, with a corresponding twist of 0.0044 rad.

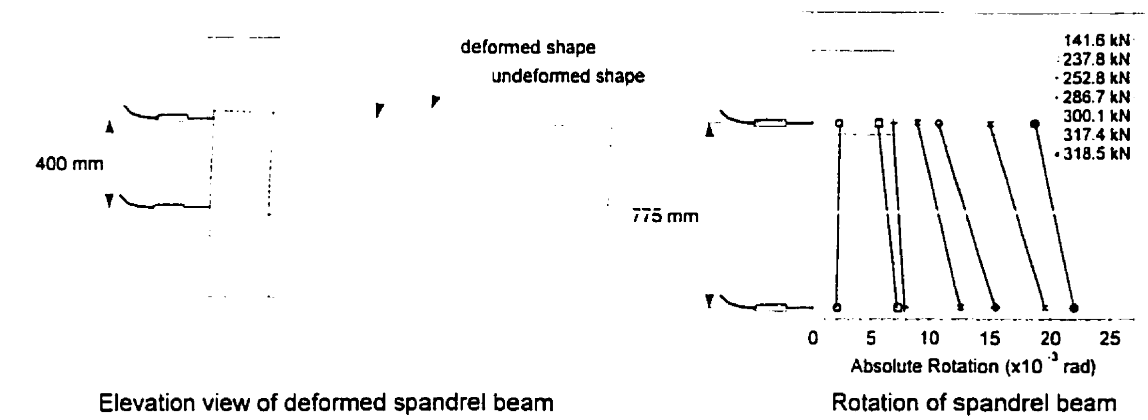

(a) Vertical deformation of spandrel beam

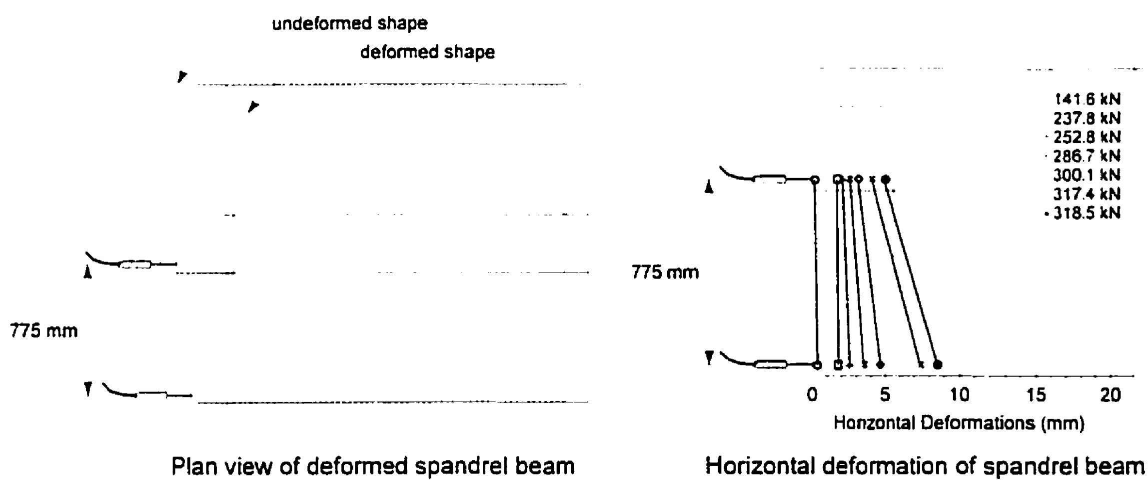

(b) Horizontal deformation of spandrel beam

Figure 6.21: Spandrel beam deformations for Specimen RS2

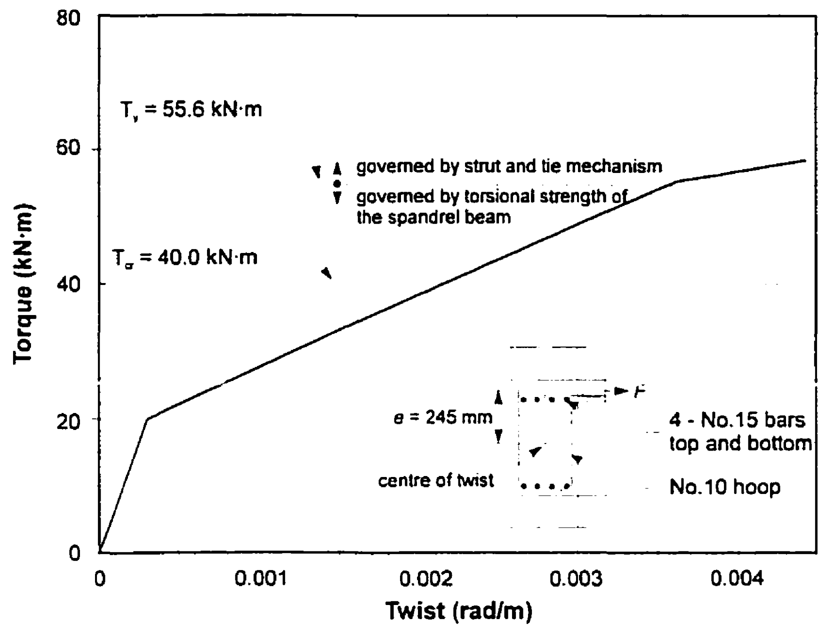

Figure 6.22: Torsional response of spandrel beam for Specimen RS2

6.6 Role of the Slab

6.6.1 Strut and Tie Mechanism for Transferring Forces from Slab Bars

As shown in Fig. 6.22, once yielding has occurred in the spandrel beam, the mechanism by which the slab forces are transferred into the joint region can be determined by a strut and tie model as demonstrated by DiFranco *et al.*(1995). The strut and tie model used for all three specimens in shown in Fig. 6.23. The disturbed region is shown in Fig. 6.23a, whereas Fig. 6.23b represents idealised flow of compressive stresses and associated tension ties making up the strut and tie model. Fig. 6.23b assumes that the slab bars are anchored near the outer edge of the spandrel beam. The top south longitudinal bar in the spandrel beam then acts as the tension chord, while the top horizontal legs of the closed hoops act as tension members. The forces in the slab bars can be calculated using these strut and tie models, the geometry and reinforcement details of the spandrel beam, provided that the tension tie forces are limited to their yield values.

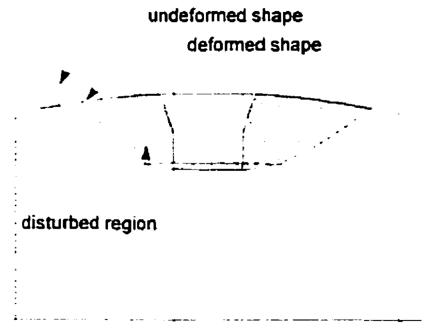

(a) Disturbed region of the specimens

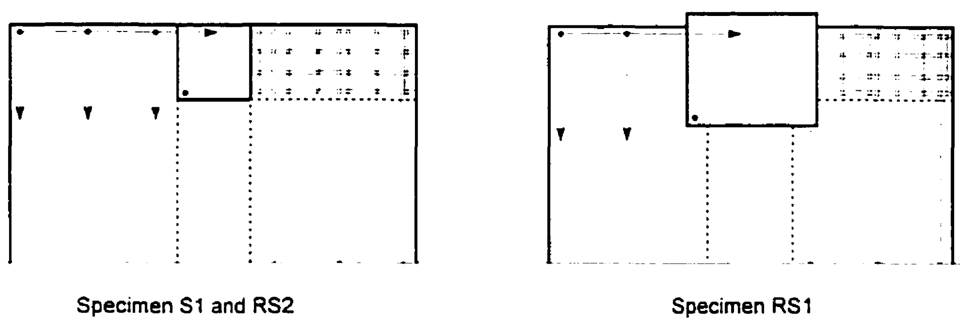

(b) Flow of forces in the disturbed region

Figure 6.23: Idealized strut and tie model for the specimens

6.6.2 Effective Slab Reinforcement

The presence of slab reinforcement will increase the negative moment capacity of the beam as well as increase the direct shear transferred to the joint. It is therefore imperative to determine the effective slab width participating in the response, since this will directly influence ductility levels, as well as the hierarchy between yielding of the columns and the beams. Underestimating the contributions of the slab bars will result in a flexural strength ratio between the columns and the beams significantly lower than those specified in the codes. Table 6.6 summarises the effective slab widths recommended by the Canadian, American and New Zealand codes for exterior joint connections. Many tests, including the one in this thesis, have demonstrated that yielding of the longitudinal slab bars occurs over a greater width then that which is recommended by the codes.

Table 6.6: Effective slab widths used in current design codes

Standard	"Effective Slab Width" in Tension
CSA Standard (CSA, 1994)	Clause 21.4.2.2 specifies that slab reinforcement within a width of $3h_f$ from the side faces of the beam be considered effective.
ACI Code (ACI,1995)	Chapter 21 which contains the special provisions for seismic design does not specify an effective width. Section 8.10, however, specifies that the effective width of T-beam flanges must be less than 1/4 of the span of the beam, and the effective overhang flange must be less than: (a) $8h_f$ (b) 1/2 clear span to next web
New Zealand Standard (NZS, 1995)	Clause 8.5.3.3 specifies that for an exterior joint with a transverse beam the slab reinforcement within a width defined as the lesser of the following should be considered effective: (a) 1/4 of the span of the beam, extending on each side from the centre of the beam. (b) 1/2 of the span of the slab, transverse to the beam, extending on each side from the centre of the beam (c) 1/4 of the span of the transverse edge beam extending on each side from the centre of the beam.

6.6.3 Determination of Effective Slab Reinforcement

Table 6.7 summarises the calculations to determine the number of slab bars which contribute to the negative moment capacity of the beam. This table compares the number of bars predicted to yield determined using the compression field theory and strut and tie models with the number of slab bars which yielded during the experiment.

Table 6.7: Predicted and experimentally determined number of yielded bars

	Experimental values		Prediction from modified compression field theory		Prediction from strut and tie model	Final Prediction
Specimen	Torque (kN·m)	Number of Bars	Predicted Torque (kN·m)	Number of Bars	Number of Bars	Number of Bars
S1	54.0	5.0	56.5	5.2	4.5	5.2
RS1	65.4*	6.0*	56.5	5.2	6.2	6.2
RS2	63.7*	6.0*	55.6	5.2	4.2	5.2

* these values were limited by the size of the slab used for the experiments. If a wider slab had been provided, thus more slab bars would have been present, then it is predicted that these values may have been higher.

To determine the number of effective slab bars using the modified compression field theory, the predicted yielding torque is divided by the eccentricity between the centroid of the spandrel beam and the line of action of the slab forces in the bars, see Fig. 6.24. This value represents the tensile force in the slab bars. Dividing the tensile force by the yield stress of the No. 10 slab bars will determine the area of yielding bars. For example, for Specimen RS2 a yielding torque of 55.6 kNm was determined. Dividing by the eccentricity, e = 245 mm, and then by the yield stress of the No. 10 bars (434 MPa) results in a area of yielding bars equal to 522.9 mm^2. This area is equivalent to 5.2 No. 10 slab bars on each side of the column.

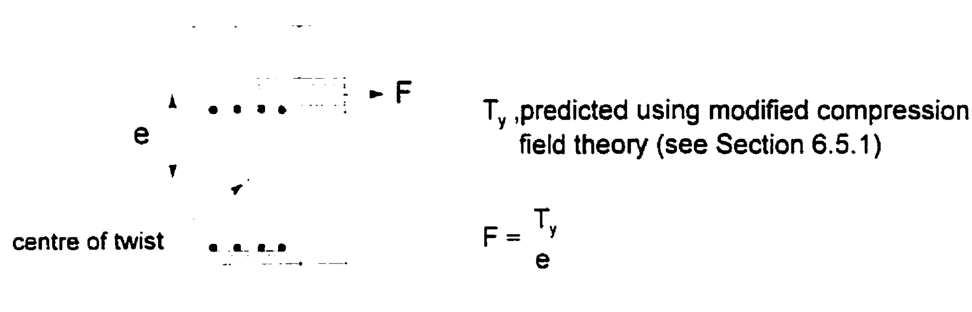

Figure 6.24: Determination of slab bar forces from torsional strength of spandrel beam

The strut and tie model was used to predict the number of effective slab bars, that is the number of bars able to reach yield. The load carrying capacity of the strut and tie model is limited by the force that can develop in the tension ties. For this analysis, the tension tie force in the strut and tie resisting mechanism is limited to A_sf_y. The tension resultant force in the top of the spandrel beam was determined considering 2-No. 15 bars (As = 400 mm^2) contributing to the tension tie force. Furthermore, the node where the compressive forces converge resulted in an assumed lever arm for the truss model of 0.8c, where c is the column dimension. Figure 6.25 illustrates the equivalent truss model for each of the three specimens and shows the total forces in the slab bars which can develop when the main tension tie force reaches yield. As can be seen from Fig. 6.25, this resisting mechanism is capable of developing 4.5, 6.2 and 4.2, for Specimens S1, RS1 and RS2, respectively. These results were obtained by dividing the sum of the forces reached in the slab bars by the yield stress. The final predictions for the number of slab bars that will yield, shown in Table 6.7, are governed by the strongest mechanism. It is noted that Specimen S1 failed by severe distress in the column and joint area and hence could not fully develop yielding in the beam and slab.

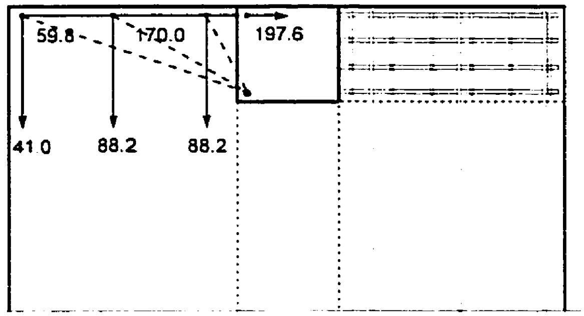

(c) Specimen S1

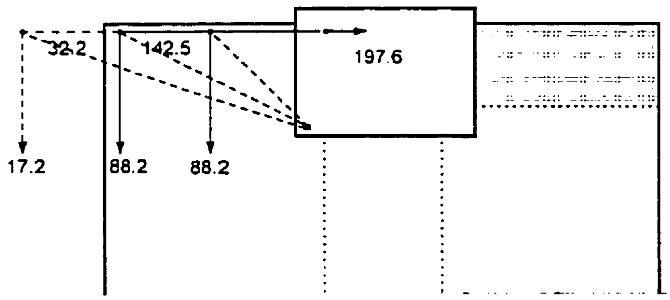

(b) Specimen RS1

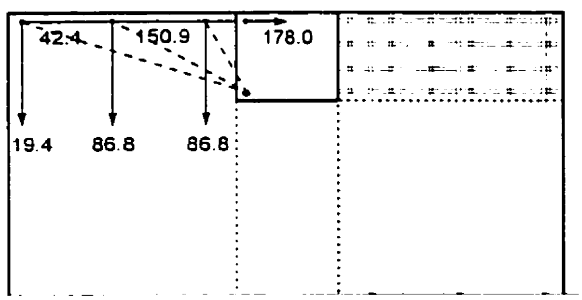

(a) Specimen RS2

Figure 6.25: Strut and tie models showing corresponding forces in slab bars

6.6.4 Simplified Determination of Effective Slab Reinforcement

A simplified method for determining the effect slab reinforcement was developed by DiFranco *et al.* (1995). This method involves the use of Equation 6-4 (Collins and Mitchell, 1974) to determine the torsional strength and assumes and angle of principal compression equal to 45°, therefore Equation 6-4 becomes:

$$T_y = \frac{2 A_o A_t f_y}{s} \tag{6-8}$$

and when equated to the induced torque created from the slab bars:

$$T_y = \frac{2 b_o h_o A_t f_y}{s} = \frac{h_o}{2} n A_s f_y \tag{6-9}$$

Where h_o and b_o are the dimensions of the between the corner longitudinal bars in the spandrel beam, as shown in Fig. 6.26, and n equals the number of effective slab bars. Therefore solving for n results in:

$$n = \frac{4 b_o A_t}{s A_s} \tag{6-10}$$

A further simplification is possible if the area of the slab longitudinal bars is equal to that of the closed hoops in the spandrel beam, which is often the case. Equation 6-10 is then further reduced to:

$$n = \frac{4 b_o}{s} \tag{6-11}$$

The number of effective slab bars estimated using this equation is shown in Table 6.8. It is noted that the values obtained are slightly overestimated since the contribution of shear to the yielding of the spandrel beam in torsion is ignored in this method.

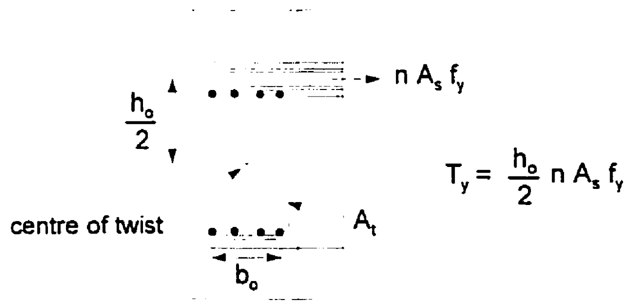

Figure 6.26: Torsion induced by slab bars

Similarly, a simplification to the strut and tie model calculations to determine the number of effective slab bars can also be made by noting that the limiting parameter is the magnitude of the tensile forces in the longitudinal bars at the back face of the spandrel beam. The resisting moment is provided by the force in these longitudinal spandrel beam bars multiplied by a lever arm of 0.8 times the column dimension, c. Taking moments about this nodal point results in Equation 6-12 as shown in Fig. 6.27:

$$\frac{A_s^* f_y}{s_s} \cdot \frac{x}{2} = A_{sl} f_y (0.8 c) \qquad (6\text{-}12)$$

where, A_s^* = the area of slab bars within the distance s_s

A_{sl} = the area of top longitudinal steel in the outer half of the spandrel beam

x = effective width of the slab

x/2 = the lever arm to the resultant of the slab bars

s_s = spacing between the slab bars (see Fig. 4.28)

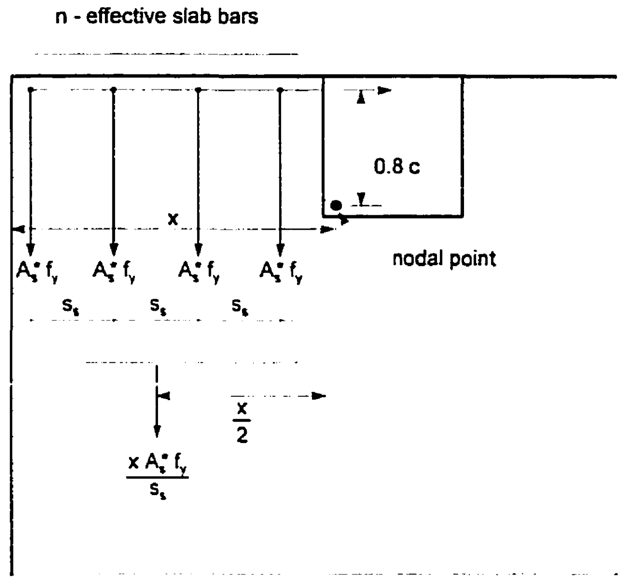

Figure 6.27: Simplified strut and tie model

Solving for x in Equation 6-12 results in:

$$x = \sqrt{\frac{1.6 A_{sl} c s_s}{A_s^*}} \tag{6-13}$$

The number of slab bars expected to yield is equal to the total number of bars within the distance x from the column face. The results of the simplified method are shown in Table 6.8. It is noted that the mechanism which involves torsional yielding predicts 9.9 bars as being effective for all three specimens. Specimen S1, which did not develop full yielding in the beam and slab developed only 4 bars. The two retrofit specimens develop all 6 slab bars and would have developed more had the specimen been wider.

Table 6.8: Simplified determination of effective slab bars

Specimen	Simplified Torsional Strength $n = 4 \frac{b_o}{s}$	Simplified Strut and Tie Model $x = \sqrt{\frac{1.6 A_{sl} c s_s}{A_s^{\bullet}}}$; $n = \frac{x}{s_s} N$	Experimental Results
S1	9.9	4.13	4.0
RS1	9.9	5.06	>6.0
RS2	9.9	4.13	>6.0

6.6.5 Flexural Strength Ratio

The flexural strength ratio, M_R, is obtained by dividing the nominal flexural strength of the column by the sum of the nominal flexural strength of the beams framing into the column. It is then evident that the greater the contribution of the longitudinal slab steel to the negative flexure strength of the beam, the smaller the flexural strength ratio. The Canadian Standard (CSA 1994) specifies a minimum M_R of 1.33 for a ductile moment resisting frame. This lower limit has been established to ensure that proper yielding hierarchy occurs in the structure. Table 6-9 lists the calculated flexural strength ratios for varying effective slab widths as well as the actual flexural strength ratios of the specimens tested. The actual flexural strength ratios are based on the recorded yield stresses of the reinforcement, compressive strengths of the concrete, and the amounts of slab steel found to be effective.

For Specimen S1, it is apparent that this design is inadequate to ensure proper hierarchy of yielding among the frame members, shown by the M_R ratio less than 1.33. The reinforced concrete retrofit applied to Specimen RS1 has significantly increased the flexural strength ratio. Assuming an effective slab width of $3h_f$, as specified by the CSA Standard (1994), a flexural strength ratio of 2.14 is calculated. In reality, the full width of the slab was effective with twelve slab longitudinal bars reaching yield, this dropped the measured flexural strength ratio to 1.58. For Specmien RS2, the addition of the vertical steel corner angles to the deficient column increased the flexural strength ratio from 1.02 to 1.58, for an effective slab width of $3h_f$. When the actual effective slab width is accounted for, the actual measured flexural strength ratio of Specimen RS2 is 1.26.

Table 6.9: Flexural strength ratio for varying effective widths

Effective Slab Width	S1 M_R	RS1 M_R	RS2 M_R
i) beam only, no slab bars effective	1.2	2.52	1.88
ii) 3 h_f, 4 slab bars effective	1.02	2.14	1.58
iii) 4 h_f, 8 slab bars effective	0.88	1.86	1.38
iv) full width of slab effective, 12 slab bars	0.78	1.66	1.24
Measured, M_R	0.96	1.58	1.26

CHAPTER 7

CONCLUSIONS AND RECOMMENDATIONS

7.1 Conclusions

7.1.1 Column Retrofit Specimens

Three column specimens were constructed and tested, one which represented a deficient column and the other two to determine the effectiveness of two different retrofit techniques. One of the retrofit techniques used a reinforced concrete sleeving, while the other involved the attachment of vertical steel corner angles and welded batten plates. From these tests it was concluded that:

- The unretrofit specimen, column C1, displayed a very brittle post-peak load deflection response, due primarily to the deficient design and detailing of the transverse reinforcement.
- The reinforced concrete sleeved specimen, RC1, was very effective in increasing the axial compressive resistance of Specimen C1 by a factor of 2.6, as well as an increased loading stiffness 2.3 times that of Specimen C1. However, the post peak response of Specimen RC1 was very similar to that of the unretrofit Specimen C1, being very brittle.
- Specimen RS2, which used vertical steel corner angles and batten plates to retrofit the deficient column specimen, S1, showed an increase of 20% in compressive resistance and a 31% increase in loading stiffness. More importantly, the effectiveness of this column retrofit was demonstrated in the ability to sustain significant compressive loads after the peak load had been reached, dropping only 21% instead of 50% (Specimens C1 and RC1) immediately after the peak load was reached.

7.1.2 Beam-Column-Slab Subassemblage Specimens

This experimental program investigated the response of a full-scale concrete beam-column-slab subassemblage subjected to reversed cyclic loading. The response of Specimen RS2 was compared to the responses of two other specimens (S1 and RS1) previously tested at

McGill University by Castele (1988). Specimen S1 and the subassemblages for Specimens RS1 and RS2 before retrofit were designed and detailed as nominally ductile moment-resisting frames with a force modification factor, R, of 2.0 as specified by the 1994 CSA Standard.

The main objective of this research program was to investigate the influence of using two different column retrofitting techniques on the seismic performance of nominally ductile moment-resisting frames. The conclusions from the results of these three tests are:

- The weak column design of Specimen S1 greatly influenced the response under reversed cyclic loading. The premature failure of this specimen can be attributed to the severe distress in the column and significant joint yielding due to the lack of adequate joint shear reinforcement. This specimen displayed poor hysteretic behaviour throughout the test, reaching a value of 2.7 for ductility displacement at the maximum deflection. Significant joint distress did not allow flexural hinging of the beam to occur.
- Specimen RS1 demonstrated very stable hysteretic response with excellent energy dissipation characteristics of about 5 times that of Specimen S1. This retrofit technique was successful in increasing the displacement ductility to a value of 5.3, as well as increasing the ability of the structure to dissipate energy by increasing the column strength. This strengthening technique increases the joint region and results in increased column dimensions.
- Specimen RS2, which used vertical steel corner angles and batten plates to retrofit the column, also demonstrated very stable hysteretic response resulting in improved energy dissipation characteristics. Specimen RS2 dissipated about 3.5 times the amount of energy dissipated by Specimen S1. A displacement ductility of 6.4 was reached at maximum deflection for this specimen. This retrofit resulted in considerable beam flexural hinging due to the increased column strength, however at the later stages of loading joint yielding occurred. This indicates that the collar angles placed directly above and below the joint were not that effective in resisting joint shear. The advantages of this type of retrofit are associated with the ease and speed of construction as well as the minimal increase in column dimensions.

7.2 Future Research Recommendations

It is suggested that the following aspects of column retrofit using vertical steel corner angles and batten plates be investigated:

- Practical techniques for strengthening the joint region need to be developed.
- The influence of yield strength, spacing and size of the batten plates, on the retrofitted column needs to be studied.

REFERENCES

Aboutaha, R.S., Engelhardt, D., Jirsa, J.O. and Kreger, M.E., *Seismic Retrofit of R/C Columns using Steel Jackets,* Seismic Rehabilitation of Concrete Structures, ACI SP-160, 1996, pp.59-72.

Aboutaha, R.S., Engelhardt, D., Jirsa, J.O. and Kreger, M.E., *Rehabilitation of Shear Critical Concrete Columns by use of Rectangular Steel Jackets,* ACI Structural Journal, January-February 1999, pp.68-78.

ACI Committee 318, *Building Code Requirements for Reinforced Concrete (ACI 318-95),* American Concrete Institute, Detroit, Michigan, 1995.

Applied Technology Council (ATC), Rapid Visual Screening of Buildings for Potential Seismic Hazards: Supporting Documentation ATC-21-1, Redwood City, California, April 1988, 137 pp.

Applied Technology Council (ATC), A Handbook for Seismic Evaluation of Existing Buildings ATC-21-1 (preliminary), Redwood City, California, 1989, 169 pp.

Applied Technology Council (ATC), Techniques for Seismically Rehabilitating Existing Buildings (preliminary) ATC-22, Redwood City, California, March 1989, 137 pp.

Bentz, E.C. and Collins, M.P., Response-2000, Reinforced Concrete Sectional Analysis using the Modified Compression Field Theory, version 0.7.5 (beta), University ofToronto, Toronto, Ontario, 1998.

Canadian Institute of Steel Construction (CISC), Handbook of Steel Construction, CISC 1994, Willowdale, Ontario.

Canadian Institute of Steel Construction (CISC), Limit States Design in Structural Steel, CISC 1995,Willowdale, Ontario.

Canadian Standards Association, CSA Standard A23.3-94 - Design of Concrete Structures, Rexdale, Ontario, December 1984, 282 pp.

Canadian Standards Association, CSA Standard A23.3-94 - Design of Concrete Structures, Rexdale, Ontario, December 1994, 218 pp.

Castele, D.J., Effect of Column Strength on the Seismic Response of Concrete Frames, M.Eng. Thesis, Department of Civil Engineering and Applied Mechanics, McGill University, Montreal, Quebec, 1988, 96 pp.

Collins, M.P., and Mitchell, D., Prestressed Concrete Basics, Canadian Prestressed Concrete Institute, Ottawa, Ontario, 1987.

Collins, M.P., and Mitchell, D., Prestressed Concrete Structures, Prentice Hall, Response Publications, Toronto/Montreal, 1997.

Cook, W. and Mitchell, D., *Disturbed regions in Reinforced Concrete Members*, ACI Structural Journal, Vol. 85, No. 2, March-April, 1988, pp. 206-216.

DiFranco, M.A., Effect of Spandrel Beam on the Seismic Response of Concrete Frames, M.Eng. Thesis, Department of Civil Engineering and Applied Mechanics, McGill University, Montreal, Quebec, 1993, 131 pp.

DiFranco, M.A., Mitchell, D., and Paultre, P., *Role of Spandrel Beams on Response of Slab-Beam-Column Connections*, ASCE Journal of Structural Engineering, Vol. 121, No. 3, March 1995, pp. 408-419.

Dritsos, S.E., *Jacket Retrofitting of Reinforced Concrete Columns*, Construction Repair, Vol. 11, No. 4, 1997, pp.35-41.

Federal Emergency Management Agency (FEMA), Typical Costs for Seismic Rehabilitation of Existing Buildings, Volume II - Supporting Documentation, Los Angeles, California, February 1988, 145 pp.

Frangou, M., Pilakoutas, K. and Dritsos, S., *Structural repair/strengthening of RC Columns*, Construction and Building Materials, Vol. 9, No. 5, 1995, pp.258-267.

Ghoborah, A., Aziz, T.S. and Biddah, A., *Seismic Rehabilitation of Reinforced Concrete Beam-Column Connections*, Earthquake Spectra, Vol. 12, No. 4, November 1996, pp.761-780.

Habibullah, A., ETABS: Three Dimensional Analysis of Building Systems - Users Manual, Computers & Structures Inc., Berkeley, California, February 1989, 246 pp.

Hanaa, S., Jones, R., *Composite Wraps for Aging Infrastructure: Concrete Columns*, Composite Structures, Vol. 38, No. 1, 1997, pp. 57-65.

Hoppel, C.P.R., Bogetti, T.A. and Gillespie, J.W.J., *Design and Analysis of Composite Wraps for Concrete Columns*, Journal of Reinforced Plastics and Composites, Vol. 16, No. 7. 1997, pp. 588-601.

Howie, I., Castro, P.F. and Karbhari, V.M., *Concrete Columns with composite wraps: A comparison of theoretical and experimental results*, Transactions of the Institution of Engineers Australia - Civil Engineering Transactions, Vol. 39, No. 1, 1997, pp. 1-9.

Iglasias, J., *Repairing and Strengthening of Reinforced Concrete Buildings Damaged in the 1985 Mexico City Earthquake*, The Mexico Earthquakes-1985, Factors Involved and Lessons Learned, 1986, pp. 426-439.

Jirsa, J.O., *Repair and Strengthening of Reinforced Concrete Structures*, Seismic Design for Existing Structures, Seminar Course Manual, SCM-14(1986), American Concrete Institute, 1986, 47pp.

Jirsa, J.O. and Meli, R., *Working Group Conclusions on Materials, Repair and Retrofitting,*, Reducing Earthquake Hazards, Lessons Learned from the 1985 Mexico Earthquake, Earthquake Engineering Research Institute 89-02, 1989, pp.175-179.

Jirsa, J.O., Kreger, M E. and Carrasquillo, R.L., *Repairing and Strengthening Damaged Reinforced Concrete Buildings*, Reducing Earthquake Hazards, Lessons Learned from the 1985 Mexico Earthquake, Earthquake Engineering Research Institute 89-02, 1989, pp.175-179.

Mander, J. B., Priestley, M. J. N., and Park R., *Theoretical Stress-Strain Model for Confined Concrete*, ASCE Journal of Structural Engineering, Vol. 114, No. 8, August 1988, pp.1804-1827.

Martin, I., *Seismic Rehabilitation: Why, When and How*, The Mexico Earthquakes-1985, Factors Involved and Lessons Learned, 1986, pp. 396-408.

Marquis, G.M., Effect of High-Strength Concrete on the Seismic Response of Concrete Frames, M.Eng. Thesis, Department of Civil Engineering and Applied Mechanics, McGill University, Montreal, Quebec, 1997, 117 pp.

Masri, A.C. and Goel, S.C., *Seismic Design and Testing of an RC Slab-Column Frame Strengthened by Steel Bracing*, Earthquake Spectra, Vol. 12, No. 4, November 1996, pp.645-666.

Mirmiran, A., Shahawy, M., Mukherjee, A., Ramana, V.P.V., Kant, T., Dutta, P.K. and Desai, Y.M., *Behaviour of Concrete Columns Confined with Fiber Composites*, Journal of Structural Engineering-Reston, Vol., 124, No. 9, 1998, pp 1094-1106.

Mitchell, D., and Collins, M.P., *Diagonal Compression Field Theory - A Rational Model for Structural Concrete in Pure Torsion*, ACI Journal, Vol. 71, No. 8, August 1974, pp. 396-408.

Mitchell, D., Dandurand A.and Paultre, P., *Repair and Upgrading of Concrete Structures in Mexico City after the 1985 Earthquake*, Canadian Journal of Civil Engineering, Vol. 15, No. 6, 1988, pp. 1052-1066.

Mitchell, D., and Paultre, P., *Assessment of Some Canadian Seismic Code Requirements for Concrete Frame Structures*, Canadian Journal of Civil Engineering, Vol. 18, No. 3, 1991, pp. 343-357.

National Building Code, Associate Committee on the, National Building Code of Canada 1990 and Supplement to the National Building Code of Canada 1990, National Research Council of Canada, Ottawa, Ontario, 1990.

National Building Code, Associate Committee on the, National Building Code of Canada 1995 and Supplement to the National Building Code of Canada 1995, National Research Council of Canada, Ottawa, Ontario, 1995.

Paultre, P., Evaluation of Seismic Performance of Concrete Frame Structures in Canada, Ph.D. Thesis, Department of Civil Engineering and Applied Mechanics, McGill University, Montreal, Quebec, 1987, 213 pp.

Paultre, P., Castele, D., Rattray, S., and Mitchell, D., *Seismic Response of Reinforced Concrete Frame Subassemblages - A Canadian Code Perspective*, Canadian Journal of Civil Engineering, Vol. 16, No. 5, October 1989, pp. 627-649.

Priestly M.J.N. and Calvi, G.M., Seismic Design and Retrofit of Bridges, John Wiley & Sons, New York, NY, 1996, 686 pp.

Ramirez, J.L., *Ten Concrete Column Repair Methods*, Construction and Building Materials, Vol. 10, No. 3, 1996, pp. 195-203.

Rattray, S., Reversed Cyclic Load Tests on Reinforced Concrete Frame Subassemblages, M.Eng. Thesis, Department of Civil Engineering and Applied Mechanics, McGill University, May 1986, 143 pp.

Standards Association of New Zealand, NZS 3101: 1995, Part 1: Code of Practice for the Design of Concrete Structures and Part 2: Commentary on the Design of Concrete Structures, Wellington, New Zealand, 1995, 127 pp. and 156 pp.

Toutanji, H. and Balaguru, P., *Durability Characteristics of Concrete Columns Wrapped with FRP Tow Sheets*, Journal of Materials in Civil Engineering, Vol. 10, No. 1, 1998, pp. 52-58.

Ye, L., Zhang, S. and Mai, Y.W., *Strengthening Efficiency of E-Fibre Composite Jackets of Different Architectures for Concrete Columns*, Applied Composite Materials, Vol. 5, No. 2, 1998, pp 109-123.

APPENDIX A

Design of Test Specimen RS1

A detailed description of the design of the column retrofit of Specimen RS1 is presented in this section. For more details on the design of Specimens RS1 and of companion-unretrofit beam-column-slab subassemblage Specimen S1, both, constructed and tested by Castele, refer to Castele (1988). This specimen was designed and detailed for "nominal ductility" with an R of 2.0 prior to column strengthening. It is assumed in the design that all reinforcement had a yield stress, f_y ,of 400 MPa and that the compressive strength of concrete, f'_c, is 30 MPa.

A.1 DESIGN OF SPECIMEN RS1

The design and detailing of the main beam and spandrel beam of Specimen RS1 is identical to Specimen S1 (constructed and tested by Castele, 1988). The column of Specimen RS1 was strengthened to achieve a "strong column-weak beam" mechanism. The column dimensions were increased to 700 by 600 mm from 400 by 400 mm in order to enlarge the section and to accommodate the added hoop and vertical reinforcement.

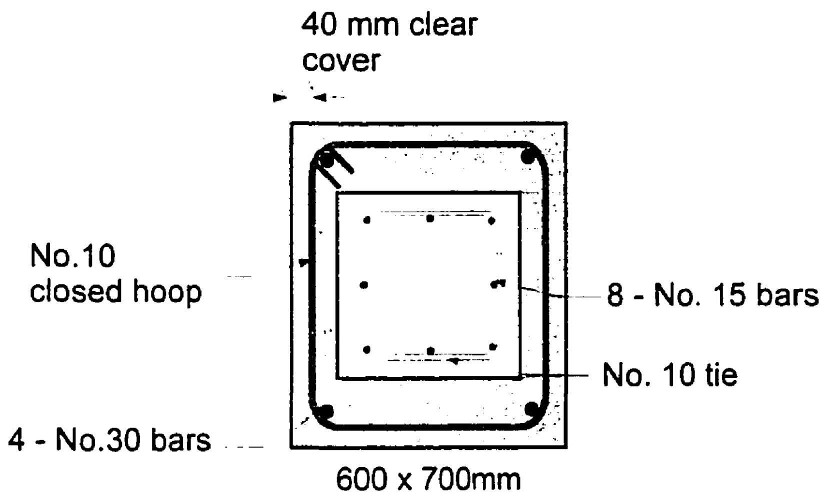

Figure A.1: Column reinforcement details of Specimen RS1

a) *Details of Strengthened Column*

The column was strengthened using 4 - No. 30 vertical bars placed around the existing column as shown in Fig. A.1. Two holes were drilled through the floor slab to allow continuity of the vertical reinforcement through the joint region. From the results of a non-linear finite element analysis, it was found that placing additional ties just above and below the joint region would assist in resisting the joint shears. Therefore, two No. 10 hoops were placed at each of these locations. The details of the added column hoops are shown in Fig. A.2.

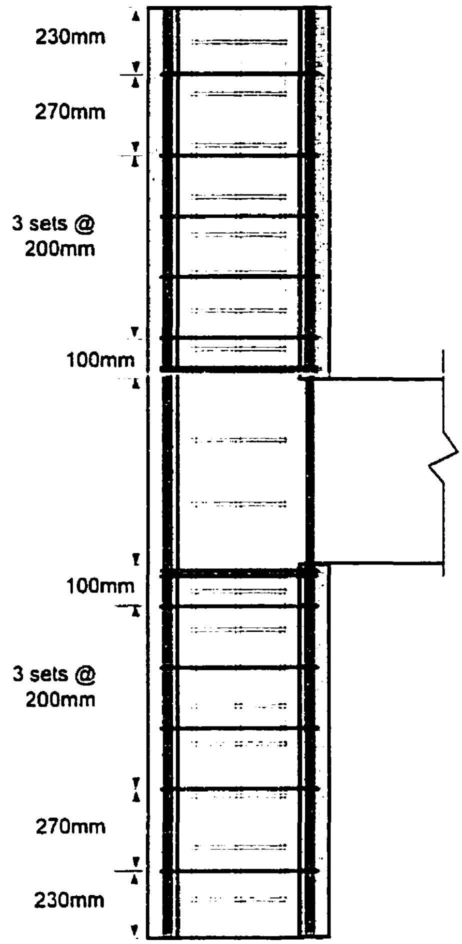

Figure A.2: Details of Column reinforcement of Specimen RS1

b) *Check Column Strength*

The maximum axial load permitted by Clause 10.3.5.3. (CSA 1994) is given by the expression:

$$P_{r(max)} = 0.8\,(0.85\,\phi_c f'_c (A_g - A_{st}) + \phi_s A_{st} f_y)$$
$$= 5876\text{ kN} > P_f$$
O.K.

From the program RESPONSE (Collins and Mitchell, 1997), an analysis of the cross section subjected to an axial load of 1076 kN, determined that the column could carry a factored moment resistance, M_{rc}, of 570 kNm. A comparison of the axial load vs. moment capacity of the columns of Specimen S1 and RS1 are shown in Fig. A-3. Due to the strengthening of the column, the bending moment capacity of this specimen has significantly improved. As a result, the plastic hinging is not expected to form in the column since Clause 21.4.2.2 (CSA 1994) has been satisfied. Clause 21.4.2.2 (CSA 1994) requires that the flexural capacity of the columns exceeds the nominal flexural resistance of the beams such that:

$$
\begin{aligned}
\sum M_{rc} &\geq 1.1\sum M_{nb} \\
\sum M_{rc} &= 570 + 570 = 1040 \text{ kNm} \\
M_{nb} &= 1.2M_r = 1.2 \times 381.7 = 458 \text{ kNm} \\
1.1M_{nb} &= 503.8 \text{ kNm} \\
\text{Thus,} \sum M_{rc} &> 1.1M_{nb}
\end{aligned}
$$

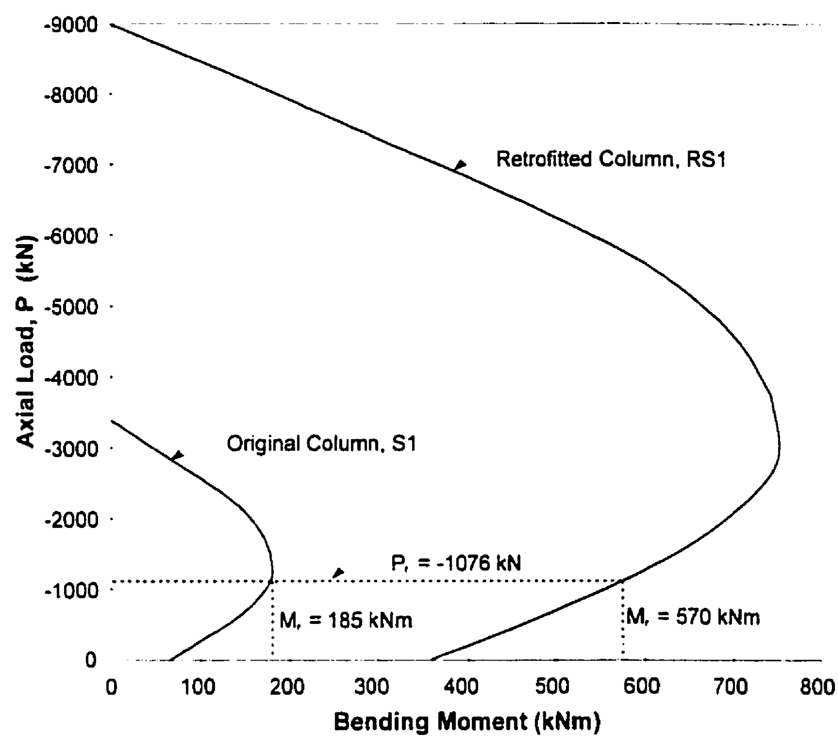

Figure A.3: Axial load versus Moment Capacity of Specimens S1 and RS1

As seen in Fig. A.4, the factored design column shear, V_f is 191 kN. The shear resistance of the concrete, V_c of the strengthened column as specified by Clause 21.7.3.1 is one-half of the value calculated by:

$$
\begin{aligned}
V_c &= 0.2 l f_c \sqrt{f_c'} b_w d \\
&= 0.2 \times 0.6 \times \sqrt{30} \times 700 \times 535 \\
&= 246 \text{ kN}
\end{aligned}
$$

Therefore V_c is 123 kN according to Clause 21.7.3.1.

The shear resistance provided by the original transverse column reinforcement, V_s is calculated by using Clause 11.3.7.

$$\begin{aligned} V_s &= \frac{f_s A_v f_y d}{s} \\ &= \frac{0.85 \times 200 \times 400 \times 342.5}{125} \\ &= 186 \text{ kN} \end{aligned}$$

The shear resistance provided by the added transverse column reinforcement, V_s is calculated by using Clause 11.3.7.

$$\begin{aligned} V_s &= \frac{f_s A_v f_y d}{s} \\ &= \frac{0.85 \times 200 \times 400 \times 535}{200} \\ &= 182 \text{ kN} \end{aligned}$$

Therefore, the shear resistance provided by both the added and original transverse reinforcement is 368 kN.

The shear resistance, V_r provided by the strengthened column of Specimen RS1 is defined in Clause 11.3.4 as,

$$\begin{aligned} V_r &= V_c + V_s \\ &= 123 + 368 \\ &= 491 \text{ kN} > 191 \text{ kN} \end{aligned}$$

but V_r cannot exceed,

$$\begin{aligned} V_r &= V_c + 0.8 l f_c \sqrt{f_c'} b_w d \\ &= 123 + 985 \\ &= 1108 \text{ kN} \end{aligned}$$

Hence the shear capacity is adequate to develop the nominal flexural capacity in the beam.

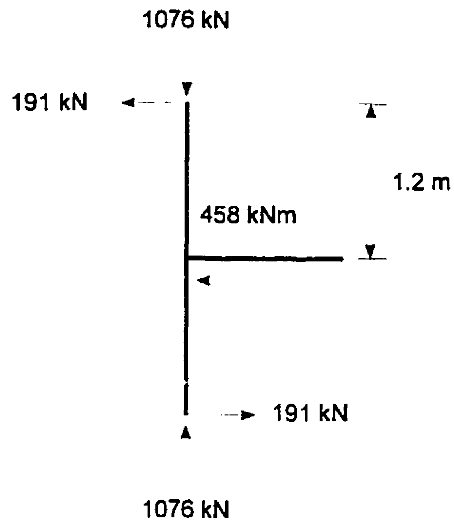

Figure A.4: Determination of design shear force in the column

c) *Check Joint Capacity*

The design joint shear is 449 kN (see Castele, 1988) The strengthening procedure has reduced the required joint shear which must be resisted by the joint reinforcement to:

$$\begin{aligned} V_s &= V_j - V_c \\ &= 449 - 246 \\ &= 203 \text{ kN} \end{aligned}$$

The shear resistance provided by the original joint ties is:

$$\begin{aligned} V_s &= \frac{f_s A_v f_y d}{s} \\ &= \frac{0.85 \times 200 \times 400 \times 342.5}{150} \\ &= 155 \text{ kN} \end{aligned}$$

The shear resistance provided by the original joint ties is significantly less than the design joint shears. Therefore four additional joint hoops were used, two hoops placed directly above and two hoops placed directly below the joint region, as shown in Fig. A.2. The shear resistance of the added hoops is:

$$V_s = \frac{f_s A_v f_y d}{s}$$
$$= \frac{0.85 \times 400 \times 400 \times 535}{600}$$
$$= 121 \text{ kN}$$

The total shear resistance provided by the added hoops and the existing ties is 155+121=276 kN which is greater than the design joint shear of 203 kN. It should be pointed out that this specimen was originally designed according to the 1984 CSA Standard and was a satisfactory design to meet the requirements of this code. However, the calculations shown above are according to the 1994 CSA Standard. It is evident that from the changes of the 1984 CSA Standard to the 1994 CSA Standard, Specimen RS1 has remained adequately designed and detailed.

APPENDIX B

Design of Test Specimen RS2

A detailed description of the design of the column retrofit of Specimen RS2 is presented in this section. For a full design of unretrofit companion beam-column-slab subassemblage Specimen S1, constructed and tested by Castele, refer to Castele, (1988). This specimen was designed and detailed for "nominal ductility" with an R of 2.0 prior to column strengthening. It is assumed in the design that all reinforcement steel bars had a yield stress, f_y ,of 400 MPa, while the structural steel had a yield stress, f_y ,of 300 MPa and the compressive strength of concrete, f_c', is 30 MPa.

B.1 DESIGN OF SPECIMEN RS2

The design and detailing of the main beam and spandrel beam of Specimen RS2 is identical to Specimen S1. However, the column of Specimen RS2 was strengthened to achieve a "strong column-weak beam" mechanism. The column dimensions were slightly increased due to the addition of the vertical corner angles. The details of the column retrofit are described in Section 2.3.4.

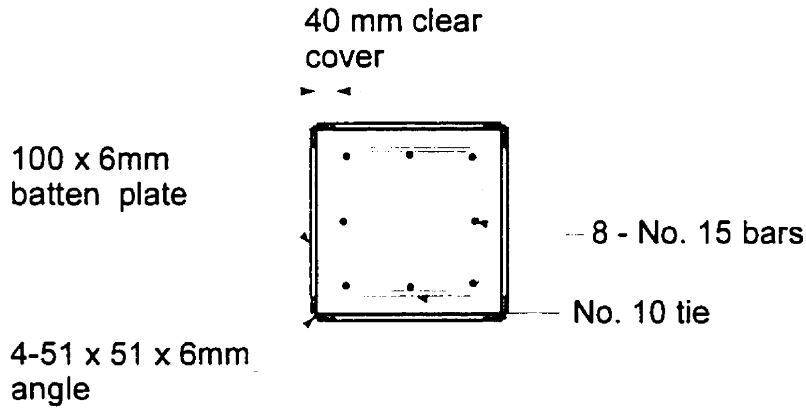

Figure B.1: Column reinforcement details of Specimen RS2

a) *Details of Strengthened Column*

The column was strengthened using 4 - 51 x 51 x 6 mm thick steel angles (A_s = 605 mm^2) placed at the corners of the existing column. Added transverse reinforcement, provided in the form of 100 by 6 mm thick steel batten plates (A_s = 600 mm^2) which were welded to the corner angles, as shown in Fig. B.1. The details of the strengthened column are shown in Fig. B.2.

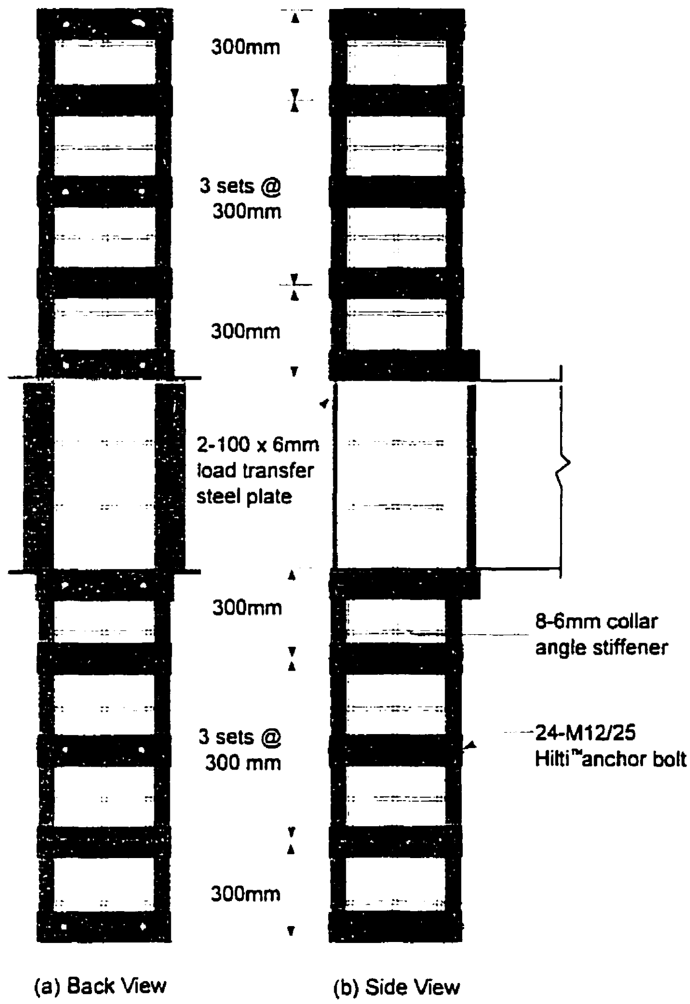

Figure B.2: Details of Column reinforcement of Specimen RS2

b) *Check Column Strength*

The maximum axial load permitted by Clause 10.3.5.3. (CSA 1994) is given by the expression:

$$P_{r(max)} = 0.8\,(0.85\,\phi_c f_c^{'}(A_g - A_{st}) + \phi_s A_{st} f_y)$$
$$= 2838 \text{ kN} > P_f$$
O.K.

From program RESPONSE (Collins and Mitchell, 1997), an analysis of the cross section subjected to an axial load of 1076 kN, determined that the column could carry a factored moment resistance, M_{rc} of 396 kNm. A comparison of the axial load vs. moment capacity of the columns of Specimens S1 and RS2 is shown in Fig. B.3. Due to the addition of the steel corner angles the bending moment capacity of this specimen has increased. As a result, plastic hinging is not expected to form in the column since Clause 21.4.2.2 (CSA 1994) has been satisfied. Clause 21.4.2.2 (CSA 1994) requires that the flexural capacity of the columns exceeds the nominal flexural resistance of the beams such that:

$$\sum M_{rc} \geq 1.1 \sum M_{nb}$$
$$\sum M_{rc} = 396 + 396 = 792 \text{ kNm}$$
$$M_{nb} = 1.2 M_r = 1.2 \times 381.7 = 458 \text{ kNm}$$
$$1.1 M_{nb} = 503.8 \text{ kNm}$$
$$\text{Thus}, \sum M_{rc} > 1.1 M_{nb}$$

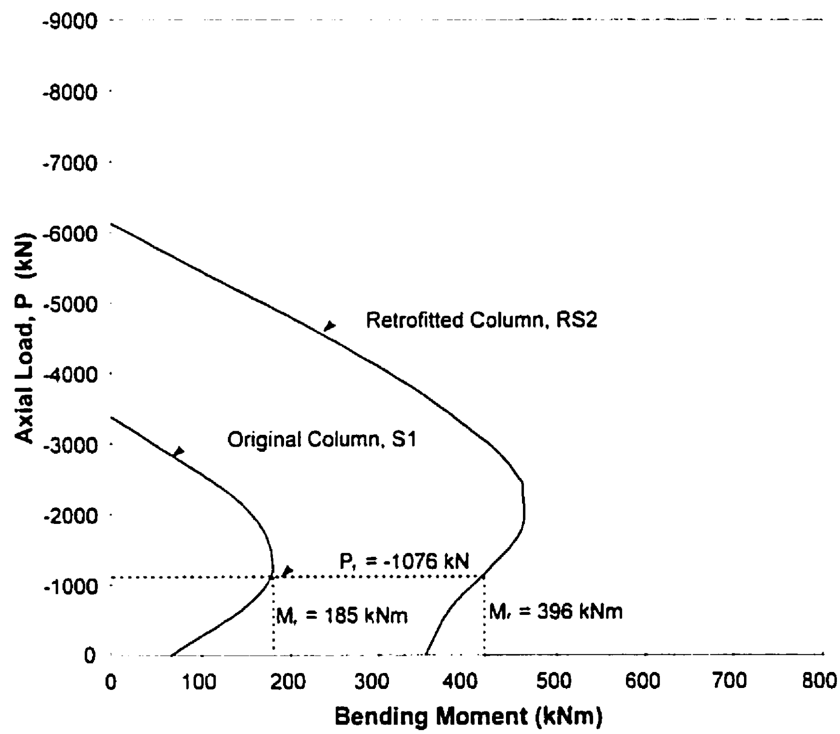

Figure B.3: Axial load versus Moment Capacity of Specimens S1 and RS2

As seen in Fig. A.4, the factored design column shear, V_f is 191 kN. The shear resistance provided by the concrete, V_c of Specimen RS2 equals:

$$V_c = 0.2 \lambda \phi_c \sqrt{f_c'} b_w d$$
$$= 0.2 \times 0.6 \times \sqrt{30} \times 400 \times 342.5$$
$$= 90 \text{ kN}$$

However, V_c specified by Clause 21.7.3.1 is one-half the value calculated above, therefore V_c = 45 kN.

The shear resistance provided by the original transverse column reinforcement, V_s is calculated by using Clause 11.3.7.

$$V_s = \frac{f_s A_v f_y d}{s}$$
$$= \frac{0.85 \times 200 \times 400 \times 342.5}{125}$$
$$= 186 \text{ kN}$$

The shear resistance provided by the added batten plates in the column is:

$$V_s = \frac{f_s A_v f_y d}{s}$$
$$= \frac{0.85 \times 1210 \times 300 \times 342.5}{300}$$
$$= 352 \text{ kN}$$

The total shear resistance provided by the original ties and the added batten plates is 538 kN.

The total shear resistance of the strengthened column of Specimen RS2 is determined by Clause 11.3.4:

$$V_r = V_c + V_s$$
$$= 45 + 538$$
$$= 583 \text{ kN} > 191 \text{ kN}$$

but V_r cannot exceed.

$$V_r = V_c + 0.8 lf_c \sqrt{f_c'} b_w d$$
$$= 45 + 360$$
$$= 405 \text{ kN}$$

The shear capacity, governed by the maximum limit on V_r, is adequate.

c) Check Joint Capacity

The design joint shear is 449 kN (see Castele, 1998). The required joint shear which must be resisted by the joint reinforcement is:

$$\begin{aligned} V_s &= V_j - V_c \\ &= 449 - 90 \\ &= 359 \text{ kN} \end{aligned}$$

The shear resistance provided by the original joint ties is:

$$\begin{aligned} V_s &= \frac{f_s A_v f_y d}{s} \\ &= \frac{0.85 \times 200 \times 400 \times 342.5}{150} \\ &= 155 \text{ kN} \end{aligned}$$

The shear resistance provided by the original joint ties is unsatisfactory. The addition of the 102 mm x 102 mm x 16 mm thick collar angles placed directly above and below the joint region provide strong bands of transverse reinforcement which could prevent the joint from failing in shear. It is believed that these collar angles could permit the joint shear resistance to be developed through strut-and-tie action.

The combined joint shear resistance of the collar angles and the existing joint reinforcement is 1025 kN, which greatly surpasses the design joint shear of 359 kN. However, Clause 11.3.4 specifies an upper limit to the value of the shear resistance of:

$$\begin{aligned} V_r &= V_c + 0.8 l f_c \sqrt{f_c'} b_w d \\ &= 90 + 360 \\ &= 450 \text{ kN} \end{aligned}$$

The joint shear resistance is limited to a value of 450 kN which is greater than the design joint shear of 359 kN. Therefore the proposed design of Specimen RS2 is adequate, satisfying all pertinent provisions of the 1994 CSA Standard.